IMPROVING USEFUL LIFE OF ENGINEERING COMPONENTS BY COATING AND OTHER TECHNIQUES

THESIS

Submitted by

T. C. PETER

for award of the degree of

DOCTOR OF PHILOSOPHY

JULY - 2003

Department of Mechanical Engineering

Government Engineering College

Thrissur.

Department of Mechanical Engineering

GOVERNMENT ENGINEERING COLLEGE

THRISSUR – 680 009

CERTIFICATE

This is to certify that the thesis entitled

"IMPROVING USEFUL LIFE OF ENGINEERING COMPONENTS BY COATING AND OTHER TECHNIQUES"

being submitted by **Shri. T. C. PETER** *for awarding of Degree of* **DOCTOR OF PHILOSOPHY** *in Engineering to the University of Calicut is a record of bonafide work carried out by him during the year 1999 - 2003 at Govt. Engineering College, Thrissur.*

The contents of this thesis, in full or in parts, have not been submitted to any other Institute or University for award of any degree or Diploma.

Dr. M. K. Balakrishnan Nayar
Supervising Teacher,
Former Prof. & Head of
Production Engg. Dept.,
Govt. Engg. College,
Thrissur.

Thrissur

10-07-2003

ACKNOWLEDGEMENT

I am indebted to Dr. M. K.Balakrishnan Nayar, Former Professor and Head of Production Engineering Department, for his guidance , supervision and constant encouragement through out the period of this research work and helped in the preparation of this Report. He was helpful in identifying the topic for Research, in collecting source materials and other datas.

I am recording my sincere thanks to Dr. R. Krishna Murthy, Professor in Manufacturing Engineering Department, IIT Madras for his continuous and total involvement for his comments, detailed discussion, positive criticism and the support extended by him through out the course of this research work. The facilities in the laboratory was made available to me for my study and enlightened me on this technology.

My sincere thanks to Prof. K. Vijayan Raja, Professor & Head of Mechanical Engineering, Govt. Engineering College, Thrissur for rendering his help and providing all facilities in the department for the successful completion of the work.

Dr. N. Premachandran, Principal, Govt. Engineering College was a source of inspiration and he gave all support and guidance during the entire course of the Research Programme. I am very much indebted to him for this gesture.

I record my sincere gratitude to Prof. K.K. George, Director of Technical Education, Kerala for his help and support.

The discussion with Dr. P. Sasidharan, Scientist, C – MET, Thrissur has broadened the scope of the work and gave an insight into the glazing of Ceramics.

Dr. Shaji and Dr. P. Raghavan, Scientistis, CSIR Laboratory, Thiruvananthapuram have shared their experience and expertise in this field and that has contributed considerably. Dr. Gopinatha Pai of VSSC spent his valuable time with us and helped us in giving the final shape to the Project Work.

My thanks to Dr. K. P. Mohanan, former Director, College Development Council, Calicut University for helping us in getting Registration and proper recognition from the University in time.

Dr. V. M. Manoharan, Former Member of the Calicut University Syndicate and Prof. P. N. Prakasan, Member of the Syndicate for all their help and guidance, Fr. Paul Porathoor, Prinicpal, St. Thomas College, Thrissur took active interest in my Research Programme.

I would like to record my thanks to Dr. D. Balakrishnan, Jt. Director (Rtd.), Directorate of Technical Education, Kerala for his valuable suggestions during the course of this work.

The help and co-operation received from the Staff of IIT, Madras, University of Calicut, Dept. of Mechanical Engineering, Govt. Engineering College, Thrissur; CSIR Laboratory, Thiruvananthapuram; VSSC, Thiruvananthapuram in respectfully acknowledged.

I would like to thank all, who have contributed in one way or other for the successful completion of this work.

T. C. PETER

ABSTRACT

Failure of Engineering components due to surface deterioration it a common phenomena, especially in tribological applications. The productive life of components can be augmented by improving the surface quality by various finishing operations. The strength and durability of the surface can be increased by giving a proper coating with a suitable material.

The coating technique has to be developed depending upon the environment in which the component is supposed to operate. The mechanical properties of the coated surface, surface quality etc. are of paramount importance. The substrate material and its metallurgical characteristics will go a long way in identifying a process for coating.

Of late, the coating technology is becoming popular as a tool in deciding the quality of surface of Engineering materials. A wide range of coating materials and coating processes is available for diverse applications and requirements. Advanced materials such as ceramics and composites are emerging as better candidates for this emerging technology. These materials are being used currently in diverse applications requiring wear resistance and chemical stability at elevated temperatures.

This Report is an in-depth study on coating of materials. The first chapter gives an introduction to the topic, highlighting the necessity of the process and its relevance in the present context. The second chapter

explains the process in detail. The various equipments used for coating are listed out. The parameters involved in the process are also indicated. The mechanism of coating, formation of metallurgical layers on the subsurface etc. are studied. The various tests to assess the quality of the coating are also indicated. The third chapter examines the various techniques used for production of powders, its characterisation and the behaviour in the coating process.

The forth chapter discuss the structure property co-relation of Plasma Sprayed Coatings, viz Zirconia Coatings, Mechanical Tests, AE Tests and XRD Tests are discussed. Effects of coating on glazing in Porcelain has also been studied in detail. The coating was done with Alumina and the properties are studied especially on glazing and wear mechanism.

The fifth chapter consolidates the findings and gives a direction towards the scope of further work in this field.

CONTENTS

List of Tables

ABBREVIATIONS

AE	Acoustic Emisson.
APS	Atmospheric Plasma Spraying
AT	Alumina – Titania
DCB	Double Cantilever Beam
FFT	Fast Fourrier Transformation
IR	Infra Red.
PSZ	Partially Stabilised Circonia
RMS	Root Mean Square
SEM	Scanning Electron Microscope
STF	Strain to Fracture
TEM	Transmission Electron Microscope
VHN	Vickers Hardness Number
VPS	Vacuum Plasma Spraying
XRD	X – ray Diffraction

CHAPTER – 1

INTRODUCTION

Advances in Technology calls for introduction of new materials and processes to cope up with the operating parameters. Failure of Engineering Components can be due to mechanical or metallurgical factors.

Mechanical failure might be defined as any change in the size, shape, or material properties of a structure, making it incapable of performing desired functions. Failure of a component or structure can be due to damage by plastic deformation, formation and propagation of cracks, corrosion or by associated modes of wear.

Further, failure can be of body type (bulk failure) or of surface type. Bulk failure is mostly associated with plastic deformation of a component, resulting in the component being unable to support the forces, perform the intended function or even avoid interfacing with other operating components. Fracture is another bulk type of failure leading to sudden and catastrophic separation of a machine part into two or more pieces as a result of initiation and propagation of cracks. Corrosion and related wear are mechanisms, which primarily deteriorate the surfaces of components by metallurgical factors.

Concentrated research has resulted in achieving considerable improvements in bulk properties through microstructural refinements and reinforcements and thus avoids bulk failure. However, surface deterioration / degradation is still a serious problem in many engineering industries / applications. Surface deterioration leads to rapid loss in quality, impaired performance , unwanted noise or vibration etc. Abrasion, erosion and corrosion constitute major contributory factors for this (quality loss), necessitating rapid replacement of components. Replacement of components is time consuming, costly and added cost of down time and increased maintenance etc. This demands new approaches towards material selection and processing for optimal use. Surface engineering is concerned with the application of both traditional and innovative surface technologies to produce a composite material with properties unattainable with either the base or surface material individually.

The growth in surface engineering has been encouraged by two factors. The first has been the recognition that the surface is the most important part in any engineering component. It is at the surface where most of the failures originate. The second has been the development of new coating and treatment methods, which provide coating, the requisite characteristics, which were previously unachievable.

Corrosion, fatigue and related wear are the most impending among surface failures, resulting in the loss of huge amount of materials. Ever increasing demand for materials and the rapid depletion of their

natural sources have created an urgent need for the conservation of materials. Surface engineering has become an effective approach for minimizing this loss by optimally combining desirable bulk and surface properties.

In other words surface engineering enables designer to choose bulk material from the stand point of structural and economic criteria and surface material to deal with severe external conditions and meet specific design demands like resistance to corrosion, abrasion and other modes of wear.

Broadly speaking the underlying techniques of surface engineering can be divided into those involving the modification (whether by mechanical, thermal or chemical means) of the existing surface chemistry and structure of the component and those involving the deposition of overlay material, albeit often in the form of a thin / thick layer of coating over the bulk or substrate. The former generally referred to as diffusion process has now attained some saturation in terms of performance enhancement and added limitations of its dependence on inherent quality of the substrate materials, and is resulting in diminishing returns. On the other hand the latter referred to as surface coating has experienced rapid strides in technology development and applications. Coating technology is one of the most innovative techniques found in modern economy.

Among various coating techniques, the thermal spraying process exhibits certain unique characteristics, making it the most sought after

process to deal with corrosion and related wear problems in many critical engineering applications.

In thermal spraying process, substrate temperatures is rarely 2000°C; even when very high melting point alloys or materials are used to form droplet spray. This means that not only coating of refractory (and thus high melting points) metals and ceramic can be applied, but also the choice of substrate materials is much wider than for hard facings. In thermal spraying the coating material is fed as a wire or fine powder into flame, usually oxy-acetylene, which has a temperature of about 3000°C. The droplets are heated to about 2000°C and strike the target surface at about 100m/s.

Plasma spraying methods are also widely used. The plasma is formed by an inert gas, usually Argon, using a high-energy electric arc into which the coating material is introduced as a fine powder. The very high temperatures of the arc (15000°C or more) enable a wide range of coating materials to be sprayed. Rapid expansion of hot gas, accelerates the molten droplets to more than 250 m/s and the combination of temperature and kinetic energy leads to coating of lower porosity than those produced by flame spraying.

To achieve enhanced tribological performance, the coating must, of course, remain firmly bonded to the substrate, and for this reason correct surface preparation prior to coating is essential. The bonding mechanism of hard faced coatings is mostly metallurgical, where as

for flame and plasma sprayed layers it depends more on mechanical interlocking. Even a strong interfacial bond will fail if sufficient stress is applied to it, and an important source of such stress can be differential thermal contraction between coating and substrate as they cool. Residual stresses from this source can limit the usable thickness of many ceramic coatings to less than 0.5mm. In order to improve the interfacial strength of some sprayed coatings, particularly ceramics, intermediate bond coats are sometimes used.

The choice of material is governed by the condition of use and the cost of the component. Ceramic materials have distinct advantages in several wear applications, especially under aggressive environments. The properties of advanced ceramics that make them suitable for tribological applications are high hardness, compressive strength, retention of mechanical properties at elevated temperatures, resistance to chemical reactions, low density, high stiffness, and good thermal properties. The disadvantages include low fracture resistance, high cost of processing raw materials such as powders and fabrication cost.

Abrasive wear is one of the prominent modes of material loss in many of the engineering applications. Abrasive wear arises when a hard, rough surface slides against a relatively softer surface, digs into it, and plows a series of grooves. Abrasive wear can also arise in the form of three body abrasion, when hard abrasive particles are introduced between sliding surface and abrade material from both the sliding surfaces. Hardness and corrosion resistance of the surface of

the engineering component, are vital properties, when they are exposed to abrasive and chemically reactive environment. These and other modes of wear can be combated by spray deposition of hard and wear resistant ceramics.

Motivation

The present work is an in-depth study on the various coating techniques, influence of operating parameters and the properties of the Products. New avenues are explored for the application of coating techniques.

CHAPTER – 2

LITERATURE SURVEY

2.1 INTRODUCTION

The main objective of the present study is to understand various techniques used for coating, the various parameters involved and the influence of those parameters on the quality of the end product. The performance of the various products are studied under diverse operating conditions.

2.2 NECESSITY FOR SURFACE MODIFICATION

Ever increasing demand for materials and the rapid depletion of their natural resources has created the need for their conservation. Majority of engineering failures are surface originated. Corrosion, fatigue and wear are the most impending among these, resulting in the loss of huge amount of materials. An effective way of minimizing this loss is by improving the surface properties of engineering materials. This is achieved presently by employing a surface modification process, either by altering the surface chemistry or microstructure. However, recent developments in the surface coating technology offer a more viable and attractive solution with a much greater flexibility. There is an emerging

philosophy that surface coating is a cost-effective way of minimizing the use of expensive or scarce materials. From the economic point of view, the recovery of expensive machine parts, (after corrosion or surface damage) is very desirable. Surface coatings are increasingly used in this role, for example in the recovery of jet engine turbine blades, crankshafts of automobiles etc.

The latest surface coating technology enables the engineer to obtain the precise coating properties required for functional surfaces in various ways. A range of coating materials and coating process is available for different applications and requirements. Thermally sprayed coatings have excellent wear resistant properties (Erich Lugscheilder, 1994)

2.3 Coating Process

The coating technology is one of the most innovative techniques found in modern economy. The different functions of the coatings such as wear and corrosion resistance, thermal or electrical insulation etc. can be achieved using different coating techniques and coating materials. The importance of these coating techniques is wear protection, often combined with corrosion resistance.

Metal spraying as a process of enhancing useful life of engineering materials have been clearly established. The

properties required by the coating are more and more sophisticated(good or high mechanical ,thermal, corrosion, wear resistance) and it is necessary to understand in detail about what phenomena involved in coating. The numerous spraying parameters depend on too many macroscopic elements.

Plasma spraying has to be regarded as one of the most universal coating techniques. Different plasma spraying processes allow to work with all kinds of materials from low melting plastics to high melting compounds. The high temperature which are reached by the plasma process and high grade of atomisation of commercial plasma spray devices enable us to achieve high quality coatings of hard metals, hard alloys ,high alloy steels and inter-metallics.

Plasma spraying, as a process developed in the fifties was used primarily for refractory materials. But now it is established that it can be used on almost any type of substrate. Applications include corrosion, temperature, and abrasion resistant coating and production of monolithic and near net shape. Taking advantage of

the Rapid Solidification Process (R.S.P), Powders of glassy metals can be plasma sprayed without changing their amorphous characteristics. Recently high temperature super conductive materials have been deposited by the plasma spray process.

The advent of Low Pressure Plasma Deposition (LPPD) provided an impetus for further developments, in particular in the aircraft industry. Today, turbine blades and other components of aircraft engines are coated with corrosion and temperature resistant coatings using LPPD Process. This provides better mechanical and thermal properties of the coatings. Also this allows chemically reactive materials to be sprayed.

2.4 Plasma Spray Technology – as a System

Plasma spray is regarded as a system having components substrate, coating materials, and coating processes. (Erich Lugseheilder, 1987). Analysis of the complex service condition of the engineering surface, the characterization of the spray powders and powder quality controls ,the process optimization and characterization of the sprayed coating are gaining more and more importance in plasma spraying technology. (Ahmed et al 1991, Berndt, 1994).

2.4.1 Basics of plasma spraying

Figure 2.1 shows a schematic arrangement for plasma spraying using a dc spray torch.

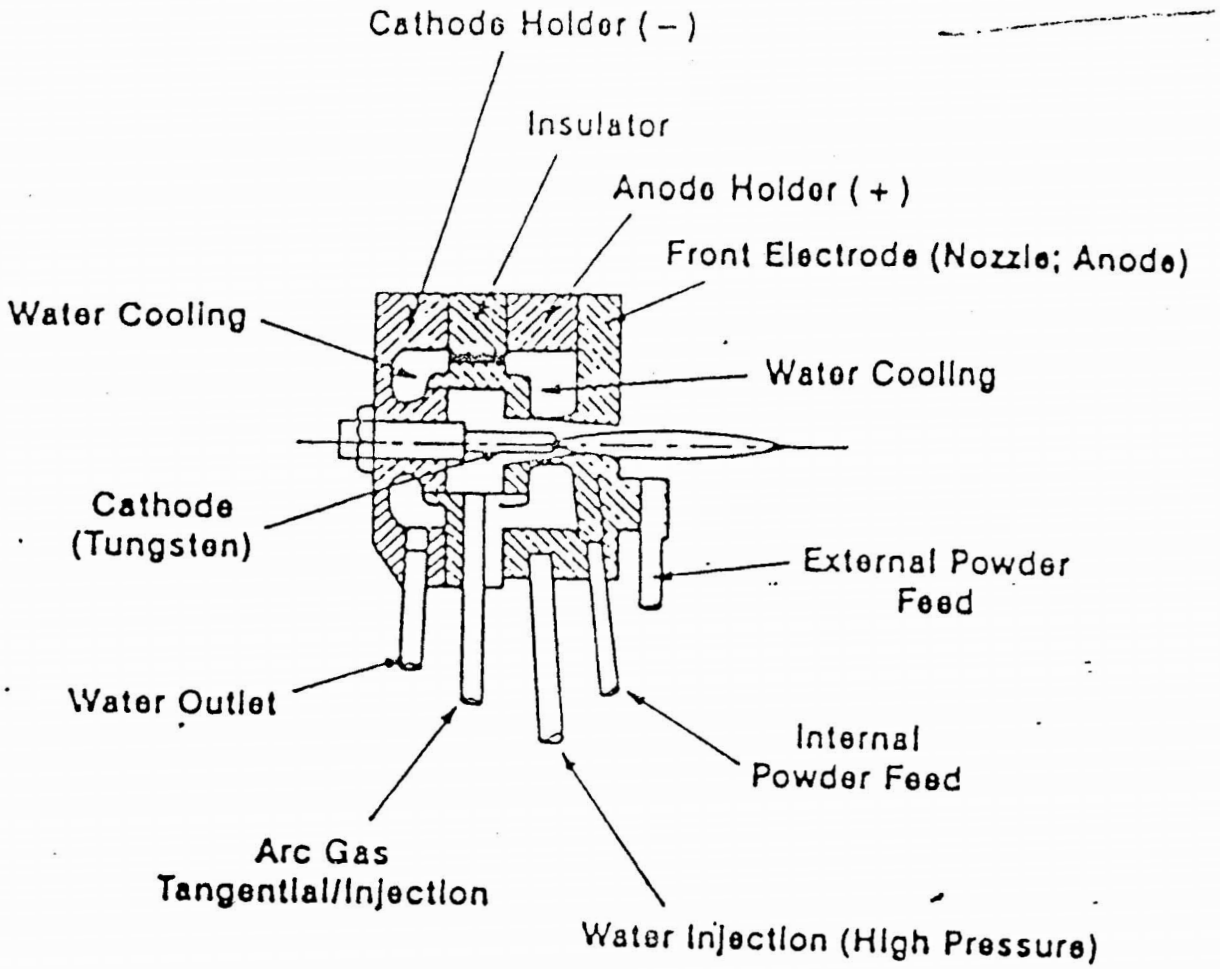

Fig. 2.1. Schematic of Typical Plasma Spray Gun

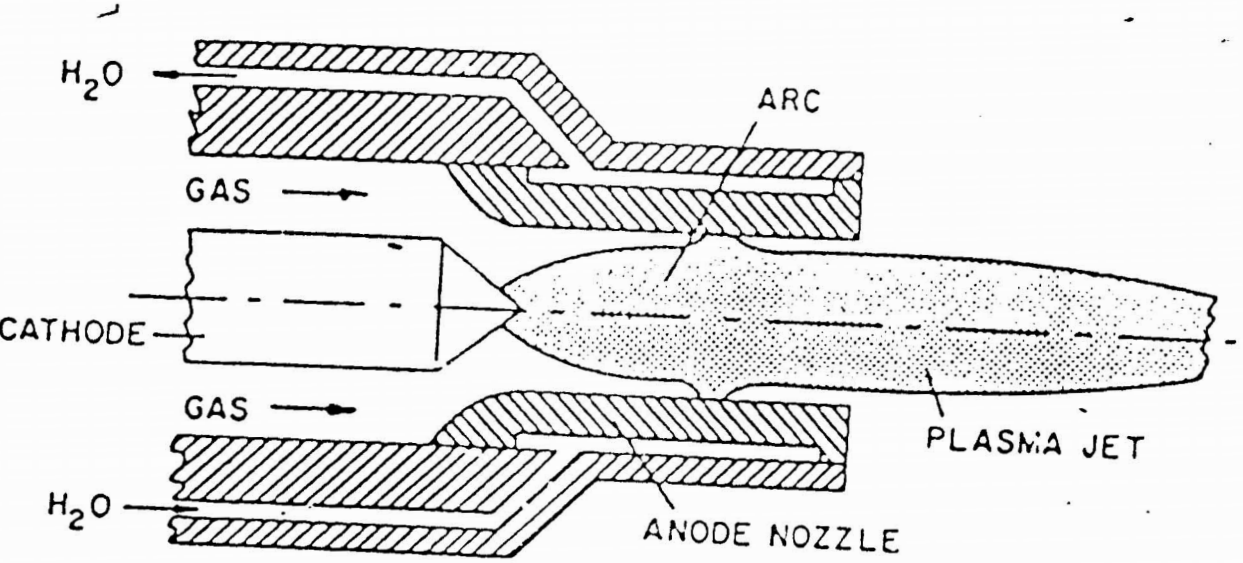

Fig. 2.2. Schematic of a Plasma Torch

A high intensity arc is operated between a stick type cathode and a nozzle shaped water cooled anode.

Plasma gas, introduced along the cathode, is heated by the arc to plasma temperature leaving the anode nozzle as a plasma jet or plasma flame.

Fine powder suspended in a carrier gas is injected into the plasma jet where the powder particles are accelerated and heated as the molten powder particles impinge with the high velocities on the substrate, they form more or less a dense coating.

2.4.2 *Basics of plasma spraying*

We discuss on a D.C plasma torch operated at atmospheric pressure, which are the most common tools for plasma spray. Figure 2.2 shows the essential components of the plasma torch. The arc is initiated at the tip of the cathode (typically thoriated tungsten)and water cooled anode nozzle may be converging , converging diverging or essentially straight depending on particularly sprayed application. The working gas is introduced either axially or with additional wire components. The latter improves arc stability in the vicinity of the cathode and rotates the anode are root which may be desirable for reducing anode erosion.

The gas heated by the arc emanates as a plasma jet from the torch orifice. The gas flow rate is sufficiently high to ensure a highly turbulent jet with a visible length of several centimetres.

The maximum temperature of the jet is a function of the design and of the operating parameters. It may reach values upto 20,000 K. in general a smaller diameter results in higher axis temperatures of the arc as well as the plasma jet if the operating parameters (mass flow rate and current) are kept the same. Although D.C arc are considered to be steady and stationary discharges, arcs are exposed to strong flows, as in the case of typical plasma spray torch, show high levels of fluctuation. The anode arc roof may travel axially as well as circumferentially (in case of vortex flow).

In addition, the arc may experience "shunting" effects which have been extensively studied in the sixties.

These arc fluctuations result in corresponding fluctuation of the plasma jet. (Fig. 2.3). With a frequency spectrum in the 10 k Hz ranges. Because of this fluctuation, temperatures and velocities measured in such plasma jets must be considered as average values. Besides these fluctuations, plasma jets show more or less deviations from the ideal two dimensional behaviour which is usually postulated for the temperature and velocity measurement as well as for modelling work

a.

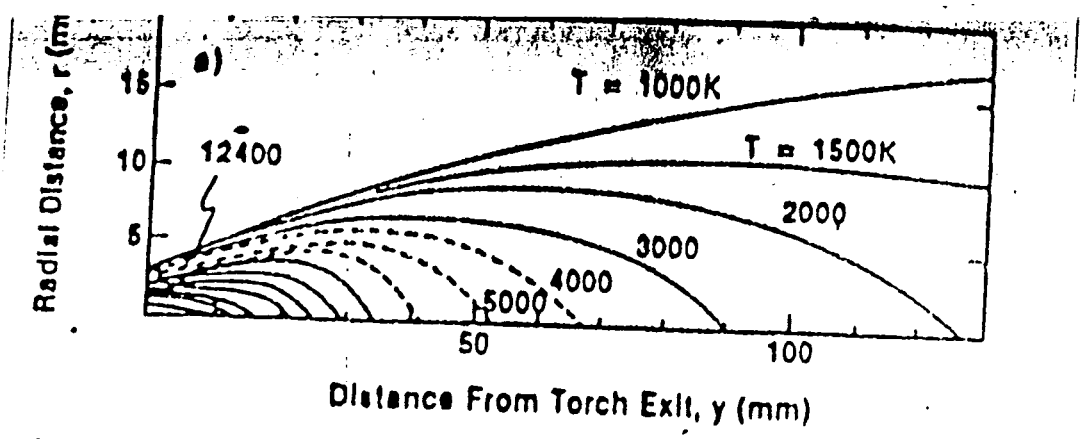

b.

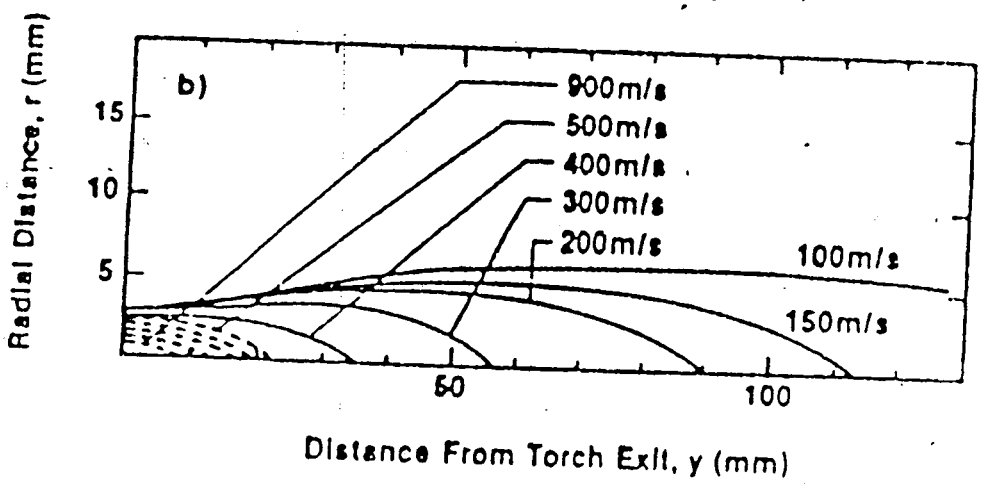

Fig. 2.3a - Temperature Profile of a DC N^2H_2 Plasma Jet.

Fig. 2.3b - Velocity Profile of a DC N_2H_2 Plasma Jet.

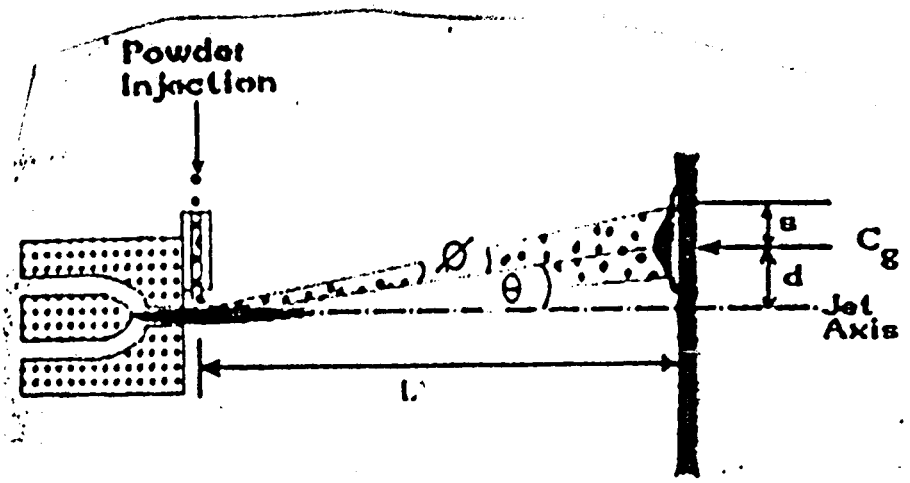

Fig. 2.4 - Spraying process and relevant data used in calculation

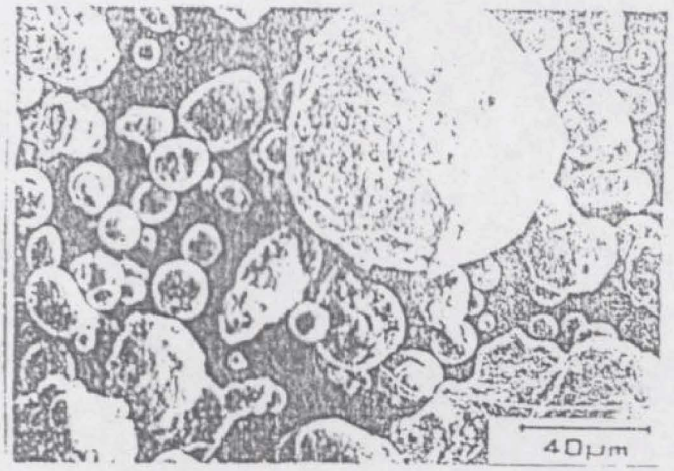

Fig. 2.5a - Scanning electron micrograph of the Ni - Cr powder

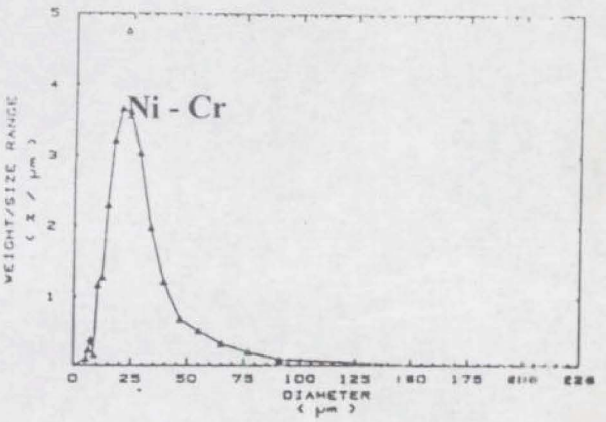

Fig. 2.5b - Particle size distribution of the Ni-Cr powder

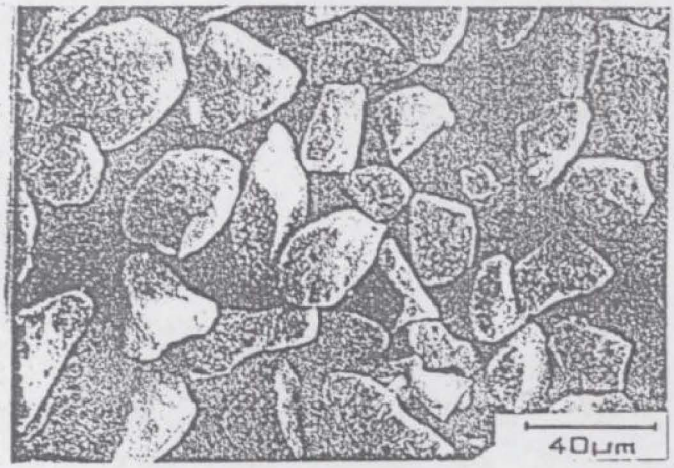

Fig. 2.6a - Scanning electron micrograph of the Alumina powder

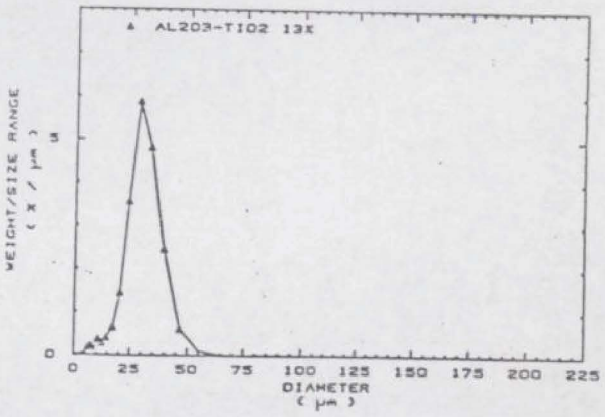

Fig. 2.6b - Particle size distribution of the Alumina powder

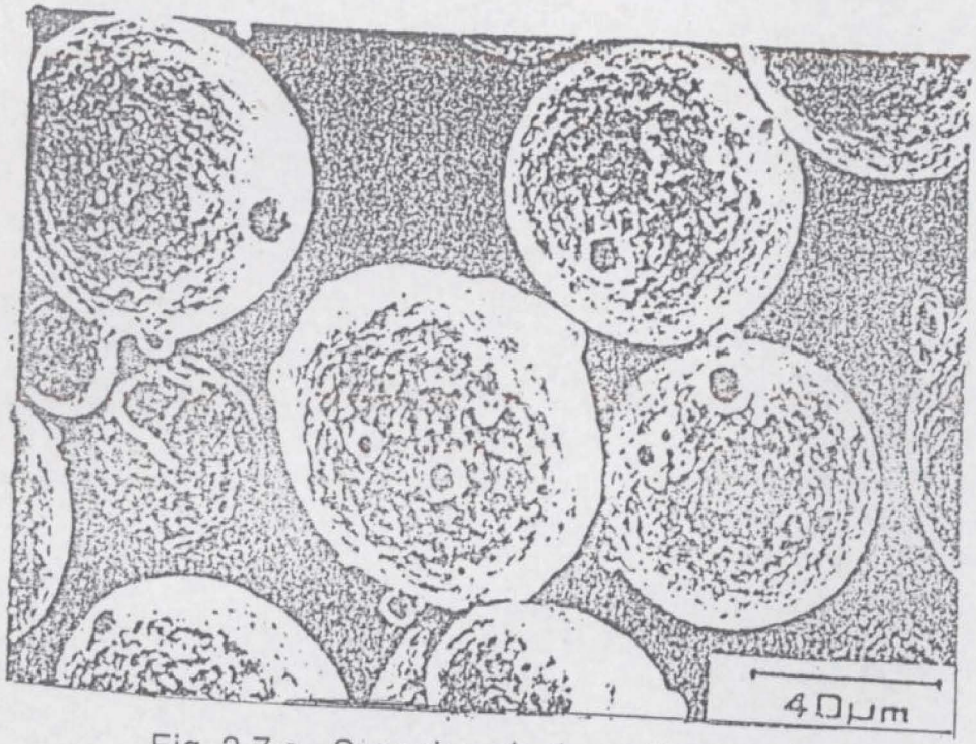

Fig. 2.7 a - Scanning electron micrograph
of the Ni - Cu- In powder

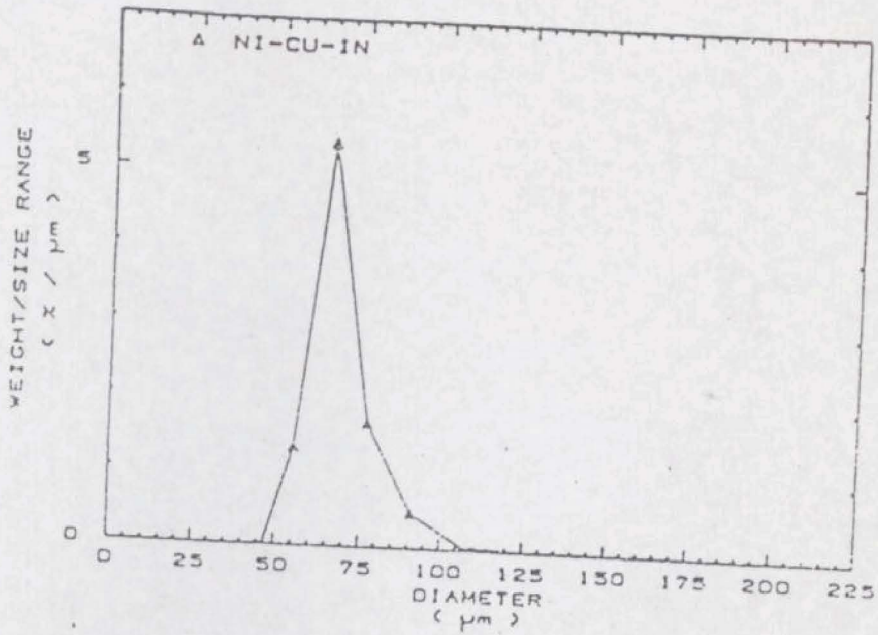

Fig. 2.7 b - Particle size distribution
of the Ni - Cu - In powder

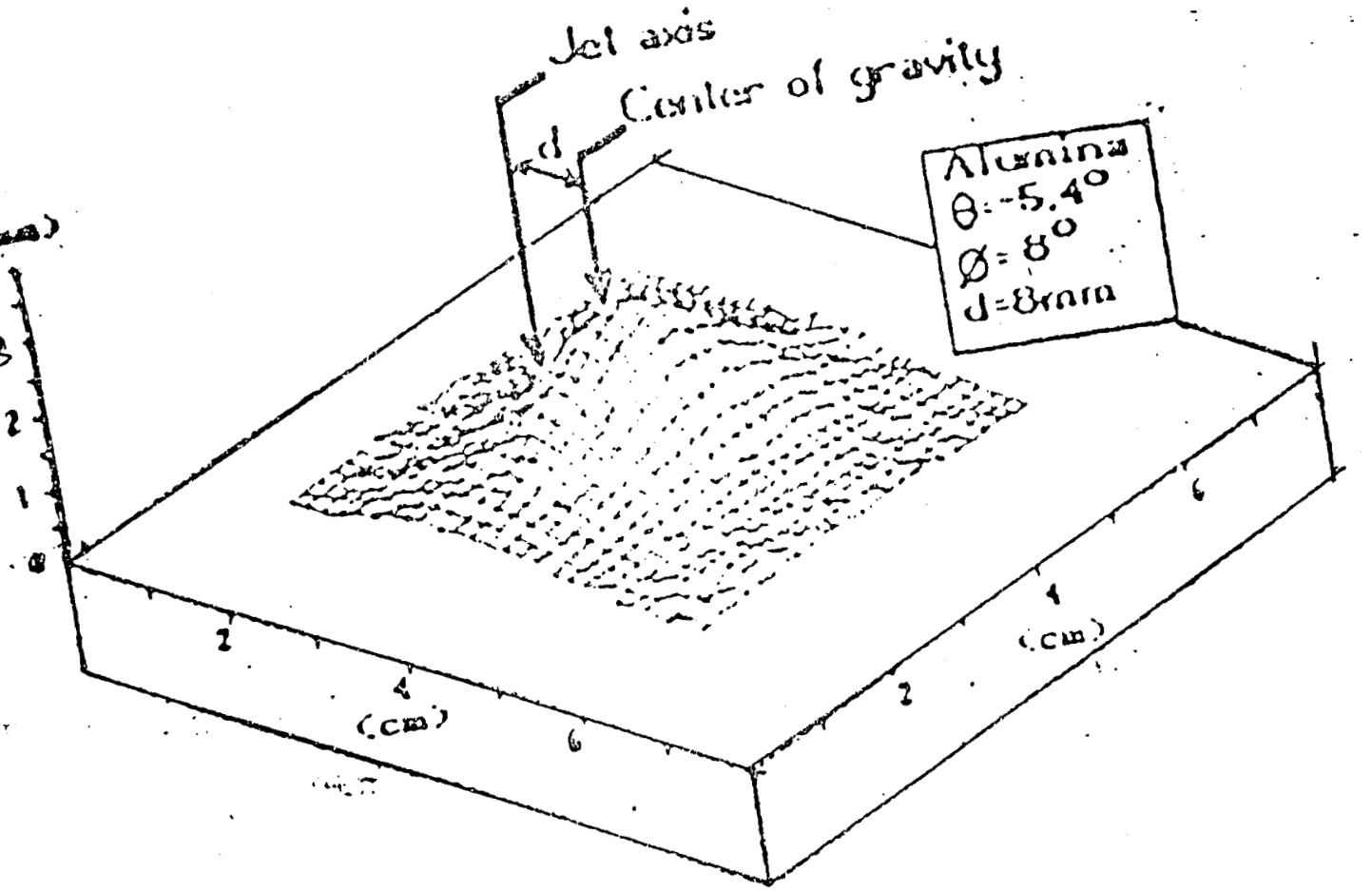

Fig. 2.8 - Typical 3 - D profile of a spray deposition pattern

2.4.3 Spraying Parameters

The effect of parameter injection on the spraying efficiency and adherence and microstructure were studied in detail by Champagne and Dallaiere (1994). They observed that after they have been transported from the powder feeder to the gun, particles may follow three types of trajectory. The particles with high momentum pass through the plasma jet and splash on to the substrate below the jet axis. Particles with low momentum are deflected by the plasma and strike the surface above the jet axis. The particles which are centrally transported for the near the jet axis. Flow of gas and particles towards the substrate form an asymmetric spray cone. When the gun is maintained in a stationary position ,a spray deposition pattern or a profile is built up on the substrate. Coatings are then nearly done when this deposition is scanned over the substrate.

The analysis of spray deposition pattern could provide a powerful means of characterizing different spraying parameters and more particularly, the particle injection mode.

$\text{Tan}\Theta = d/L$ ---------- (2.1)

(Figure – 2.4)

This is a measurement of the particle deviation from the jet axis where L is the spraying distance. By assumption, positive values correspond to particles that are deflected by plasma and negative values to particles which pass through it. Particles may deviate from the jet axis and also from the spray cone axis. The angle Φ formed between the spray cone axis and the directrix of the spray cone is called the spray divergence. This angle is defined as

$\text{Tan}\,\Theta = S/L$ ---------- (2.2)

Where s is the standard deviation of the sprayed particles from the centre of gravity and L has the same measuring as defined earlier. The value of Θ and Φ are therefore the main characteristics that can be used to assess the injection mode. Θ assesses the main trajectory of particles while Φ is the measurement of its dispersion.

By controlling the injection, the mean trajectory particle Θ can be modified. The trajectories of the higher particles and particularly their dispersion are affected not only by the nature of the plasma but also the size, shape, density of the spraying powder. Because the dispersion of the trajectory called spray divergence is very

sensitive to particle size distribution and the nature of the spray material, a supplementary variable should be defined to make compression possible between two materials. The relative spray divergence

$$\Phi(r) = \Phi / \Phi\ (\Theta = 0) \quad \text{---------- (2.3)}$$

Where Φ is the spray divergence for a specific injection mode and $\Phi\ (\Theta = 0)$ is the spray divergence when the axis of the spray cone coincides with the jet axis, i.e. when most of the particles are centre line injected.

L= spraying distance.

The injection of the particle plays an important role in plasma spray by determining the trajectories of the particles and their state upon impact; it contributes to the final coating quality. The particles which follow a quasi axial trajectory crossing the most energetic zones of the plasma leads to dense and adherence coatings. The measurement and characterization of spray deposition patterns can be considered as a powerful means of optimising spraying parameters.

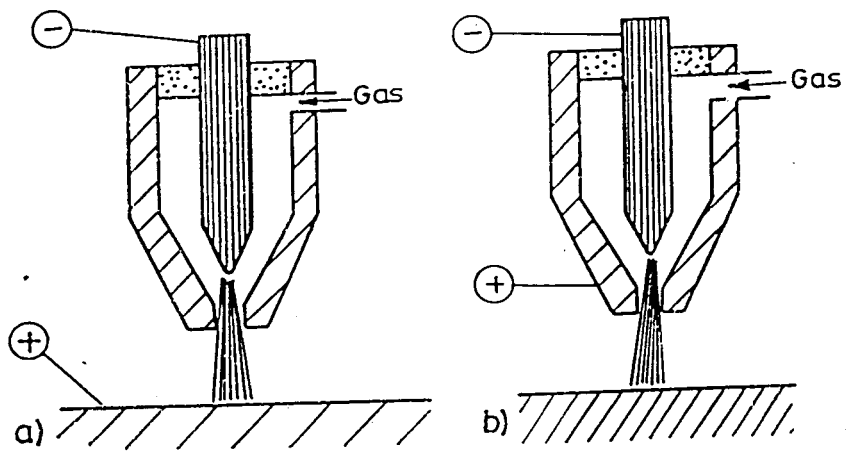

Fig. 2.9 - Schematic representation of
a) Transferred arc and
b) Non - Transferred arc plasma

2.5 PLASMA SPRAYING

Ceramics can be used as monolithic structure or as coating / deposition. Ceramics as coating / deposits have wider applications. Deposits of ceramics can be obtained by suitable spraying technique. Plasma spraying is a well-established process, for coating a metal with almost any material (metallic or ceramic) which can be melted without decomposition or excessive vaporisation on the plasma jet. The process has been developed from combustion flame spraying, the only essential difference being the higher gas temperatures and velocities obtainable in a plasma jet and the use of inert atmosphere.

Plasma can be generated by imparting sufficient energy to a gas to cause ionisation. Plasma guns operate through either transferred arc or non-transferred arc mode. In the transferred arc process, the work piece acts as an electrode, the arc carrying a large portion of heat to the surface. In the non-transferred arc, the plasma flame is confined between two water-cooled electrodes within the chamber. Fig. (2.9).

In a non-transferred arc plasma gun, electric arc is produced between a Tungsten cathode and a Copper anode in the form of a nozzle. The plasma gas (inert gases like Argon, Helium, Nitrogen etc) entering the nozzle is heated by the electric arc energy to a high temperature, causing dissociation of either mono-atomic gas or dissociation and partial ionisation of di-atomic gas as the case may be. The inert gas gets transferred into a plasma state, and a

large volume of thermal and kinetic energy is released in the form of plasma beam. (Fig. 2.10).

The temperature in the plasma arc centre even attains 30000°K and the outlet velocity of the plasma beam jetting from the nozzle is supersonic (about 1000ms^{-1}). The spray material, supplied to the plasma beam in the form of powder, is melted by high temperature, taken up by the beam and thrown on to the substrate at high velocity. The temperature of a plasma beam depends mainly on the ionisation degree, which is in turn influenced by the kind of plasma gas and the working parameters of the plasma gun. A typical temperature distribution in a plasma beam is shown in Fig. 2.11 *(Matejka, 1989).*

2.6 APPLICATION OF CERAMIC COATINGS

Plasma spray technology facilitates deposition of high quality coatings for wear applications. It has the outstanding advantage that it can be used to deposit functional layers onto economically priced substrates, thus opening a wide field of applications. The main area of use of the high-energy plasma is the spraying of high melting point materials, utilizing the high process temperature and energy density of the plasma process. Thermal spraying of ceramics has become an attractive and affordable solution for many industrial problems (wear resistance, electric insulation, thermal barrier etc) and, as a result, the technology has undergone

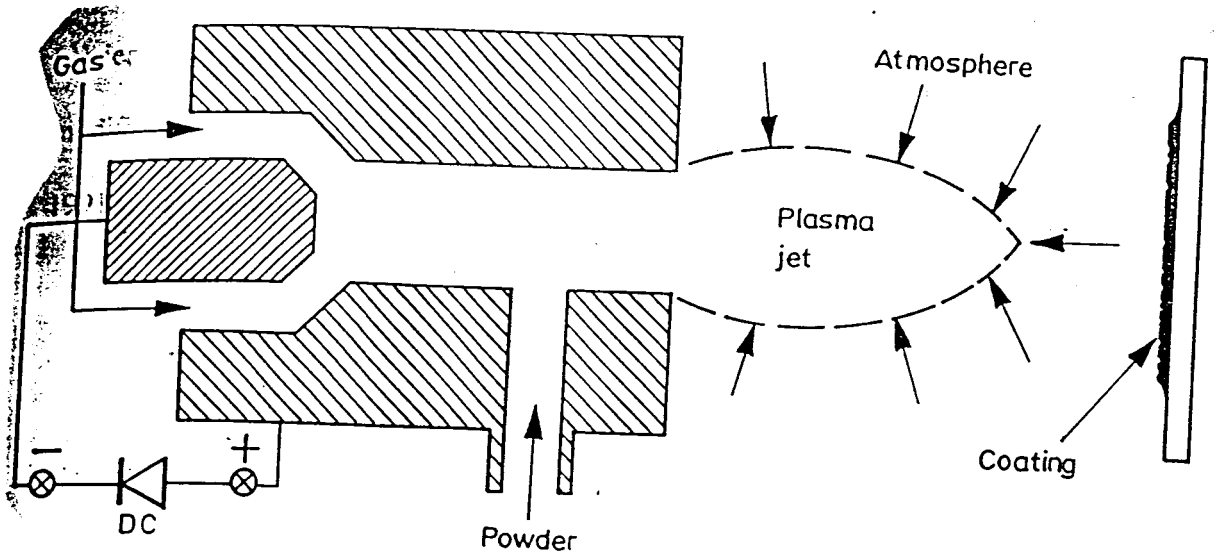

Fig. 2.10 - Schematic representation of a Plasma Gun

many changes and modifications concerning sprayed materials and the technique itself. *(Lech Pawlowski, 1991).*

Some of the very typical applications are coating of $A1_2O_3$, $A1_2O_3$-T_1O_2 in the textile industry, Cr_2O_3 for pumps, printing presses and reactor applications, WC-CO in aviation and turbine industries and MO coatings in automotive industry. (Erich Lugscheider, 1987).

Rhys-Jones (1990) has discussed the use of thermally sprayed coatings for compressor and turbine applications in aero engines. Coatings are applied to the surfaces of engine components, when protection is required against surface degradation process such as physical wear, fretting, oxidation, corrosion and erosion. In addition to their use as surface protection systems, coatings are also used for sealing (clearance control) application in the compressor and turbine.

The surface modification technique has also attracted much interest in the biomaterial field, where functional improvements in dental and orthopedic implant devices have been sought. *(Filiaggi et al, 1991).*

In IC engines, the combustion gases are highly corrosive, and may contain particles, which can cause severe wear. This has created demands for improved protection of engine parts. Plasma sprayed Zirconia coating is the principal heat and erosion resistant

material for many engine components. ZrO_2 and Cr_2O_3 coatings on IC engine parts have been found to increase the performance of the engine. *(Ingard Kvernes et at, 1992).*

Under unlubricated sliding, ceramics behave differently from metals. The wear resistance does not decrease and the coefficient of friction does not increase due to adhesion as in metals. This advantage of ceramics makes them more promising as components in vacuum and precision equipment, where working condition is unlubricated sliding and high wear resistance and precision are required. (Zhou *et al,* 1994).

With increased scope for applications of plasma sprayed ceramic coatings in critical areas, there is a necessity for undertaking the mechanism of coating formation and the influence of plasma spray parameters on the coating quality, so that, the desired functional specifications can be attained.

2.7 MECHANISM OF COATING FORMATION

McPherson (1981) has discussed about the mechanism of coating formation, during plasma spraying process. Spray coatings are formed by the build up of successive layers of liquid droplets, which flatten and solidly rapidly on impact to give the lenticular microstructure. Solid particles will tend to bounce off the substrate or previously solidified material. Therefore the essential requirement for efficient plasma spraying is to melt completely the

particles injected into the jet. For a given system, the only factors, which can control the coating microstructure, are the velocity, temperature and particle size distribution of the spray droplets at the plane of impact. The main beam requirement to melt the spray particles completely is that of supplying the heat of fusion so that there tends to be a concentration of particles at the melting point. Increasing the power input eventually produces a hump in the mean temperature, ensuring that most particles are completely melted.

When a liquid drop strikes a flat surface at low velocity, it flattens to a disc then retracts, passing through the equilibrium shape of spherical cap to form a cone and then spreading again to form the final equilibrium shape determined by static surface tensions forces. At high impact velocities, however, the radially flowing thin sheet of liquid becomes unstable and disintegrates at the edge into many small droplets. Studies on the particles adhere and that the degree of adhesion is influenced markedly by droplet size and velocity. There tends to be a critical velocity, for a given particle size, for which high retention is obtained; above and below this value the retention is much less. The real area of contact between the flattened droplet and substrate is probably much less than the apparent area due to the voids present at the interface. as the liquid droplet spreads to form a thin film, its cooling rate will rapidly increase by conduction into the substrate. The rate of heat extraction from an impinging droplet will rapidly increase as it flattens against the substrate, as the surface area available for heat

transfer increases. The liquid layer will cool to below its equilibrium melting point and solidification will commence and further spreading will be arrested.

An increase in temperature of the liquid droplet, produced by release of the heat of fusion during rapid crystal growth, would tend to suppress further nucleation because of the large temperature dependence of nucleation rate, and columnar crystal growth from the interface into the droplet can be expected. If however, the rate of heat loss by conduction through the substrate interface were greater than the rate of heat liberated by crystallization, the temperature would continue to decrease, the nucleation rate would increase and crystallization would be controlled by nucleation to give a fine equiaxed microstructure. The crystal growth rate is therefore an important factor in determining the microstructure produced in sprayed coatings, but the heat extraction rate is so great that the time interval for solidification will be extremely small whether it is controlled by growth or nucleation. In practice usually lamellar texture (extended equiaxed) is observed; which can be attributed to higher heat extraction rate.

2.8 COATING MICROSTRUCTURE

Many of the properties of plasma-sprayed coatings depend upon their microstructure; therefore, to properly understand coating properties and to develop new ones, the coating microstructure must be understood. The microstructure, which depends mostly

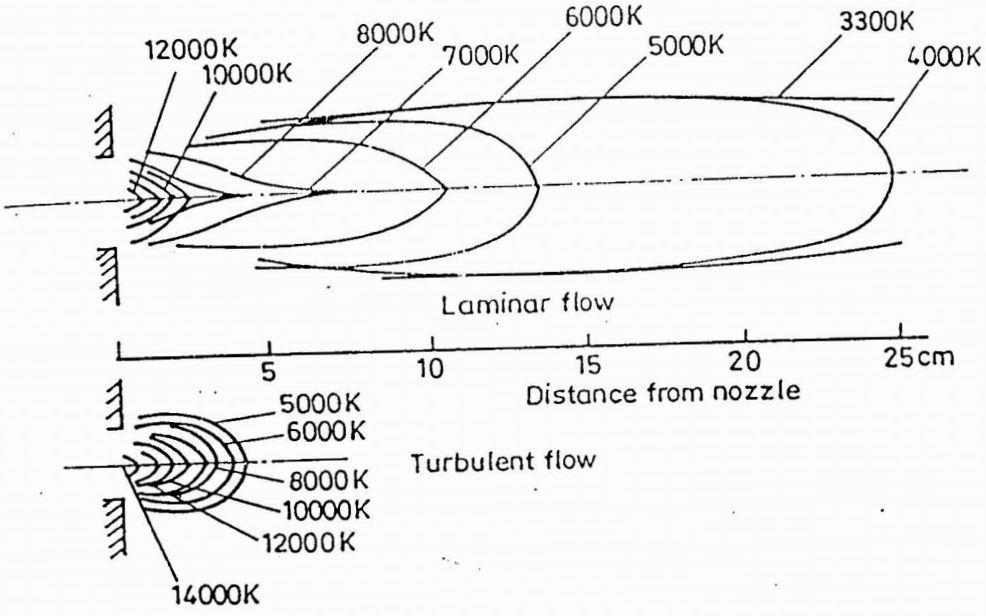

Fig. 2.11 - Typical temperature distribution in a plasma beam (Matejka, 1989)

upon the mechanism of coating formation, is the common factor linking properties to processing details. The microstructure of plasma-sprayed coatings is related to the mechanism of formation through two predominant factors: the nature of the interfaces between individual lamellae, and the internal structure within lamellae produced by their rapid solidification. Incomplete contact between lamellae during the process of coating formation results in the formation of extremely fine, narrow pores between lamellae. Fig. 2.12 is a schematic illustration of a typical cross section, where the individual lamellae of plasma-sprayed ceramic coatings has shown a network of fine cracks perpendicular to the lamellar plane which are formed by the stresses produced by restraint of the thermal contraction of the lamellae by the underlying material during cooling from the solidification temperature. These cracks will not form in metallic coating because the thermal strain may be accompanied by plastic flow. In addition to the cracking, porosity also generally degrades the mechanical properties of sprayed materials. Brittle fracture is extremely sensitive to defect size and the strength is determined by the largest crack-like defect present. Many other properties such as electrical and thermal conductivity and elastic modulus are reduced by the presence of pores, which reduce the effective cross-sectional area of material.

The influence of porosity on these properties depends on the pore size and morphology. However, finely distributed porosity tends to improve the thermal shock resistance of brittle materials

and studies of the failure of some ZrO_2 based thermal barrier coatings under thermal cycling conditions have shown that increased porosity does in fact increase the number of cycles to failure. This can be attributed to the possible toughening of zirconia ceramics due to stress induced transformation (the porous sites facilities accumulation of stressed zone and consequent phase transformation); however, the observation on the influence of porosity on fatigue can not hold good for other ceramics.

The elastic modulus of coatings is much lower than that of the bulk material. Heat treatment of the sprayed coating causes sintering of fine pores, which change shape to spherical, and the elastic modulus tend to increase towards that of the bulk polycrystalline material. The thermal conductivity of plasma – sprayed coatings is also much lower than that of the bulk material. Conduction occurs only across the true region of contact between lamellae so that the low conductivity can simply be related to the relatively small true contact region in plasma-sprayed coatings. Inter lamellar contact may be expected to improve in coatings sprayed in a low-pressure chamber, with consequent rise in conductivity (McPherson 1989).

2.9 STRENGTH ENHANCEMENT OF SPRAYED COATINGS

The coating properties may be modified by altering its microstructure. The coating strength property may be improved by mixing metal and ceramic powders (cermets) prior to spraying.

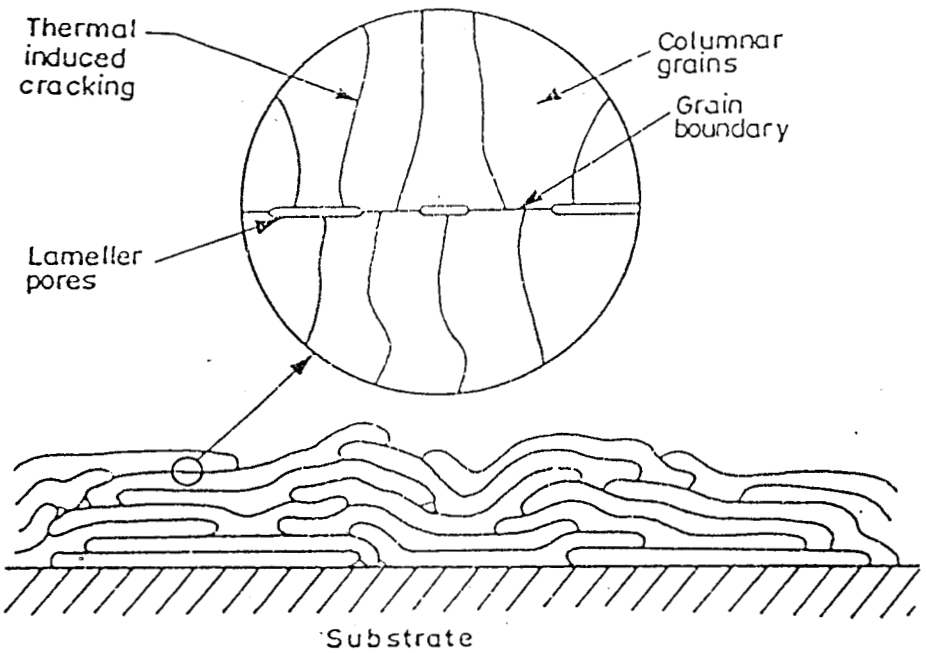

Fig. 2.12 - Schematic representation of coating structure (McPherson, 1989)

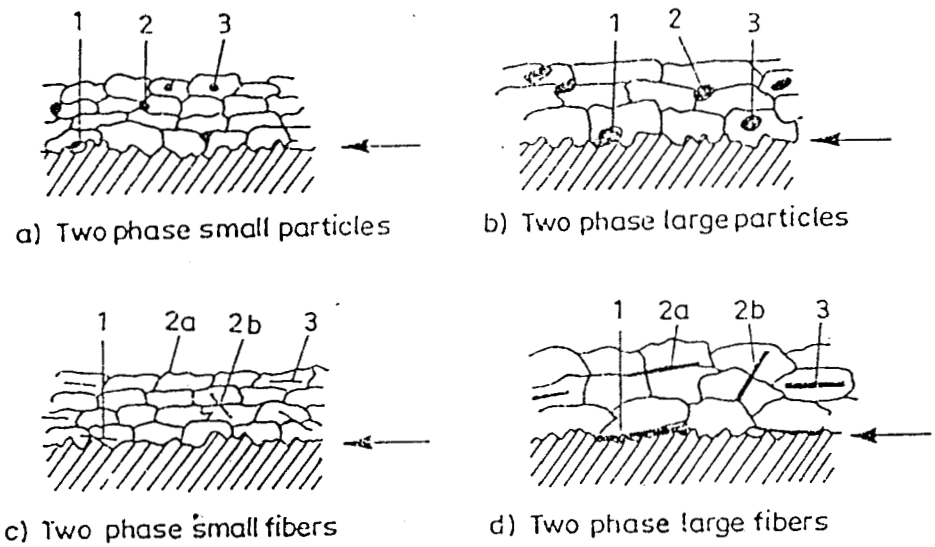

Fig. 2.13 - Schematic representation of composite thermal sprayed coatings (Berndt, 1987)

The metallic species confers some ductility to the coating system and thereby impedes crack growth. Such a coating may have excellent wear resistant characteristics. However, cermet coatings generally do not posses high temperature resistance, since isolated metallic particles will lead to an increased oxidation rate. Addition of second phase ceramic particles / fibres to the basic coating structure may improve the cohesive strength/toughness of the coatings. Schematic of composite structure is shown in Fig. 2.13. Second phase ceramic material can increase the strength of the coatings only if it establishes some mechanical or chemical bonding with the matrix phase.

Berndt *et al,* (1987) have investigated the production and microscopic investigation of fibre reinforced thermally sprayed composite coatings. These fundamental studies have shown that the fiber morphology can be retained in the coating structure. The enhanced continuum of the matrix can account for increase in thermal conductivity.

The microstructure and important properties of different sprayed coatings have been studied by Ke-Shun Shi *et al,* (1988). Bending strength and stress-strain relationship has been studied by four-point bending method. The stress-strain relation of the coatings has been found to exhibit non-linear behaviour, determined by laminar structure of the coatings. (The weakest links between laminae). The bending strength of the coating was found to decrease with an increase in the grain size. Thermal shock

resistance of a coating can be enhanced by increasing the fracture strain of the coating, considering the important effect of grain size on the fracture strain.

Ekkehard (1994), has observed 11-20% porosity in plasma sprayed ceramics with relatively low values of Young's modulus and strength. Most of the pores found were crack like grain boundary gaps. Because of their characteristic laminar grain structure, plasma sprayed ceramics were not as brittle as porous sintered ceramics. The thermal expansion and densification behaviour, on, heat treatment of plasma sprayed ceramics has been studied. It has been observed that the grains of the loose, as sprayed structure sinter together as a result of heat treatment. It has also been observed that wider the grain size distribution of the as sprayed coating, higher will be the increase in density after heat treatment. Young's modulus and strength have been found to increase with heat treatment.

Thermally sprayed coatings though proved to exhibit excellent wear resistant properties, do not fully meet the requirements for corrosion proof coatings because of surface porosity. As a result, the corrosion resistance of the coating itself, and its ability to protect the substrate, is insufficiently developed in many cases. Sealants are frequently applied to close the pores in thermally sprayed coatings in order to improve corrosion resistance. During spraying, air or gas inclusions form, which are associated with turbulence and the sublimation of individual material component;

this may lead to a submicroscopic system of cracks in addition to the microscopic porosity (Lugscheider, 1994). Of late, defects are being eliminated by laser glazing process.

2.10 RESIDUAL STRESSES IN COATINGS

In addition to formation of lamellar structure, with associated porosity/micro-cracks, the spray coating can also posses residual stress, induced during spraying. A large temperature gradient exists across the interface between flattened droplet and substrate (or previously solidified material) so that, after each particle has solidified, its thermal contraction is restrained by the underlying solid and microstress distribution will be established within the particle. In brittle materials this results in the formation of a network of fine microcracks. The stresses would be relaxed by plastic deformation in metallic coatings so that the final residual stress would be comparable with the ambient temperature yield stress. In addition to these microstresses a pattern of macrostresses may be developed because of the mismatch of thermal expansion between coating and substrate. (McPherson, 1981).

Internal stress is an important parameter in coating technology since it also often relates to the maximum coating thickness which can be deposited without spallation. The mechanisms by which residual stress is built up or locked into a coating depend markedly on the deposition process. The powder particles injected into the

plasma jet are melted and subsequently impinged on the substrate surface where incident particle cooling rates are very high. (Approximately 10^5 – 10^6 KS^{-1}). Moreover, as cooling takes place, continuously further particles arrive at the substrate. The build up of particles produces growth of coating at a high velocity. During deposition, it is assumed that the heat is transferred to the substrate from the coating and also redistributed radiatively and / or convectively to the surrounding atmosphere. The net rate of heat extraction will decide the status of the deposit, including the built-in stress levels. Changes in stress distribution as a result of changes in deposition rate for plasma-sprayed ceramic (Zirconia) and metallic (tungsten) coatings have been analysed by stress modelling. (Rickerby *et al,* 1987). According to the predictions of the model, for plasma-sprayed Zirconia, with increasing deposition rate, there is a change in the stress state from compressive to tensile due to a rise in the effective deposition temperature, while for tungsten coatings, owing to a high thermal conductivity, residual stresses are virtually independent of deposition rate; also of great importance is the variation in residual stress with coating thickness since it is often observed that coatings fail at some critical thickness.

The model has shown that for a Zirconia coating, the stress distribution swings from being totally compressive for thin deposits to showing a maximum in compressive stress close to the substrate with large tensile stresses in the outer regions of thicker coatings. In contrast, for plasma-sprayed tungsten, the residual stress

distribution remained compressive everywhere and increased with coating thickness since a high thermal conductivity coating ensures that each incremental layer of coating is effectively being deposited on an increasingly hot substrate.

The experimental study has indicated a low compressive stress at the outer surface, which increased towards coating-substrate interface, The existence of stress maximum close to or at the coating-substrate interface may explain the spallation of coatings when they reach a certain thickness, since the fracture strength of the coating may be exceeded locally in these regions of high stress. The presence of pores and included oxide, although they may be second-order effects, will obviously affect the thermal conductivity of a plasma sprayed deposit, and thereby influence the distribution of residual stress in the coating.

It is seen that the mechanism by which the residual stress is build up or locked into a coating depends markedly on the deposition process and on subsequent cooling. Two processes can produce stress during the subsequent cooling phase: one is the temperature gradient within the substrate and the other is the difference in thermal expansion coefficients of the coating and the substrate. If the heat flux onto the sample during spraying is high and the thermal diffusivity of the coating is low, a high temperature gradient develops within the coating. As a consequence, a high temperature gradient develops within the coating. as a consequence, a high tensile stress may develop at the coating

surface after cooling, which may induce surface cracking. Even if the temperature gradient is low, a difference in thermal expansion coefficients can produce a significant stress after cooling. The actual failure in a coating system is generally within the ceramic layer, near the metal-ceramic interface. (Ferrari *et al,* 1997).

Residual stresses can influence markedly the substrate-coating adhesion. Microcracks or incipient cracks propagate along the interface under the action of the residual stresses and can lead to complete debonding. The value of the rate of strain energy release can be taken as a parameter regarding the debonding of the coating. It can be calculated from the stress distribution during spraying and the time taken for debonding can be evaluated. (Sobolev *et al,* 1991).

2.11 EFFECT OF TEMPERATURE DISTRIBUTION

The temperatures in a coating during plasma spraying have a marked effect on the physical properties of the coating, such as the residual stresses and the crystalline structure. these parameters are particularly important for sprayed ceramic coatings, which crack easily as a result of stress. Knowledge about the temperature distribution in coating and the substrate is essential for the analysis of residual stresses and metallurgical interactions in the coating system. This will also help in qualitative appraisal of coating properties in relation to spraying parameters. Precise parametric

studies on stress behaviour in coating composites are required for individual applications.

Evaluation of temperature distribution in plasma-sprayed coating has been attempted by Lech Pawlowski et at (1982) by taking into account both the physical properties of sprayed material and the effect of thermal resistance between the coating and the substrate. The theory was used to determine the temperature distribution in alumina coatings plasma sprayed onto copper or mild steel substrates. A comparison between the theoretical predictions and experimentally determined surface coating temperatures has been made. The experiments were carried out using IR thermography. The influence of, the spraying distance, the substrate material and cooling of the sprayed samples, on the coating surface temperature has been investigated. The predicted temperatures were found to be within 20% of experimental values. In thermal spraying processes, extreme increase in substrate temperature may occur during application of the coatings. Because of steep temperature gradient between the coating and the substrate, there can be numerous fluctuations in the thermal history of the coating also.

Knotek *et al*, (1988) have made quantitative evaluations of temperature distribution in coating and substrate, during spraying process, as well as during the cooling period. The influence of the properties of composite materials and significant spraying parameters has been taken into account. The observation of the results indicated that over a short duration, the maximum

temperatures occur at the current spraying surface; however the most extreme fluctuations in temperature take place in the lowest layers of the coating, their levels and frequency being dependent on the substrate and the coating thickness. This thermal behaviour of the coating system explains the reason for the tendency of the coating of ceramic composites to fracture primarily over the lowest coating layers when subjected to tensile stress.

Influence of substrate temperature on adhesion/cohesion of plasma sprayed alumina ceramics has been studied by Mellail *et al*, (1996). The adhesion/cohesion was found to be best for substrate temperature between 300 and 500°C for substrates, whose expansion coefficients were as close to that of alumina. When the expansion mismatch is too high, the compressive residual stress generated upon cooling does not allow the coating to adhere to the substrate.

Residual stress evaluation of plasma sprayed NiCrAlY coatings, has been carriedout by Richard *et al*, (1996). The test results show higher order residual stresses in the as sprayed (APS) coatings. Also, the stress level is high at the substrate-interface compared to the surface. The stress value has been found to reduce after heat treatment of the coating system. In VPS (vacuum plasma spray) system, the residual stresses are found to be low, both before and after the heat treatment. Adhesive strength of the coatings not only reduces the stresses, but also increases the adhesive strength. It can be

summed up that the performance of the coating, especially its retentivity is largely dependent on the residual stress/stresses pattern induced during spraying.

2.12 PHASE TRANSFORMATION DURING PLASMA SPRAYING

During spraying, the deposition can undergo phase transformation, compared to the starting material, depending on the spray parameters and the material composition. Experiments conducted by McPherson, (1981) with thermally sprayed Al_2O_3 deposits showed that the metastable γ-Al_2O_3 structure was produced rather than α-Al_2O_3, which was supplied as spray powder. This can be explained on the basis of nucleation kinetics: γ -Al_2O_3 is more easily nucleated from the melt than α-Al_2O_3 because of lower interfacial energy between crystal and liquid and, at sufficiently rapid cooling rates, the metastable form is retained at room temperature. Al_2O_3 coating generally contain some α-Al_2O_3, and this can be explained by the fact that all the particles fed are not melted completely and partially melted particles incorporated into the coating have an α-Al_2O_3 structure.

2.13 SPRAY PARAMETERS – A REVIEW

The properties of thermally sprayed coatings are influenced by multiple parameters which can be subdivided into process control variables (flame temperature, gas pressure, powder flow rate, geometry of the nozzle, working distance etc.), surface treatment of

the substrate (mechanical, chemical etc.), and powder properties (chemical composition, melting point, solidification range, heat capacity, morphology, distribution of partcle size etc.).

2.13.1 Effect of powder size

Within the scope of quality control of sprayed coatings, one important test is the determination of the size distribution of the powder particles. It is well known that different particle size affect the processing of the powder as well as the properties of the coating. size distribution in combination with shape and surface condition of the particles will determine the flow behaviour of the powder to the spray gun. During plasma spraying, small particles will evaporate, reducing the deposition efficiency. Microstructural defects in combination with residual stress in the coating can cause cracking or spalling. In thermal spraying, if the particles are larger than critical size, they do not melt completely during their flight to the substrate. these unmelted powder particles do not facilitate a flawless coating. Therefore most thermally spray methods require powder with a well-defined range of particle sizes. (Poech *et al*, 1993)

2.13.2 Spray parameters on interface status

Plasma-sprayed coatings consist of a highly an isotropic layered structure with individual splats oriented parallel to the substrate

surface. The adhesion of coating to substrate has been explained by three mechanisms (Mellali *et al,* 1996).

Chemical Adhesion : This implies both (possible) chemical reaction and the melting of the substrate by the impinging particle. However, once the first layer is sprayed, the adhesion between the splats (coating cohesion) is no longer governed by the same mechanism.

Diffusion : This mechanism is promoted if the substrate is kept at high temperature during spraying, as is the case of alloys or metals sprayed vacuum conditions on a metallic substrate.

Mechanical Anchorage : Studies have shown, that this is the only possible method of adhesion for ceramic materials.

Different spraying parameters influencing the adhesion and cohesion property of oxide coatings on metallic substrate have been identified. Orientation between the torch axis and the substrate has been found to be important, the best adhesive/cohesive values being obtained for 90° orientation. for cold substrate, adhesion/cohesion properties were found to increase with surface roughness upto a certain limit, related to particle size.

When preheating the surface upto a certain limit (which depends on the residual stresses generated upon cooling due to expansion

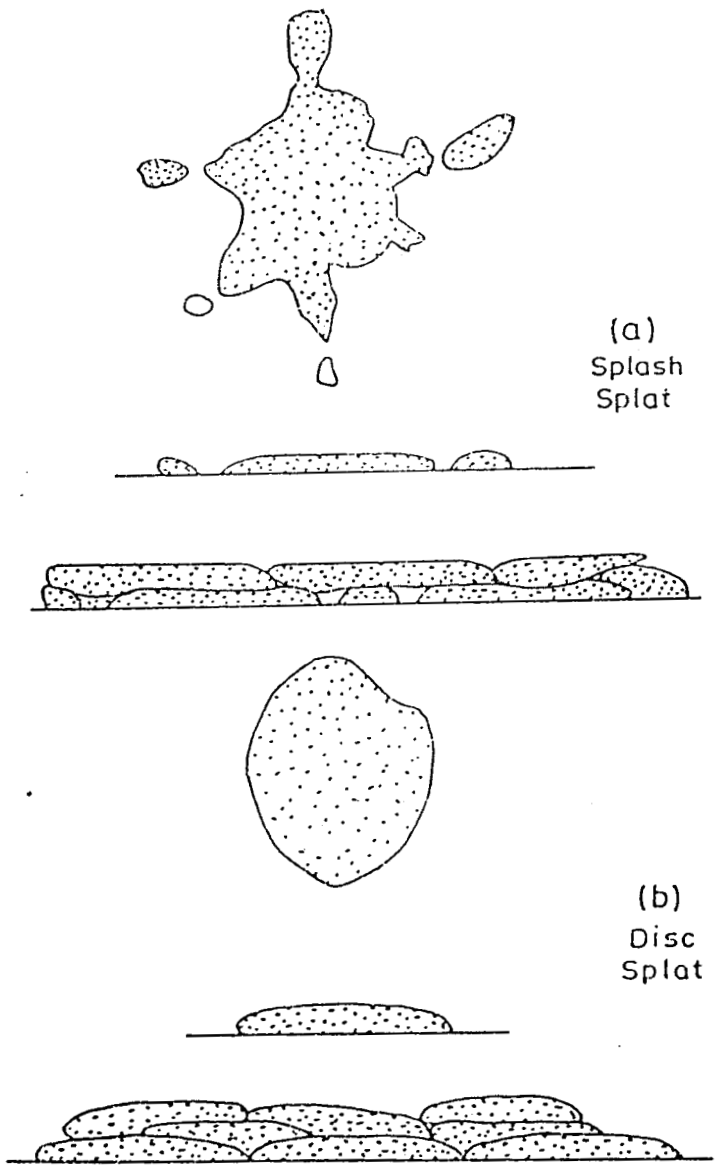

Fig. 2.14 - Schematic representation of Disc and Splash splats (Griffiths, 1997)

coefficient mismatch between substrate and coating), the adhesion/cohesion properties was found to increase with preheating temperature for a given surface roughness. Adhesion/cohesion property has been found to decrease with increase in particle size for same spraying conditions. The adhesion decreases if the preheated surfaces are oxidized.

An experimental investigation has been made on the process of atmospheric plasma spraying of high performance ceramics such as Alumina, Titania and partially stabilized zirconia, on steel substrates. coating properties like bond strength and porosity have been evaluated by varying the spray process parameters like stand-off distances, power and coating thickness. bond strength of the coating was found to decrease with increase in the thickness of coating and was found to increase with power input. Porosity of the coating was found to reduce with increase in power input. (Gowri, 1997).

2.13.3 Effect of substrate topography

Adhesion of the thermal plasma sprayed coating and subsequent performance is critically depended upon the surface conditions of the metal substrate and in particular the surface finish, texture and topography. The normal substrate preparation procedure is to chemically degrease the surface and then grit blast it, followed by cleaning in air stream to remove loose material if any. Two types of impacted particles have been identified; these

being disc and splash types of splats Fig. (2.14). The effect of surface topography on the splat shape, form and flow were studied by conducting tests on polished surfaces, ground surface and grit blasted surfaces. The ground and polished topographies were much less complex than that produced by grit blasting. The surface topography of the grit-blasted surface has a significant effect on the build up of the initial coating. The initial layers build up preferentially in the valleys. Although the coating adhesion increases with increasing roughness, there is an optimal valley spacing for maximum adhesion. (Griffiths *et al,* 1997).

The adhesive strength of ceramic coatings deposited by plasma-spraying may be generated by various factors such as mechanical interlocking, adhesion and adsorption, chemical reaction, diffusion, electrostatic force, etc. Considering a rapid solidification process with a cooling rate of about 10^6 KS^{-1} for ceramic coatings, the most effective factor may be the mechanical interlocking force. It is well known that the adhesive strength of coating depends on the surface roughness of their substrate. However roughness is a physical quantity representing the level of humps or indentations on substrate surfaces. It neglects hook shaped indentations, which are part of their topography, and which can generate a mechanical interlocking force. From the experimental results, it was observed that the adhesive strength increased with average roughness initially, but found to reduce, beyond a certain critical roughness value. The critical average surface roughness was found to change with the type of spray particles, spraying conditions,

blasting conditions, substrate materials, the spraying method, etc. Thus average surface roughness is not a proper measure to relate to the adhesive strength. Experimental observation have shown an increasing relations between adhesive strength and a blasted surface with a larger number of anchor-shaped surfaces. (Shigeyasu Amada *et al,* 1996). The disc type of particles were found to be associated with high adhesion and a high-integrity interface, whereas the splash type particles were associated with poor adhesion and a low integrity interface.

2.13.4 Effect of interlayer for bond strength improvement

Double cantilever beam approach has been used successfully to measure the strain energy release rate Gc for cohesive failure and the strain energy release rate Ga for adhesive failure of Al_2O_3 – TiO2 coatings on grit blasted steel and also for Al_2O_3-TiO_2 with Ni-Al bond coat on mild steel. (McPherson, 1981).

It has been observed that for $A1_2O_3$ – TiO_2 coatings range of values of Ga was less than Gc; whereas with Ni-a1 coatings, Ga was found to be greater than Gc, An interesting feature of the cohesive fracture of all coatings was that it appeared very similar with the occurrence of failure between the lamellae. The only significant difference was evidence of plastic deformation in the metallic coatings and fracture within lamellae in

the case of ceramics. This difference is vital and would explain the higher values of Gc for metals by the energy dissipated in plastic deformation of lamellae as the crack propagated between them.

The role of Ni-Al bond coat in improving the adhesion of ceramic coatings can also be explained in a similar manner. The failure in the vicinity of the bond coat interface results in dissipation of energy by deformation of the metallic lamellae as the crack passes between lamellae in both layers, an effect which cannot occur for a ceramic sprayed directly onto a solid metallic substrate. Thus Ga for failure between the bond coat and ceramics is considerably higher than Ga for ceramic directly sprayed onto steel.

The Ni-Al coating provides interesting results because Ga on steel is so much higher than Gc. The excellent bonding characteristics of sprayed composite Ni-Al has been explained by the formation of a metallurgical bond between the substrate and coating, in addition to the mechanical keying to the substrate. The fact that Ga is very high compared with Gc, however suggest that such a bond does not occur between lamellae. for Ni-A1 coatings the fact that Gc is very low compared with that expected for the bulk material is consistent with poor contact between lamellae owing to the formation of oxide and entrapped gas. However, the very high Ga for Ni-A1 on steel suggests that good contact has been achieved between steel and the impinging droplets, an effect which may be due to chemical interaction between the molten

droplet and oxide film on the steel surface and also mechanical anchorage.

2.13.5 Effect of spraying environment

Plasma spraying can be carried out either in open atmosphere (APS) or in vacuum (VPS) conditions. For non-oxide materials, VPS coatings give better performance than APS coatings, as observed by Kingswell *et al,* (1991). Erosive wear behaviour of tungsten coatings (both APS & VPS) has been investigated in terms of coating properties and microstructure. It has been observed that in case of APS tungsten, erosion occurs predominantly by fracture at the weak intersplat boundaries, which are formed by the inclusion of oxide during spraying. In case of VPS coatings, there is an increase in cohesive strength and material loss occurred mainly by micro chipping and ploughing deformation. Thus APS coatings have been observed to be having higher erosion rate than the VPS coatings.

2.14 BOND STRENGTH EVALUATION FOR COATING SYSTEMS

Adhesion between coating and substrate as well as cohesion within the coating are frequently the limiting factors of thermal sprayed coatings. Therefore test methods for general, quality control purpose and for optimisation of the coating properties are of great importance.

Conventional bond strength tests of thermally sprayed coatings yield only overall strength values. It is not possible to differentiate between adhesion at the interface, which is influenced by bond contamination and surface roughness, and the cohesive strength, which is related to the intrinsic properties of the coating and influenced by defects or internal stresses occurring in the coating microstructure. Failure occurs mostly within the coating, i.e. , the coating layer with its defects is the weakest part of the spray deposits.

Various methods of evaluating the adhesion strength of thin coatings, like indentation, scratch, hammering, coining and metal stamping have been evaluated by Arai *et al*, (1987). Indentation and scratch tests have been found to be useful to determine the critical load of the coating, when the adhesion strength is extremely low.

Of all the methods reviewed, indentation and scratch adhesion methods have been found to be best suited for relating practical levels of adhesion to the performance of real engineering components in service (Rickerby 1988).

Different methods for evaluating the coating substrate adhesion of thin coatings have been reviewed by Chalker *et al*, (1991). Tests like pull off test, indentation test and scratch test have been analysed, for their ability to assess the critical load for failure of

adhesion between coating and the substrate. The authors stress the need for the development of a reliable, non-destructive technique like scanning electron acoustic microscopy for evaluating the coating-substrate adhesion.

In order to obtain information about the influence of preparation of substrate surface on the adhesion of a coating, tensile bond strength test and modified crack-opening displacement test have been conducted, using specimen, after deliberate crack initiation at the interface (Schweitzer *et al,* 1991). Crack initiation was achieved by weakening of the interface at the outer diameter in the case of bond strength specimen or at the notch root in the case of crack opening displacement specimens. This made it possible to look at the influence of surface roughness and grit contamination on the coating adhesion separately.

The method most commonly used to characterize the bond strength of thermal-sprayed coating is the pull-off (tensile) test. One major disadvantage of pull-off tests is the necessity to adhesively bond the counter bar to the coating, which means that the test load is limited by the strength of the adhesive. A new test method (shear test) has been developed, which allows the determination of the shear stress necessary to cause adhesive or cohesive failure of plasma-sprayed coatings. The shear stress measurement from the test has been found to be very sensitive to change of spraying parameters and the quality of substrate surface preparation and has been found to be well suited to describe the

quality of the substrate/coating system for metallic as well as ceramic coatings. (Heinrich Grutzner *et al,* 1991).

The success of the plasma sprayed ceramic coating relies on adequate bonding between the ceramic coating and metal substrate. Interface fracture toughness of plasma sprayed alumina ceramic on metal substrate has been studied using modified double cantilever beam (DCB) tests. Dependence of fracture toughness on initial crack length has been studied. Conventional tensile adhesive bond strength testing has also been conducted. Effect of the variation in plasma – spraying parameters have shown significant changes in the mechanical integrity of metal/ceramic interface (Filiaggi *et al,* 1991).

Plasma-sprayed ceramic coatings are utilised particularly of their refractory properties and wear resistance, but their use is limited by relatively poor adhesion to the substrate. Zirconia coatings partially or fully stabilised with Y_2O_3 or CeO_2, containing varying proportions of transformable tetragonal phase have been tested using double cantilever beam technique to determine the toughness. Coatings containing tetragonal phase zirconia have been found to be having significantly higher fracture toughness than fully stabilised (cubic) coatings. Cohesive fracture toughness has been found to be greater than adhesion toughness (a phenomena attributed to stress induced toughening of ZrO_2). Transformation toughening effect has been found to be operative in coating containing transformable tetragonal phase. Tetragonal

ZrO_2, if formed will transform to monoclinic on cooling if the transformation temperature is above room temperature, but will persist as non-transformable tetragonal if the transformation temperature is below room temperature. (Heintze *et al,* 1988).

One property of hard coatings that limits their use is the tendency to crack under load. Four-point bend tests have been conducted on sprayed WC-CO coating system. The test involves placing a coated beam in pure bending with the coating in tension and detecting cracks using acoustic emission (AE). The strain in the coating monitored and the results are presented as strain to fracture (STF) (Linda C. Cox 1988). Analysis of the test results has shown that the four-point bend test is an excellent method for investigating the mechanical properties of a coating. The bending strength of the coating system, evaluated during the test will be influenced by the coating-substrate interactions, stress distribution at the interface and the residual stress left over from the coating process.

2.15 DEFECT CHARECTERIZATION

The defects that lead to fracture in structural ceramics can be classified as either extrinsic or intrinsic . Intrinsic defects are induced during the manufacturing process and are generally volumetric voids or inclusions. Extrinsic defects are generally surface breaking cracks that form during matching, impact damage or thermal cycling. (Khuri-Yakub, 1982).

Any non-destructive testing technique, which is able to characterize the coating itself and its adhesion to substrate, will be highly useful for defect identification. Such techniques would also be useful to follow the in-service damage of the coating, under cyclic loading. Ultrasonic waves are most suitable for testing the interfaces of a plasma assisted coated system. Ultrasonic waves are reflected at an interface between two solids with different acoustic impedance. Any variation from a perfect adhesion between two surfaces, due to the presence of a flaw at the interface, induces a change in the amplitude of the reflected wave, which in turn, can be used to reveal this flaw. (Lescribaa *et al,* 1996).

Summary

The literature survey illustrated above presents the mechanism of deposit formation, strength-property relationship, distinction between adhesion and cohesion strength and also different techniques being adopted for evaluation of adhesion/cohesion strengths and also for defect identification. The importance of residual stress at the interface and the consequent need for surface preparation has also been highlighted.

2.16 WEAR BEHAVIOUR OF CERAMICS/CERAMIC COATINGS

In this section, an account of the literature survey concerning wear of ceramics/coatings and associated mechanism is presented

Mechanical failures attributable to wear are probably the most common cause of direct or indirect engineering component failure, since most of the failures are surface originated. Surface engineering, properly practiced, offers the choice and flexibility, in terms of design and materials selection, to effect optimised remedial action specific to the problem in question. Ceramics/coatings are used for combating abrasion/erosion/corrosion environments. Abrasion is the dominating mode among them.

2.16.1 *Mechanism of abrasive wear*

Abrasive wear is the removal of material caused by hard particles or asperities penetrating a softer surface during sliding contact. The hard particles may be contamination from the surroundings or may be produced within the tribosystem itself during the wear process. e.g. work hardened wear debris, fragments of oxide layer or second-phase particles already present in one or both the surfaces. Abrasion, in many cases, is a wear mechanism, which, one uses even deliberately, as in machining process such as grinding, lapping and polishing.

2.16.2 *Deformation modes during abrasion of ceramics/ceramic coatings*

The observations form the detailed scanning electron microscopic study of the surfaces of polycrystalline alumina

abraded under various environments have been presented by Swain, (1975). It has been observed that ploughing accounts for only a small fraction of the volume of material removed by abrasive wear. In case of polycrystalline alumina, dislocation and twins are generated during abrasion and grinding. It is possible that these dislocations and twins can propagate through the grain and pile up at the subsurface grain boundaries. A crack will nucleate by this mechanism at the grain boundary, provided stress relief by slip in adjacent grains does not occur. Stress relief is unlikely to occur because of the absence of any elastically stronger material to generate slip in the adjacent grain and the inherent weakness of the grain boundary. On continued abrasion, more cracks will be generated at the grain boundaries and eventually coalescence of these cracks will form a continuous intergranular crack somewhat paralleling the surface. Simultaneously, the ploughing of the surface by the abrasive particles is likely to produce a plastically welded surface layer. This welding of the near surface region tends to hold together the deformed surface layer and suggest why layers rather than individual grains are the wear product. The basic mechanism proposed to account for the above referred delamination type of wear in alumina is further supported by observations of the wear debris indicating that both chipping and delamination mechanism occur during the abrasive wear of polycrystalline alumina.

Donald *et al,* (1984) have conducted wear studies on ceramic materials to understand their physical and chemical properties

which will affect their behaviour when in contact with themselves or with other ceramics or metals.

In general, metals readily deform plastically whereas ceramics, while having high strengths are normally brittle and fracture with little or no evidence of plastic flow. At the interface between two ceramic in solid state contact under load and relative motion, plastic flow has been observed in the surface layers of some ceramics. When a silicon carbide surface is placed in contact with a diamond under relatively low contact pressure, elastic deformation can occur in both the silicon carbide and the diamond. Sliding occurs at the interface. No groove formation due to plastic flow and no cracking of silicon carbide with sliding were observed. With an increase in the applied load, plastic deformation occurred in silicon carbide, causing permanent grooves during sliding with very small cracks being generated in the silicon carbide. The frictional energy dissipated during sliding was due to shearing at the interface and plastic deformation of the silicon carbide i.e., ploughing of silicon carbide by the diamond. When a much higher contact pressure due to high concentrated stress in the contact area is provided, the sliding action produced gross surface and subsurface cracking following plastic deformation. Under such condition debris particles and large fracture pits due to cleavage are observed. The coefficient of friction is strongly influenced by the bulk properties of the silicon carbide such as crystallographic orientation and the presence of the grain boundaries.

The presence of surface and subsurface defects such as dislocation vacancies, voids impurities and micro cracks in the surface of the materials in the contact will generally dictate the zones from which wear damage and wear particles are generated. The extent and distribution of such defects will, to large extent, determine the size of the wear damage and wear particles generated.

Ayayi et al, (1988) have observed different mechanisms of wear in ceramic materials subjected to tribo-contact. These are plastic deformation, tribochemical mechanism and brittle fracture. Although ceramics are considered to be brittle, plastic deformation has been observed during surface contacts. Plasticity in otherwise brittle materials occurs through the inhibition of fracture by hydrostatic pressure associated with concentrated contact of surfaces. Thus plastic flow is seen in some cutting processes, some fatigue processes and in mild wear processes. Tribochemical mechanism involves interfacial chemical reactions at the sliding interface, followed by removal of material by sliding contact. An example is the oxidation of Si_3N_4 in water to form SiO_2, which is easily removed.

Studies relating wear to fracture properties infer wear rates from the types of damage that is seen in static indentation studies. Two types of cracks have been observed. Those that are normal to the surface and extend in a radial direction from the small region in the

material. These cracks are instrumental in removal of material during brittle fracture.

Wear mechanism of ceramics have been discussed by Kato, (1990) from the viewpoints of mechanical wear and tribo-chemical wear. Because of brittleness of ceramics, various types of cracks are induced by friction around the contact zone, such as hertzian, lateral, median and radial cracks. Depending on the value of contact pressure at the contact point, the predominant wear particles are formed by propagation of some of these cracks.

The phase and structural composition of the surface material under the interaction of mechanical, chemical and heat components of tribosystem is an objective indicator of the tribotechnical qualities of the surface layer. The contact interaction of the surface with abrasives is by way of an intensive and heterogeneous plastic deformation of the former. This deformation is followed by structural transformations in the subsurface layer such as growth of dislocation density, structural grain fragmentation and subsurface texture formation. Depending on the degree of deformation, one or more of the above can occur. (Sorokin *et al,* 1991).

Vijande – Diaz, *et al*, (1991) have studied the wear resistance of plasma sprayed $A1_2O_3$ and Cr_2O_3 under dry friction, abrasion and lubrication conditions, at different loads and speeds. It has been

observed that wear mechanism takes place according to the following stages.

1. An initial stage, consisting of the appearance of flat zones resulting from plastic deformation of the ceramic particles owing to the specific contact pressures at the actual contact zones and to the associated temperatures in that area.
2. A crack nucleation and propagation stage in the previously deformed area probably caused by accumulation of deformation/material fatigue.
3. A third stage of fracture and individualized loosening of particles.

Ahmed *et al,* (1991) have studied the wear resistance of plasma sprayed WC – Co and Ni-A1 coatings. Preliminary investigations on the coatings have shown that there is a reduction in porosity level in the coating, with the increase in the coating thickness and wear studies have shown that the wear resistance increases with decrease in porosity level of the coating, i.e. Increased coating thickness has led to an increase in wear resistance. Also, it has been observed that in case of Ni-Al coatings, there is an increase in wear resistance, with heat treatment of the coatings.

In the case of abrasive wear of ceramics, the severest mode is characterised by the formation of lateral cracks. Such a severe mode may occur only when sharp and hard abrasives slide on ceramics with sufficient penetration depth. The wear modes of

ceramics have been studied in situ, by observing the sliding of hemispherical diamond against different ceramic discs in a scanning electron microscope. (Hokkirigawa, 1991). On the basis of in situ observations of wear processes, the mechanical wear mechanisms of ceramics are classifieds into three microscopic wear models; ploughing, powder formation and flake formation.

The occurrence of wear transition in alumina during sliding has been investigated experimentally, using a four ball wear tester by Seong-Jai *et at*, (1992). Examination of alumina wear surfaces after various periods of wear confirmed that the observed changes in friction and wear rate behaviour is related to a fundamental change in the process of wear. During initial stages of wear, the wear surface is primarily characterised by the presence of fine scratches or furrows in the direction of sliding. Prolonged sliding ultimately resulted in rough, irregular wear surfaces, which could be related to the occurrence of fracture. Consequent increased friction and the onset of appreciable material removal coincides with intergranular fracture. The fracture process initially occurs within patches of grains and then proceeds rapidly over the entire contact area appreciable wear occurs after prolonged sliding, primarily by continued intergranular fracture and grain pullout. The manner in which grain boundary cracking occurs after a period of mild wear suggests a damage accumulation model, in which internal stresses associated with damage accumulated during the initial stage leads to crack initiation and propagation. TEM

examinations of worn surfaces revealed high densities of dislocations and deformation twins.

The occurrence of grain boundary cracking only after a prescribed period of initial stage wear can be related to the fact that subsurface damage is produced incrementally by the action of isolated, small asperity contacts during initial wear stage. As such, the damage from repeated contact events accumulates to a critical level. During the initial stage of wear, the contacting asperities are microscopic-scale irregularities on the polished surfaces, together with similar scale wear debris particles, and penetration into the surface is limited. The onset of grain pullout however, dramatically changes the contact geometry, due both to the change in surface topography and to the inclusion of grain sized abrasive particles in the contact zone. With this change in contact geometry, there will necessarily be significant changes in the magnitude and distribution of contact stresses which, apparently leads to spontaneous grain boundary cracking, facilitating continued material removal by a fracture dominated process.

Dominant wear mechanisms of ceramic materials in different operating regimes have been studied by Yushu Wang, *et al*, (1996b) to understand the wear transition mechanism. The experimental results show that wear mechanisms of ceramics are predominantly dependent on contact stresses, at low contact stress, the removal of material is controlled by plastic deformation induced microfracture on the asperity contact scale. Wear debris

is produced when the plastic deformation exceeds the plasticity limit of the material, which is very limited for ceramics. As the contact stress increased and reaches a critical point, various kinds of cracks (such as partial cone cracks, lateral/shallow cracks and radial cracks etc.) are initiated. These cracks can propagate owing to subsequential contact or at high contact stress. When these cracks intersect each other, chunks of material are detached from the bulk material and crushed by the subsequential tribological contact into fine particles and carried away from the contact region as wear debris. Wear transitions from deformation to crack/fracture controlled wear in ceramics can be attributed to the change of wear mechanisms during the sliding contact stress exceeding the critical microcrack stress.

Sliding wear caused by microfracture in polycrystalline alumina has been studied by Haiyan Liu *et al,* (1996). Microfracture occurs when superimposed stress exceeds a critical threshold. The decrease in surface conformity due to surface roughening and trapping of pulled-out grains can significantly increase as influenced by the applied load, surface non-conformity and apparent contact area of worn surfaces. The apparent contact area increases with increasing test time and applied load. As the apparent contact area increases, the contact stress tend to decrease, and wear occurs over a larger contact area. Subsequently as contact surfaces become rougher and third-body particles accumulates during wear, the super imposed stress exceeds a critical value and thus microfracture occurs. Wear

transition is triggered by onset of grain pullout. The study has shown that decrease in surface conformity due to surface roughening and trapping of pulled-out grains can significantly increase the magnitude of contact stresses, which lead to high wear rate. These observations have been acquired during the present study also.

2.16.3 *Environmental influence on deformation modes of ceramics under tribocontact.*

Donald et al, (1984) have studied the tribological behaviour of ceramic materials under different environmental conditions. It has been observed that the presence of surface films such as absorbates markedly influences the adhesion, friction and wear behaviour of ceramics. Further, with ceramics and other ionic solids, the presence of surface films such as water and surface-active organics can influence adhesion, friction and wear by altering the amount of plastic deformation that occur during sliding interfacial adhesion and surface chemistry plays a very important role in the friction and wear behaviour, when two such solids are brought into contact. Lubrication of ceramic under sliding or rubbing; heating of ceramics such as silicon carbide to high temperatures resulted in graphitisation of the ceramic surface with the graphite functioning to reduce abrasion and friction.

Unlubricated sliding behaviour of ceramic bodies has been tested by exposing ceramic materials to dry sliding at different

temperatures in a controlled environment by Yust *et al*, (1985). The trends in wear coefficient variation with temperature indicates the effect of temperature on materials such as hardness, yield stress and fracture toughness, which, in turn affects the wear resistance of the material.

Alumina has been of interest as a tribomaterial in aqueous environments for many different applications. ranging from abrasives, to ball valves, and hip joint replacements. Alumina-water tribosystem has been investigated by Gates *et al*, (1989) to determine the chemical interaction between these two materials under rubbing conditions.

The mechanism of tribochemical interaction of alumina-water is explained as follows:

1. Contact conditions induce a phase transformation from alpha (a) to transition alumina.
2. Chemical reaction occurs between water and transition alumina under high temperatures and pressures to produce aluminium hydroxides.
3. These aluminium hydroxides are layer lattice structures and serve to lubricate the contact junction.

Wear tests conducted using aluminium hydroxide powders confirmed their ability to act as solid lubricants.

The fundamental frictional properties of ceramics have been analysed and discussed by Kato, (1990) with major emphasis on understanding of tribological properties of ceramics. For ceramics, the values of friction coefficient in high vacuum are found to be less than unity, whereas the frictional coefficients of metals in high vacuum can be larger than 10. This is the difference in frictional properties between ceramics and metals. In metals, the high values of friction coefficients are due to the gross junction growth at a contact point. In ceramics, because of brittleness, junction growth by plastic deformation is not allowed. Because of such lack if junction growth in ceramics, the surface films of oxides or contamination can reduce friction more effectively than in case of metals.

The effect of load, sliding speed and lubricant temperature on the tribological performance of polycrystalline α-alumina has been investigated by Deckman *et al,* (1991), using a four ball test geometry with a purified paraffin oil lubricant. The test results showed that mild to severe wear transitions occurred at particular loads, lubricating temperature and sliding speed. The transition load has been found to reduce with increase in lubricant temperature or sliding speed. The onset of transition is due to the failure of lubricating film, due to the increase in flash temperature.

The factors influencing the friction and wear between metals and ceramics have been studied using a pin on disk type of friction test rig, having controlled environment. (Hiratsuka *et al,* (1992).

The friction and wear are influenced by the following factors :

1. the oxidation activity of the metals.
2. the relative shear strength of the metal and oxide.
3. amospheric oxygen.

Yushu Wang, *et al*, (1996a) have conducted systematic wear tests with varying speeds, loads temperatures and conditions of lubrication to investigate the influence of the operating parameters and environment on the wear and wear transitions of alumina. Observations of the tests indicate that wear transitions are usually accompanied by the sudden change of the friction coefficient and the surface morphologies at the contact regions. Wear and wear transition of alumina depends on operating parameters, environment and microstructure of materials. As either load, speed, time and temperature increases either in dry air, in water or in paraffin oil, wear increases and the wear transition load decreases. Lubricants such as paraffin oil, wear increases and the wear transition load decreases. Lubricants such as paraffin oil and water effectively reduce wear and friction, and increase wear transition load. Smaller grain size in alumina strengthens the load-dependent wear transition resistance of the material under paraffin oil lubricated condition. Rougher surface results in severe wear-in of alumina, though the influence of surface roughness diminishes after the wear-in.

2.16.4 *Influence of hardness on wear resistance*

Axen *et al,* (1994) have found that, in contrast to normal hardness dependency of metallic materials in abrasion, the wear rate of ceramics can increase with increasing hardness. In abrasion, with initially loose particles, the wear rate passes through a transition region around a hardness ratio equal to one and the wear of a material is higher when the counter body, is softer. This is because, the abrasives are embedded in the softer surface and consequently groove the harder counter surface. The wear can be higher, if the area of the soft surface in which the abrasives are embedded is large. This is because, the wear of the abrasives is less pronounced if the abrasives are crushed during the test or if multiple layers of abrasives are present between the surfaces orif the macro roughness of the surfaces in the relative motion is too high.

2.16.5 *Mechanism of material removal during abrasive type of tribocontact of coating*

The mechanisms of removal of coating material during wear have been studied by Tong Zhaohe *et al,* (1992). The effect of lamellar structure of ceramic coatings on wear mechanism has been considered. WC and Cr_2O_3 coatings on stainless steel surfaces by plasma spray technique were tested. Wear tests were conducted, using a block on ring arrangement, with the coated ring sliding against a steel block, with out lubrication.

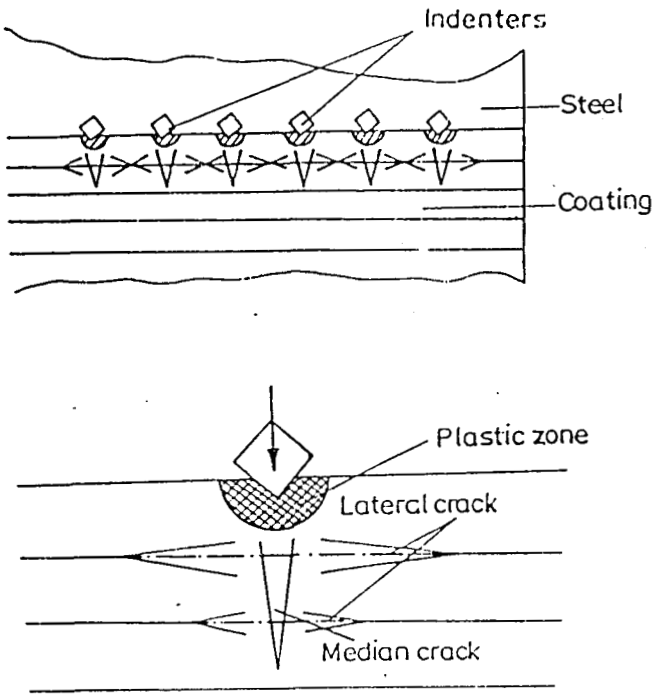

Fig. 2.15 - Schematic representation of cracking of the coating structure (Zhaohe,1992)

Test result showed that many WC particles fractured from the coating surface and were trapped in the mating steel surface. when the coating slides against worn steel surface these small hard ceramic particles interact with the coating surface like moving intenders. These indenters cause median and lateral cracks on coated surfaces when the coating slides against the mating material. For the coating materials, it has been determined that their bending strength is 5-10 times greater than the cohesive strength between layers. Therefore, cracks between layers can be formed more easily than the median cracks, The coating flakes off when the median crack reaches the interface between the lamellar structures of the coating. Fig (2.15).

With the exception of oxidation wear, the common failure of all wear mechanisms is due to the creation of loose wear debris, which requires fracture. Therefore any design of a tribological system which inhibits fracture must lead to improved wear behaviour. One obvious possibility could be to ensure that tribological contacts are totally elastic in the engineering sense, so that the only possible fracture process would be fatigue failure. This condition would clearly result in a reduction in wear (Halling *et al*, (1984). This concept of maintaining elastic stress in ceramic contacts has been used in ductile machining of ceramics for achieving high quality surfaces.

2.16.6 *Effect of material composition on wear resistance of alumina ceramics*

Even though advanced structural ceramics have potential for high performance engineering applications, some of the tribological behaviour of ceramics has to be better understood. Ceramic materials are highly susceptible to contact-induced localized surface cracking when impacted by a stream of hard particles. The erosion behaviour of pure alumina, alumina with silicate glassy phase and alumina with Zirconia particulate reinforcement has been studied by Jianren Zhou *et al*, (1991), under various structural and operational parameters. It has been found that the erosion resistance of pure alumina is very low, and that the resistance is improved by the presence of glassy phase (silicate) and second phase (Zirconia) particles in alumina. The erosion damage has been found to occur in the form of intergranular and transgranular cracking, the extent of each type depending upon the composition and microstructure of the material. Hardness of alumina has been found to be reduced with the addition of Zirconia and silicate glassy phases compared to single-phase alumina; but the toughness has been found to be higher. Erosion test results have indicated that the addition of a small amount of secondary phase, which may be either glassy phase or zirconia, results in significant reduction in erosion rate. When the percentage of second-phase materials is further increased, the erosion rate has also been found to increase considerably. Thus, there is an

optimum percentage of secondary phase which, when added to alumina, results in lowest erosion rate.

It has been observed that there is a major lack of understanding of the significance of the physical and mechanical properties of the coating materials in monolithic form, the corresponding values for the same materials as coatings, the reported differences in these parameters and their importance in the performance of coated systems. There is paucity of published date on the large number of compounds-oxides, carbides and nitrates-which, are major coating materials. As a result, a systematic approach to the design of the most suitable coating system is inhibited. (Strafford K.N., 1996).

Summary

The wear of ceramics, especially the abrasive mode, is mostly dominated by the cracking of the material. Thus it is very important to limit the working parameters, to avoid cracking, if one has to achieve minimum wear situation in ceramics. Further, the successful use of ceramics in wear resistant applications is limited more often by tribological problems than by material properties or processing deficiencies. Hence, there is a great need for a fundamental understanding of the surface intractions of ceramics with themselves and other materials. (Kazuhisa Miyoshi, 1988).

2.17 SIMULTANEOUS ABRASION THROUGH STATIC INDENTATION

Ceramics are hard wear resistant materials used for combating abrasion modes of wear and other thermal related wear forms. In order to evaluate the response of ceramics exposed to such wear environment and select the material, it is preferable to carry out studies simulating the wear process. In this section, an account on simulation of abrasion working of ceramics is illustrated.

Ceramics are utilised in situations, in which they are often subjected to abrasive wear and erosion. The machining of fine ceramics also will be carried out using abrasives; because of the higher hardness of ceramics, the most common abrasive used is diamond. The machining method can be grinding, lapping, or polishing.

The machining applications mostly involve elastic-plastic indentation, i.e. the indent (particle) radii are sufficiently some irreversible deformation is associated with the indentation process as discussed by Tong Zhaohe *et al,* (1992). The resulting subsurface plastic zone is involved in the damage of the specimen through either microcrack initiation, or subsequent crack growth. Hence, in all of these abrasive methods, indentation can be used as a very simple model for understanding the deformation and removal mechanics of the work piece. Indentation of brittle materials produces idealized model flaws. Study of such flaws

provides valuable insight into the mechanism of failure due to surface damage in brittle materials subjected to abrasive environment. Therefore it becomes important to understand the concept underlying crack initiation and propagation in ceramics, In order to optimise operating performance, it is important to know the parameters like load, crack shape corresponding to the threshold for damage in a given ceramic, as e\well as the influence of deformation and fracture properties in establishing this threshold for a given ceramic.

In many material shaping and wear processes, particularly where ceramic components are involved, surface material is removed through localized brittle microfracture. Macroscopic properties concerning abrasion and erosion may therefore be viewed in terms of summation over a vast number of discrete indentation fractures. Thus indentation tests provide a physical basis for the general science of material removal process involving abrasion. (Brian Lawn *et al,* (1975)

Bernard J. Hockey, (1971) has studied the deformation mechanism of Al_2O_3 ceramics under microhardness indentations and low load abrasion process (Diamond polishing) at room temperature. Transmission Election Microscopy has been used for the analysis. The observations showed that high densities of dislocations are produced under indentations and within the surface regions of mechanically polished Al_2O_3 crystals. The experimental conditions at room temperature were sufficient to

cause plastic deformation by both slip and mechanical twinning in the test material. Plastic deformation during these processes was thought to be a consequence of the nature and magnitude of the local stresses under indenters and abrasive particles. The high densities of dislocations observed indicate that a significant fraction if the work involved in abrasive wear of Al_2O_3 may be consumed in plastic deformation.

A sharp indenter usually concentrates very high level of stress and thus induces irreversible deformation in localized regions of the test surface. Hockey *et al*, (1975) have reported on the observations of microcrack patterns around small scale point indentations in Al_2O_3 and SiC. According to the observations made, dislocations and twins were present at the edges of the impressions; cracks, extending radially outward from the corners of the indentations were also observed. The existence of such cracks due to contact events can degrade the strength of structural ceramics, and this degradation may vary subjected to subsequent mechanical and thermal treatments.

Static indentation of SiC has been studied by James Lankford *et al,* (1979a) to determine the extent of plastic deformation beneath a sharp indenter and to relate the observed indentation microfracture patterns to the plastic zone. It has been fond that the extent of plastic zone beneath the indent is about five times the impression radius. the first cracks to form, under conditions of sufficient plasticity have been found to be radial rather than median cracks.

Further, indentation experiments have been conducted by James Lankford *et al,* (1979b) to study the threshold for crack nucleation in a wide range of ceramics. Scanning electron microscopy and acoustic emission techniques have been adopted to determine the threshold for indentation cracking. The threshold for indentation cracking was found to correspond to the lowest load at which acoustic emission could be detected. Threshold cracking is seen to relate to radial rather than median cracking.

The susceptibility of brittle materials to indentation cracking involves two major questions: initiation, how and where in the indentation field the cracks start?; during propagation, what paths do the cracks take? and what will be the extend of their growth? A model has been proposed by Lawn *et al*, (1977) for the initiation of microfracture beneath sharp indenters. Using a simple approximation for the tensile stress distribution in the elastic/plastic indentation field, fracture mechanics procedures have been applied to determine critical conditions for the growth of penny-like median cracks from sub-surface flaws. The analysis provides a functional relationship between the size of the critical flaw and the indentation load necessary to make this flaw extend.

Robert F. Cook *et al,* (1990) have reviewed the observations of indentation induced deformation and crack formation in brittle materials. The observations have found that the surface traces of cracks at indentation contacts are those of radial cracks, rather than median-nucleated half penny cracks. Also, it has been

observed that, in crystalline materials, radial cracks from almost immediately on loading of the indenter. Also it has been observed that none of the cracking events in the material results in any discontinuity in the load-displacement curve.

Ma *et al,* (1995) have studied the indentation behaviour of TiN coating on tool steel substrates of various hardness values. Under indentation loads radial cracks were observed for the hardened substrates. However, the annealed substrate samples exhibited ring or nest cracks, because a coating can not conform to the deformation produced in the substrate, which results in coating cracking, rather than adhesive failure between coating and the substrate. Indentation crack patterns of hard coatings reflect the toughness of the coating and its ability to conform to substrate deformation.

Diao *et al,* (1994) have conducted indentation tests on $A1_2O_3$ and TiN thin coatings deposited on cemented carbide substrate using diamond and SiC indenters fracture patterns). Fracture pattern diagrams as afunction of normal load and coating thickness have been introduced. It has been observed that the critical normal loads for generation of lateral cracks and spalling of coating are strongly affected by coating thickness. While, for $A1_2O_3$ the critical load decreases with increase in thickness, in case of TiN, critical normal load for generation of lateral cracks is minimum at a particular coating thickness, and increases with any change in the coating thickness.

2.17.1 Indentation test for physical property evaluation

Indentation hardness testing has been done to study the deformation and fracture behaviour of TiC & Tin coatings in a range of steel substrates. The variation of hardness with indentation size and depth has been compared with numerical models for the composite hardness behaviour of coated systems. Also the variation of hardness with temperature for coated systems has been investigated. For the coating/substrate composites studied, hardness has been found to fall rapidly with increase in temperature. The change in the hardness with temperature may be due to the changes in the microstructure of the coating with temperature and the relaxation of the residual stress within the coating.
(Knight *et al,* (1989a).

Swain, (1994) has discussed about the ability of indentation methods to characterise the mechanical properties of thin films. Measurement of hardness and elastic modules from force – displacement date, using pointed and spherical indenters has been discussed. Application of these indenters to measure film fracture and delamination has also been discussed.

Takashi Taniguchi *et al,* (1996) have used Vickers indentation method for characterizing the mechanical properties of polycrystalline Cubic Boron Nitride. It has been observed that the

indentation hardness is strongly dependent on the applied load. It has been observed that initially hardness decreased with increase in load and then remained constant. This is attributed to the fact that Vickers hardness relates not only to the indentation size but also to the cracks initiation from the corners of the indentation. when the cracks occur during indentation, a portion of the energy, which should be used to create the indentation, will be dissipated by the crack formation. Fracture toughness has been estimated, making use of the measured crack lengths at different loads, assuming E/H as constant.

Fouad Attar and Thomas Johannesson (1996) has observed that, in case of thin coating the composite hardness of the coating system would increase, with a reduction in the applied load. This indicates the influence of base material in composite systems. i.e. the indentation depth decreased with load, reducing the influence of the substrate. Also higher hardness values have been observed for similar coatings of higher thickness. Determination of the size of plastic deformation underneath the indentation, which encapsulates only within the coating thickness, is basically required to calculate the coating hardness precisely.

Coating produced by thermal spray methods can contain defective laminar structures, with weak interfaces and voids between solidified splats. This directly weak interface structure primarily characterizes the properties of the coatings. Whereas defects can degrade the strength of the coated structure, they can

also accommodate mismatch strains and even improve thermal insulation.

Antonia Pajares *et al*, (1996) have examined the plasma sprayed ceramic coating systems, by conducting Hertizan indentation (contact) tests, using spherical indenter, to study the stress-strain behaviour, also, bonded-interface specimens have been examined to study the damage process within the coating and the substrate material. Indentation stress strain curves have been used to quantify the relative role of the coating and substrate in the net deformation response. Test results indicate a transition from a coating-controlled response at low strains to a substrate-controlled response at higher strains. Damage process within the coating and substrate has been studied using bonded-interface specimens. coating degradation has been found to occur by laminar cracking at the interface with the substrate and within the coating itself. Plastic deformation primarily in the metal substrate, but also in the coating contributed to the crack driving force. Elastic modulus and yield stresses were also evaluated from the stress-strain data.

Knowledge of mechanical properties, such as elastic modulus, is generally necessary to interpret the behaviour of a material under static or dynamic loading. Direct determination of elastic modulus is generally not possible for coating of relatively smaller thickness. A new method has been developed, by Chicot *et al,* (1996) to determine the elastic properties of the coating material, based on the assumption that the difference between the shapes of the

theoretical and experimental indents are linked to the elastic recovery and then to the elastic modulus of the material. Evaluation of the entire volume of indent is based on geometric approximations. It has been found that the new methods give a good indication and confirms that elastic properties may be derived from the study of deformed indents.

2.17.2 *Evaluation of the fracture toughness through indentation*

The advent of indentation fracture mechanics has provided a fundamental basis for analysing the deformation/fracture response of ceramics to controlled sharp contact events. Evans *et al*, (1976) have studied the indentation fracture in ceramic materials. Fracture toughness values of different ceramic materials were evaluated in terms of indentation crack length and the impression radius.

The nature of stress distribution, which occurs at an elastic plastic indentation under static load, has been analysed by Perrott (1977). The analysis provides an explanation to the fractographic nature of the cracks and the potential for the growth of these cracks in the near surface region adjacent to an indetation.

Anstis et a, (1981 have critically examined the application of indentation techniques to the evaluation of fracture toughness of various ceramics. The approach adopted involves direct

measurement of radial cracks as a function of indentation load. The results of the observations indicate good correlation between the fracture toughness values obtained by conventional means and those obtained by indentation method.

Application of indentation fracture analysis using Knoop & Vickers indentation has been examined by David B. Marshall (1983). Vickers indentation has been found to be better suited than Knoop indentation for toughness determinations using crack-length measurements. However, in strength testing of ceramics, knoop indentation has been found to be a good as Vickers indentations as a source of controlled flaws.

Cook et al, (1995) have studied the nature of subsurface cracks formed under and around Vickers indentation for different engineering ceramics, using die penetrant technique and flow dimensions were recorded. The resulting date was used to investigate various aspects of indentation cracking, such as crack shape, functional relationships between indentation load and flaw dimension, and the usefulness of different indent fracture equations.

An alternative indention method has been proposed for determining the toughness of ceramics, by adopting strength equations. Routine bend-test facilities were used to investigate various aspects of indentation cracking, such as crack shape, functional relationships between orientation load and flaw

dimension, and the usefulness of different indent fracture equations.

As alternative indentation method has been proposed for determining the toughness of ceramics, by adopting strength equations. Routine bend-test facilities were used to measure the strengths of the Vickers-indented test specimen. Crack size has been eliminated as a test variable in favour of indentation load, which is much more easily monitors. This method is suitable to those materials, which do not produce well-defined radial crack pattern. But the main disadvantage is than only one result is obtained per specimen, unlike crack length measurement technique, where, number of trials could be conducted on a single specimen. (Chantikul *et al*, 1981).

2.18 SIMULTANEOUS ABRASION THROUGH SLIDING INDENTATION

Because of their inherent brittleness, local fracture can play a central role in the wear of ceramics. Under high local stress, surface and subsurface cracks can interact, causing the detachment of small chips of material and resulting in high wear and surface roughness. Cracks nucleated close to the surface may also propagate further into the bulk leading to maroscopic brittle failure. During machining (grinding/polishing) the material is subjected to abrasive type of surface contact; however, under macroscopically brittle ceramics can therefore be machined and

polished under suitable conditions without fracture (ductile regime machining of ceramics). Plastic flow in ceramics is nevertheless generally very limited compared with metals. An understanding of, and the means to measure, the onset of local fracture in ceramics are therefore very important.

Scratch testing, in which a hard stylus is slid over a sample surface under controlled conditions, provides one method of experimentally evaluating the response of a material to the high local stresses to which it may be exposed in wear and machining process. A hard stylus sliding over a brittle ceramic surface generates damage by a series of different mechanisms at different loads. To separate these mechanisms and determine at what load they occur is a general problem in scratch testing. Microscopy of the surfaces after scratching is useful in understanding the surface deformation/damages. Detection of acoustic emission originating from deformed surface is also useful in understanding deformation behaviour.

Obtaining per specimen, unlike crack length measurement technique, where, number of trials could be conducted on a single specimen. (Chantikul et al, 1981).

Perry, (1983) has discussed about the usefulness of scratch testing for studying the adhesive & cohesive failures of thin, hard coatings on a range of substrate materials. It has been found that the combination of acoustic emission and microscopic observations

are useful tools for understanding the modes of coating failures. The critical loads for coating failure have been found to be dependent on coating thickness, toughness and also hardness of the substrate material. coefficient of friction of the coating also appears to play an important role in coating failure.

Perry et al, (1981) have conducted scratch tests on thin coatings using different types of commercially available scratch test equipments, to study the consistency of the tests. The effect of wear of stylus, on the critical load of the coating has also been found to be independent of instrumentation. The critical load doesn't appear to vary to any significant extent, as the diamond stylus wears (self-sharpening of diamonds).

Different techniques for determining the critical load of thin coating, using scratch lest have been discussed by Sekler et al, (1988). Microscopic observation of the scratch is considered as the most straight forward technique, which gives maximum information. Among the methods based on the use of physical measurement, acoustic emission detection is considered as most effective. The main advantage of this technique is that the ratio between the signal amplitude below and above the critical load is notably significant. Tangential force measurement may be useful as an addition to the information acquired by the AE analysis and microscopic examination. The authors also state that there is no general criterion for characterising a coating failure. For each

coating-substrate system, the failure criteria have to be independently defined.

Knight et al. (1989a) have carried out scratch testing to study the surface deformation & frictional behaviour of thin coatings or TiN and TiC deposited on steel substrates. The coefficient of friction has been found to increase with increasing normal load. Analysis of the frictional force identified two regimes of behaviour as the normal load is increased. The tow regimes are respectively associated with plastic flow within the coating alone and with plastic flow in the substrate by stress transmission through the coating. The transition between the two has been found to occur at a load that depends on coating thickness. The transition is also expected to depend on the mechanical properties of the coating and the substrate materials.

Knight et al, (1989b) have conducted room temperature scratch tests on thin TiN coatings on a range of steel substrates. The effect of substrate hardness and deformation response on coating

behaviour has been examined. Since the substrate may carry major part of any contact load, by transmission through the coating, its mechanical properties may be critical in determining the overall response of the composite system. Critical loads have been identified for coating-substrate system where, the properties of the coating material alone determine the mechanical properties of the composite system. It has been observed that for loads, where the indentation / scratch penetration depth is less than the coating thickness, the measured material properties can be taken as being representative of the coating material alone and could be used for coating quality control. The critical load for scratch failure of the coatings appears to decrease with increasing substrate hardness. With low substrate hardness, most of the scratching work is consumed in deforming the substrate and little ploughing of the coating takes place. As the substrate hardness is increased, the rigidity imposed by reduced plasticity results in a higher concentration of stress in the coating. Loads, which would cause widespread deformation in softer substrates, result in greater coating damage with a corresponding reduction in the critical load.

Scratch testing of hard, brittle TiN coating on high-speed substrates has been carried out by Vonstebut et al, (1989). Even though scratch testing is not a substitute for wear testing, it is considered, as an efficient method of getting information on dominating damage mechanism, a coating is likely to develop. Surface damage during scratch testing has been found to start nucleation behind the trailing edge of the diamond stylus. In the

multi pass scratch-wear operation, surface damage has been found to be dominated by delamination along the coating substrate interface. Three-dimensional surface mapping is shown to be a powerful tool for coating failure analysis. It has been also mentioned that the coating failure problems can be minimised by increasing the ductility of the hard surface coating i.e., control of thickness to enhance the tenacity of the coating.

Julia-Schmutz et al, (1991) have conducted microscratch testing to evaluate the adhesion of TiC coating on to steel substrates. According to the observations made the coating-substrate deformation caused by the scratching point is mainly dictated by the deformation of the substrate. i.e. an increasing in critical load, with the increase in substrate hardness; critical load is also found to increase with coating thickness.

Maximum tensile stress on the coating surface is an important design parameter in most tribological applications of a hard-coated solid. Surface damage, wear and spalling of the hard coating are caused by cracking at the surface, where the tensile stress is maximum. Finite element method has been employed by Diao et al, (1994) to evaluate the stress field in the hard coating and the substrate under frictional loads, and the ratio between the values of maximum tensile stress and maximum contact pressure is calculated under various contact conditions. From the stress distribution, it has been found that the maximum tensile stress always appears just behind the trailing edge of the contact.

The effects of substrate roughness and the choice of stepwise or linearly increasing load on the adhesive strength of thin coatings have been studied by Fouad Attar et al, (1996) using the scratch testing technique. The scratch test implies deformation of the material in an elastic and plastic form until the coating and substrate are separated. Cohesive & adhesive failures have been observed for all coatings tested. At the beginning of application of normal load, mild plastic deformation has been observed. At higher normal loads, regular cracking transverse to the loading direction appears. These cracks are either confined in the scratch track or extended outside the scratch borderline. At a still higher load, minute a coating debris removal has been observed at the scratch track borderline. At an even higher load, complete coating removal in the track has been observed.

During scratch testing of coated materials, ridges are formed along the sides of the track due to plastic deformation of the coated composite. The size of the ridges is proportional to the normal load used for scratching. High tensile stresses in the coating, perpendicular to the scratch, are generated at the rim of the ridges. If the coating fracture resistance is exceeded, cracks propagating in the direction perpendicular to the coating surface are formed. (Per Hedenquist et al, 1997).

Scratch testing can give useful information about the adhesion of coating provided that careful identification of the failure modes is carried out. Buckling failure modes predominate for thin flexible

hard coating on a ductile substrate. In these cases plastic deformation of the substrate leads to an interfacial defect, which initiate the failure. Wedge spallation occurs for stiffer, thicker coatings. To achieve this, a compressive shear crack forms through the thickness of the coating and propagates down the interface ahead of the indenter. Material can then spall off as the wedge lifts the coating away from the substrate. To improve resistance to buckling, it is necessary to reduce the size of interfacial defects and the extent of interfacial defects and the extent of plastic deformation immediately below the coating. This means that hard ductile substrates are preferred. To reduce the susceptibility of the coating substrate system to wedge spallation, increasing the toughness of the coating to prevent shear crack propagation and ensuring that interfacial crack propagation actually occurs in a ductile fashion is required (Bull, 1997).

Concentrated contacts induce micro-cracks in brittle materials during several types of industrial processes. These processes include machining, grinding and polishing. Concentrated contact induced micro-cracking is also an important aspect of wear and erosion of brittle solids. The generation and evaluation of these microcracks, in the above applications, generally occurs as a consequence of the stresses developed at contacts between brittle solids. The sliding micro-indentation process is fundamental to a number of such applied phenomena. For example, asperity contacts between brittle solids, which contribute significantly to their wear, may well be characterised by the sliding micro-indentation

process. Surface finishing processes such as machining, grinding and lapping can be though of as repeated application of sliding micro-indenters. Thus, analysis of sliding indentation should provide insight into the material removal mechanisms prevalent during finishing as well as in understanding the surface damage left behind on the finished surface. This could lead to the development of techiniques for controlling this surface finishing damage in structural ceramics. (Chen et al, 1991).

Swain, (1979) has carried out constant speed scratch on number of brittle materials, using Vickers pyramid indenter. Observations of the micro-fracturing around scratches in brittle solids have indicated that it is very similar to that occurring beneath quasi-static pointed indentations. Three distinct regions of crak formation have been observed with increase in normal load. At low loads, no visible surface or subsurface cracking has been observed around the scratch. The scratch track is smooth and fully plastic; the process of material removal is plastically controlled. The accumulation of a large number of such plastically controlled contact events may result in a mechanical polishing operation, which is characterised by a relatively low material removal rate and a smooth mirror-like finish. For intermediate loads, a fully plastic track and well developed median and lateral cracks occur around the scratch. At higher loads, considerable crushing was observed over the scratch track. Material removal at the contact sites took place by micro cracking resembling typical abrasion operations on brittle solids.

A new method has been proposed by Lopex et al, (1989) to measure cohesion of thick coatings by performing scratch test from the substrate to the free surface of the coating. Fixed depth scratching is conducted with concurrent recording of tangential and normal forces. In the vicinity of the coating, at a critical distance L_c (measured from the free surface), scratching leads to half cone shaped cracking. The half cone shaped cracking seems to originate from radial cracks formed in front of the indenter as the surrounding stress field reaches the free surface. Cohesion resistance has been determined as a measure of L_c.

When scratch test is performed on the cross-section of a thick coating layer, a half-cone shaped fracture is induced, as the indents reaches the vicinity of the free surface. The height of this cone has been used for characterising the intrinsic fracture toughness of the coating. During scratching of a brittle material, two main phenomena can be observed: plastic grooving and brittle cracking. The radial cracks in scratching play a determinant role in inducing half-cone fracture. An estimate of the coating cohesion may be obtained form the measurements of fracture toughness by analysis of the half-cone fracture formation during a scratch test performed perpendicularly to a cross section of a coating (Beltzung et al, 1989).

The damage caused by scratching relatively brittle materials such as ceramics is normally assumed to be a dominated by fracture process. But investigations have shown that under

sufficiently high hydrostatic pressures, brittle materials may be prevented from fracturing, so that any permanent deformation can be essentially plastic. When fracture between conditions in the plastically deforming zone and the surrounding material within which conditions an elastic. Cracks may often propagate as material in unloaded, that is effctively behind the indenter in a scratch test. (Willams, 1996).

Because of their inherent brittleness, local fracture can play a central role in the wear of ceramics. Under high local stress, surface and subsurface cracks can interact, causing the detachment of small chips of material and resulting in high wear and surface roughness. Cracks nucleated close to the surface may also propagate further into the bulk leading to macroscopic brittle failure. However, under sufficient low loads, many ceramic materials can behave in an ductile manner, and macroscopically, brittle ceramics can therefore be machined and polished under suitable conditions without fracture. Plastic flow in ceramics is nevertheless generally very limited compared with metals. An understanding of, and the means to measure, the onset of local fracture in ceramics are therefore very important.

The tangential force necessary to scratch a material depends on the properties, which control the adhesive forces, as well as on the mechanical properties of the material and the indenter geometry. The occurrence of ductile to brittle transactions, or of transitions between regimes, involving different types of fracture, results in

sudden changes in the tangential force. The detachment of debris may cause the tangential force to drop, as support of the indenter tip is momentarily lost. Small fragments within the groove bottom may cause transient increases in the friction force. For most materials, the transitions between different regimes of material response as determined by SEM examination has been observed to correspond to change in the tangential force record. (Axen et al, 1997).

2.19 SIGNIFICANCE OF ACOUSTIC EMISSION IN TRIBOLOGICAL ANALYSIS

Most of the tribological events are associated with deformation of material and subsequent friction and wear process. Thus, in any tribological study, microscopic observation of materials is an essential technique for understanding and analysing material deformation processes. Advent of acoustic emission technique, has facilitated on-line monitoring of tribological processes, in order to understand the response of the material during various stages of deformation. Acoustic emission (AE) is defined as the transient elastic waves generated by the rapid release of energy from a localized source or sources within a material under stress. Sources of AE include different mechanisms of deformation and fracture. some of these sources are moving dislocations, slip, twining, grain boundary yielding, crack initiation, crack growth etc.).

Acoustic emission is the characteristic and irreversible emission by a material when it is deformed. Hence, acoustic emission is well suited to studies associated with plastic deformation. The onset of plastic deformation in materials is limited by the presence of stress risers, such as cracks and other types of flows; hence acoustic emission provides a useful tool for flaw detection. Subcritical crack growth, such as that occurs during fatigue, stress-corrosion cracking, etc. results in the release of elastic strain energy. These processes which give rise to acoustic emission is useful in the detection of sucritical crack growth. Acoustic emissions are generated in the deforming body directly by the deformation process and so are direct indicators of the actual event.

Research work on acoustic emission has shown that the potential of using AE in the investigation of friction and wear phenomena is very promising. Jiaa et al, (1990) have studied friction and wear behaviour of metals in sliding contact, using AE signal analysing technique. It has been found that different regions of wear (running-in, steady state etc.) can be distinguished from the observations on AE rms value and measured wear rate. Frequency spectrum analysis is found to be useful in detecting events occurring during sliding contacts such as stick-slip, localised damage, etc.

Boness et al, (1991) have tried to monitor in real time the wear rate and predominant wear process occurring in wear testing of sliding metallic contacts, using acoustic emission signals. The test

results have demonstrated that measurement of acoustic emission rms values provide a valuable tool in the study of wear of sliding contacts. The time varies nature of the rms values was found to give an indication of the wear mechanism occurring. It was found that a linear relationship existed between integrated rms value and measured wear scar volume.

Acoustic emission analysis is frequently used not only for the non-destructive diagnostics of various structures but also for the detection of phase transitions in coated ceramic materials and deformations in composites in different applications. The investigation of plasma-sprayed coating behaviour at higher temperatures is important both for optimisation of the technological parameters of the plasma-spraying process and for evaluation of the coating life time under conditions usual in industry. Noval et al, (1991) have studied the usefulness of Acoustic emission signals for the monitoring of coating failure and the prediction of coating life. Tests have been conducted in order to distinguish emission due to oxidation processes, failure of coating and related phenomenon during exposure of the samples to mechanical or thermal loads and also for the prediction of the coatings lifetime on the basis of acoustic emission signals emitted from the sample,

Javad Akbari et al, (1994) have carried out Acoustic emission (AE) monitoring during indentation tests of ceramic materials to reveal different types of emission and to co-relate them with microscopic observation in order to identify plastic deformation or

cracking phenomenon. The acoustic emission generated by surface cracks have been found to be of higher amplitude, and higher frequency (burst mode of emission), compared with the phenomenon during plastic deformation. Thus, AE monitoring method is effective in examining the threshold load for cracking of the indented material and also to study the plastic deformation and fracture of fine ceramics during machining or related abrasion processes.

Tanikella et al, (1995) studied acoustic emission signals during controlled indentation of soda-lime glass, The observations have shown that the acoustic emission measurements can provide useful information on crack initiation effects. Direct correlation has been found between acoustic activity and microscopic observations. Acoustic emission also showed reproducible trends in the crack initiation points.

Microhardness and cracking during indentation in sialon based ceramics has been studied by Yurkov et al, (1996). Acoustic emission monitoring technique has been adopted for the detection of crack initiation and crack propagation.

SUMMARY

Ceramic materials are being used increasingly in industrial applications as wear resistant materials. The successful use of

ceramics for such application is limited more often by tribological problems than by processing deficiencies.

Among all ceramics, alumina ceramics are found to be most abundantly available, economically more viable and hence, are most widely accepted in industrial applications, for surface property enhancement of engineering components. In spite of their higher hardness values, the major limitation for the continued development of alumina coatings as well as expanding their range of applications lied in their poor fracture toughness. However, this deficiency can be overcome by dispersive strengthening of the alumina microstructure by addition of ZrO2. The coating properties may be enhanced if distinct second phase particles are incorporated into the coated structure. This method of coating preparation has the potential of improving the fracture toughness of the coating by a mechanism of bridging the individual lamellae or by partially absorbing the energy of deformation.

There is lack of data on physical and mechanical properties of the coating materials and their importance in the performance of coated systems. Also it is seen that in most of the tribological applications of ceramics.ceramic coatings, local brittle fracture plays an important role in the material removal process, Cracks nucleated close to the surface may propagate further into the bulk, leading to brittle failure.

Static and sliding indentation methods have been found to be extremely useful in understanding the deformation and material removal mechanics of brittle materials. In addition, static indentation method is also found useful in evaluating some of the mechanical properties if brittle materials.

The review on literature clearly underlines the significance of tenacious coating for durability; apart form tenacity of the coating, the need for suitable interfacing is also highlighted. It is seen that static and sliding indentation can be used for evaluating the response of the coating material to abrasive environment in terms of friction force, critical load for crack initiation and nature of cracking during indentation. With this in view, detailed study on static and sliding indentation of sprayed ceramic coatings has been undertaken.

CHAPTER – 3

3.1 Production of metal powders

Powders are produced using a variety of techniques to meet the required specification connected with the applications. The diverse methods of manufacture provide a wide range of powder particles morphologies and properties.

When considering materials for plasma spray application, many characteristics of the powder, both in bulk and as individual particles must be evaluated. (Hermanek *et al* 1994)

A plasma spray powder consists of an infinite number of fine grains which behave and react both individually and collectively. Therefore, magnitude of physical characteristics of the powder either in mass or as individual particles must be considered and evaluated for suitability as a spray material.

3.2 Characteristics

3.2.1 INDIVIDUAL PARTICLES

Size:

Particle size, usually referred to as diameter for spherical particles. For other configuration, precise determination is technically difficult and gives only an approximation.

Shape:

A variety of particle shape viz., spherical, rounded, angular, acicular, dendritic, irregular, porous and fragmented.

Density:

The density of a powder particle is not necessarily identical to that of the material from which it was manufactured.

Surface:

The particle surface area compared to its volume is an important consideration in prescribing spray parameters. Smooth spherical particles require more heat to melt than one irregularly shaped which may be porous, circular, dendritic, or otherwise convoluted. (Fig. 3.1)

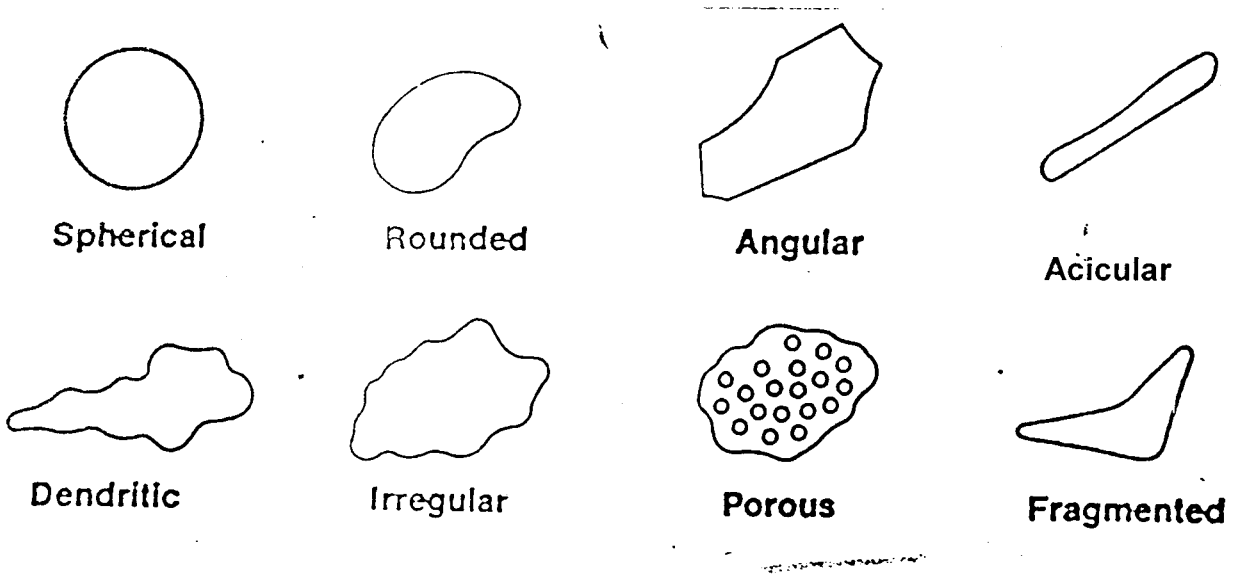

Fig. 3.1 - Various powder particle shapes (Hermanek *et al,* 1994)

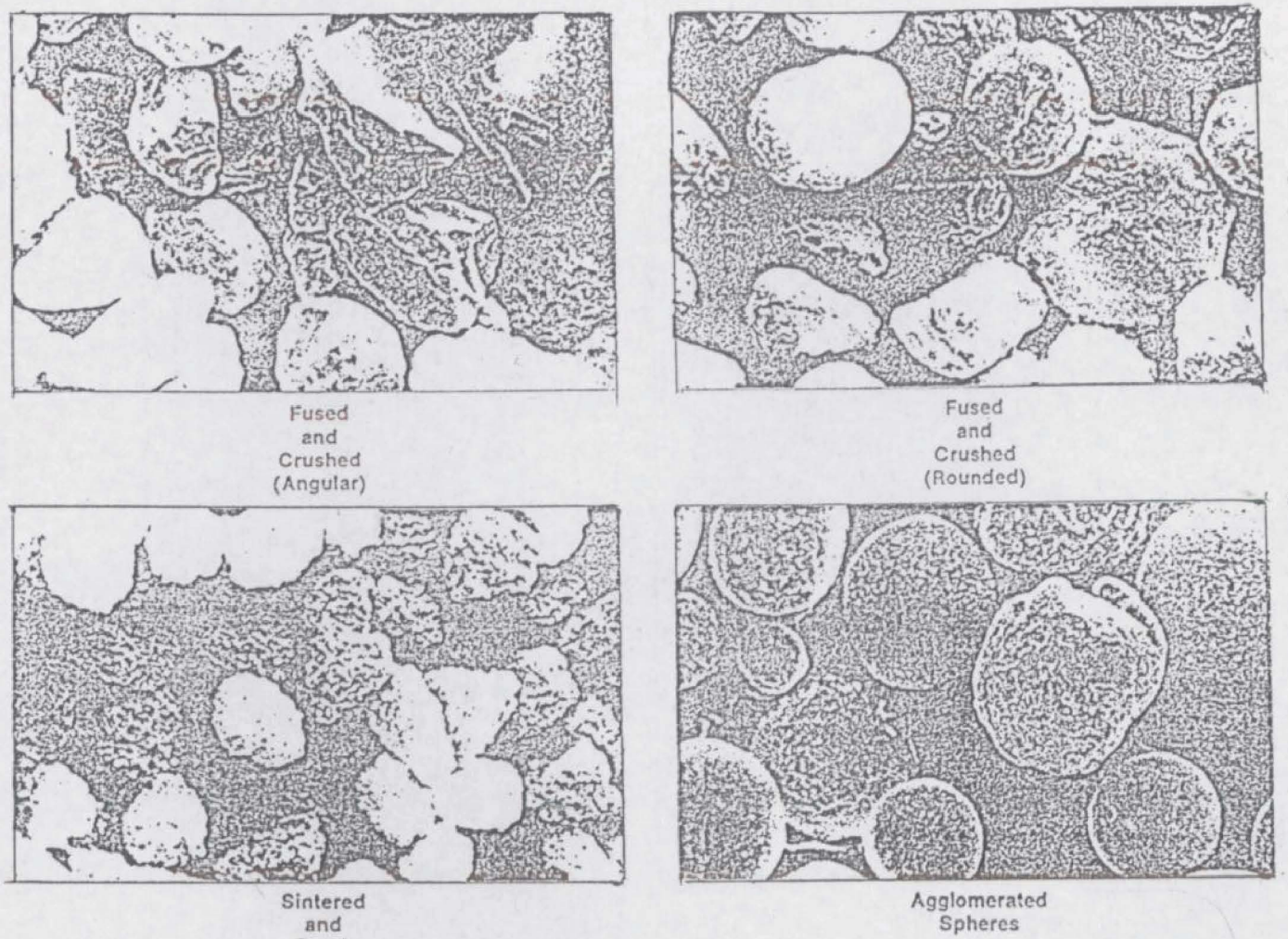

Fig. 3.3 - Typical examples of Ceramic Powders

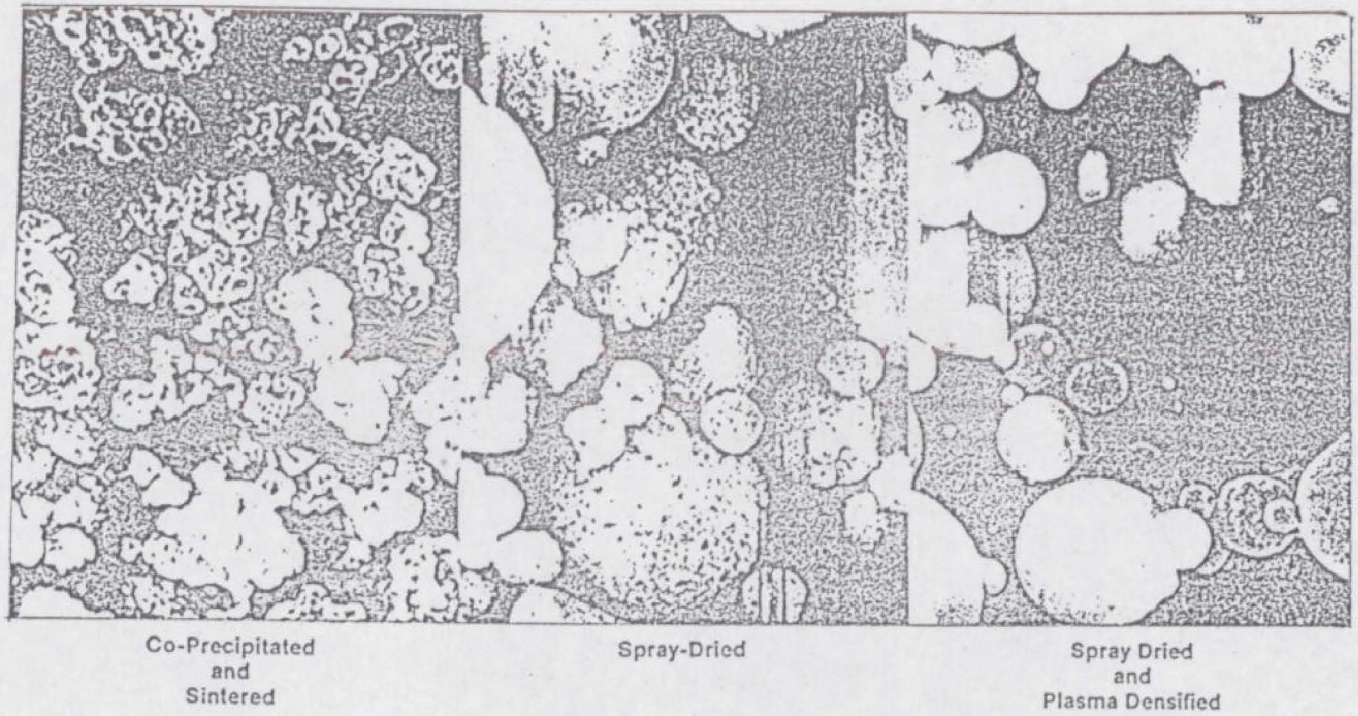

Fig. 3.2 - Typical examples of Ceramic Powders for Thermal Barrier Application

Microstructure:

Powder particles are usually monocrystalline but sometimes consist of many minute grains. Their microstructure, ie. Size orientation and shape are related to the method of manufacture. The grain structure can affect particle activity and to a certain extent its behaviour in a plasma stream.

Surface Oxide Layer:

Depending upon the manufacturing method, metal powders will contain from a few parts per million to a several percentage point of oxygen. Oxides are present as a surface layer or in solution. It will affect powder's, melting temperature, flow or wetting characteristics and there by coating quantity.

Powder Mass:

A mass of powder consists of a large quantity of particles. The most obvious properties of a good plasma spray powder are flow, particle size, distribution and configuration, apparent density and chemical stability during spraying. Particle size and distribution must be optimized for the powder to be effectively treated in the plasma. Apparent density and surface morphology are closely related as they interact relative to feed rate and melting characteristics. Additionally melting temperature must be considered especially as they relate to spray parameters, particularly gas flows and powder levels.

Average Powder Size:

Average particle size refers to a statistical diameters calculated from the particle size distribution.

Particle Size Distribution:

For most spray application, average particle size is not a decisive factor, where as particle size distribution in the total mass is

Specific Surface Area:

The total surface area of 1gm of powder in square cm per gram is expressed as specific surface area.

Apparent Density:

Apparent density of the powder depends on the friction conditions between particles, which are functions of their relative surface area and their surface condition. It further depends on the particle packing arrangement which depends on particle size, distribution and shape.

Flow:

The free flow a powder through an orifice depends upon the size of its opening. Flow therefore is influenced by friction between powder particles, but also by friction with the orifice wall. Flow is usually expressed as the time necessary for a specific amount of powder to flow through the orifice.

3.3 Powder Manufacture

3.3.1. Atomization

Atomization process consists of striking a mother metal stream with jets of gas/air/water, fragmenting it into minute droplets which solidifies into individual powder particles. The atomizing medium has a profound effect on the process yield, particle size and morphology.

3.3.2. Gas atomization

Gas atomization involves the production of liquid metal drops by the disintegration of a stream of molten metal with a high pressure jet of gas. Liquid fragmentation is accompanied by the kinetic energy of the atomizing medium typically nitrogen, argon, or air. The resulting particles tend to be smooth and spherical. When produced under inert gas cover the particles exhibit the exact chemistry of the melt, thus permitting the production of complex alloys containing W, Al, Ti, Cb, Mo, and Ta.

3.3.3 Water atomization

In water atomization a high pressure water stream is forced through nozzle to form a dispersed phase of droplets, which impact the metal stream. Droplet solidification is rapid thus causing water-atomized powders to be irregular in shape with rough oxidized surfaces.

3.3.4 Centrifugal atomization

In this process, molten metal is ejected from a rapidly spinning container. Within the spinning receptacle, centrifugal forces cause the melt to move up. The container falls to its tip where the metal is ejected in the form of droplets. The resultant particle shape can be varied from spherical to flake.

3.3.5 The Rotating electrode process (REP)

REP is a form of centrifugal atomization. A rod of the material to be atomized is rapidly rotated while being melted at one end by an electric arc or plasma. Molten droplets spin free and solidify before impacting the atomizing chamber walls. Powder particles are smooth and spherical.

3.3.6 Roller atomization

A mechanical process that feeds stream of molten metal between rapidly rotating rolls and discharging it into flakes, a circular, irregular, spherical particles. This process is mainly used for copper, tin and lead.

3.3.7 Vibrating electrode

This is a mechanical approach to produce high purity powder by vibrations of a consumable electrode. The electrode forming a resonant rod with a fixed and a free end is continuously moved between rollers towards a slow rotating water-cooled rotating

copper disc. Atomization occurs in an arc struck between the disc and vibrating electrode end. Spherical particles are formed whose size is controlled by changing the length of the resonant rod.

3.3.8 Melt drop technique

In this method molten metal contained within a closed pressurized crucible is subjected to vibrating oscillations forcing the metal through the nozzle at the bottom of the crucible and into a vacuum. Inert gas chamber causes it to expand and disperse to droplets.

3.3.9 Ultrasonic atomization

High velocity pulses of gas upto Mach2 at a characteristics frequency in the range of 60,000 – 1, 20,000 cps impinge on a molten stream causing fragmentation. This result in a spherical powder with a narrow size range, between 4& 10 μ.

3.3.10 Vacuum atomization

This technique is based upon the principle that when a molten metal is supersaturated with gas under pressure, is suddenly exposed to vacuum the gas expands causing atomization of the metal. Clean, high purity powders are formed. Alloy powders of nickel, cobalt, iron, copper and aluminium have been successfully produced.

3.4 Other manufacturing Techniques

3.4.1 Reduction:

Reduction of iron oxides or other compounds in solids or gaseous media gives sponge iron of hydrogen reduced milliscale.

3.4.2 Decomposition:

Decomposition of liquid or gaseous metal carbonyls (nickel or iron) yields a fine powder.

3.4.3 Electrolytic deposition:

Electrolytic deposition from molten metal or solutions yields either powder directly or an adherent mass that requires mechanical pulverization.

3.4.4 Precipitation:

When subjected to a hydrogen atmosphere in the autoclave nickel aluminum carbonate results in nickel powder.

3.4.5 High energy impaction

At ambient temperature or cryogenic temperature brittle coarse shapes can be impinged against a tungsten carbide

target causing them to fracture and form smaller irregular particles.

3.4.6 Mechanical comminution:

Machining: produces relatively coarse powders from soft metals.

Milling: Ball mills, impact mills, gyratory crushers and eddy mills fragment hard material (carbide refracting metals and oxides) into fine powders.

3.4.7 Condensation:

Metal solutions are caused to vaporize and condense on to a cold surface to form a deposit, which in turn may be mechanical reduced to powder.

3.4.8 Decomposition of metal hydrides

Vacuum treatment of metal hydrides produces powders of fine mesh size.

3.4.9 Reaction of metal hydrides with molten magnesium

This is the kroll process, it is used to produce titanium and zirconium spounge.

3.4.10 Rapid solidification technology (RST)

Molten metals in cast, at quench rates of 10^6 ° C/sec on to a rotating disc or drum to form powder or a continuous ribbon or flake which is subsequently pulverized into amorphous powder.

3.4.11 Intergranular corrosion

By selectively corroding carbide rich grains boundaries, stainless steel powders are produced.

3.5 Treatment of metal powders

The powders, once classified are utilized without further processing. However in some cases materials may be agglomeralise, spray dried, sintered plasma densified etc. to create a wholly new product exhibiting properties or characteristics not present in the parent material.

3.5.1 Granulation

This is the process of agglomerating fine powders into coarse granules, which flow readily, although they continue to behave as fine powders.

There are several methods by which powders can be granulated. This includes prepressing the powder into large slugs, which are then mechanically disintegrated into granules. Spray drying is a combination of atomizing, evaporation process wherein very fine powder or powders as in the case of

composites are mixed with suitable liquid binder and atomized into droplets. During free fall, the binder vaporizes producing relatively uniform spherical particles.

3.5.2 Densification

All granulated powders may be thermal sprayed as dried or in a densified condition. Densification is achieved to reduce inter particles void and increase the powders spray rate. The primary methods of densification are sintering and plasma fusing. In sintering the particles are heated for a prolonged period, at a temperature below their melting point causing them to become coherent. This doesn't result in alloying of dissimilar components or even when they are in intimate contact. Plasma fusing is essential plasma spraying the agglomerated powder to effect a dense free flowing spherical shape that under certain conditions, may be fully alloyed.

3.5.3 Powder morphology

Powder morphology will affect powder packing. Its feed rate and effective dwell time in the plasma. The latter is related to particle heat transfer characteristics. With refractory oxides morphology influences deposit efficiency and coating structure. With metallic coatings, morphology may be of even greater significance.

CHAPTER – 4

4.1 STRUCTURE PROPERTY CO-RELATION OF PLASMA SPRAYED COATING.

Sampath and Herman (1994) had conducted extensive studies at the distinguishing features between APS and VPS process correlating these processing differences to macrostructure. Ni and Ni based alloy powders were VPs processed. These powders were also plasma sprayed in air for comparative study. Plasma spraying was carried out in a plasma – technik automated APS / VPS system. The parameters used for spray coatings are given in Table 4.1.

Substrate temperature was monitored by incorporating a thin chromel – alumel thermo couple on to the back of a copper substrate. The plasma flame along with the powder carrier gas was allowed to impinge on the substrate, and the transient response was recorded. The substrate was then allowed to cool and measurement was repeated by introducing Ni powder at a known feed rate.

The coatings were deposited to 0.1 to 0.5 mm and analysis was done by X-Ray diffraction for phases and their distribution relative to coating thickness. TEM was used to substantiate the results and also to provide information on grain sizes and morphology.

APS yields rapid solidification and contains melting approaching and consolidating in one single operation. However, residual stress, porosity and oxidation of metallic components pose problems and hence limits its utility as a coating technique. It is seen that VPS produces homogeneous and dense microstructure. The results of the substrate temperature in VPS is given in Fig. 4.1.

Fig. 4.2 shows X-ray diffraction pattern of a powder and 4 VPS coatings (Sampth & Herman). The increase in intensity and decrease in the width of the Bragg peaks as the thickness increases. This shows increase in crystallinity and grain growth.

The loss of metastability in VPS coating is shown in Fig. 4.2. The superimposed diffractions patterns are for powder APS and VPS coatings of a Ni – 20% Al. alloy indicates transition from disordered state, which is undoubtedly due to self annealing.

In VPS, high substrate temperature enhances the diffusion process between coating material and substrate, favouring a strong metallurgical bond.

Gudmundsson *et al,* (1988) studied the influence of substrate temperature on the microstructure and hardness of VPS alloy coatings. They observed that higher substrate temperatures lead to larger grain sizes and lower hardness values. It was also reported that low substrate temperatures lead to higher internal stresses.

Table – 4.1
(Ref. Sampath & Herman, 1994)

Plasma Spray parameters for Aluminum and chromium Oxides.

Argon (1 min $^{-1}$)	41	41	41	40
Hydrogen (1 min $^{-1}$)	14	14	14	13
Current (Amp)	600	600	600	650
Injector (mm)	1,8	1,5	1,5	1,5
Injector Angle	90	90	90	90
Injector Distance	6	6	6 (1)	6 (1)
Powder Gas (Ar_2(1 min $^{-1}$)	3,4	3,4	3,4	2,5
Powder Feed Rate (g min $^{-1}$)	51	51	40(2)	25(3)
Spray Distance (mm)	120	120	120	110
Efficiency	34	53		

(1) 7 mm nozzle = 6,5 mm; nozzle = 7 mm.
(2) 40 g min $^{-1}$) for 5-25 micron and 45 for 10-45 micron powder respectively
(3) 25 g min $^{-1}$) for 5-25 micron and 33 for 10-50 micron powder respectively

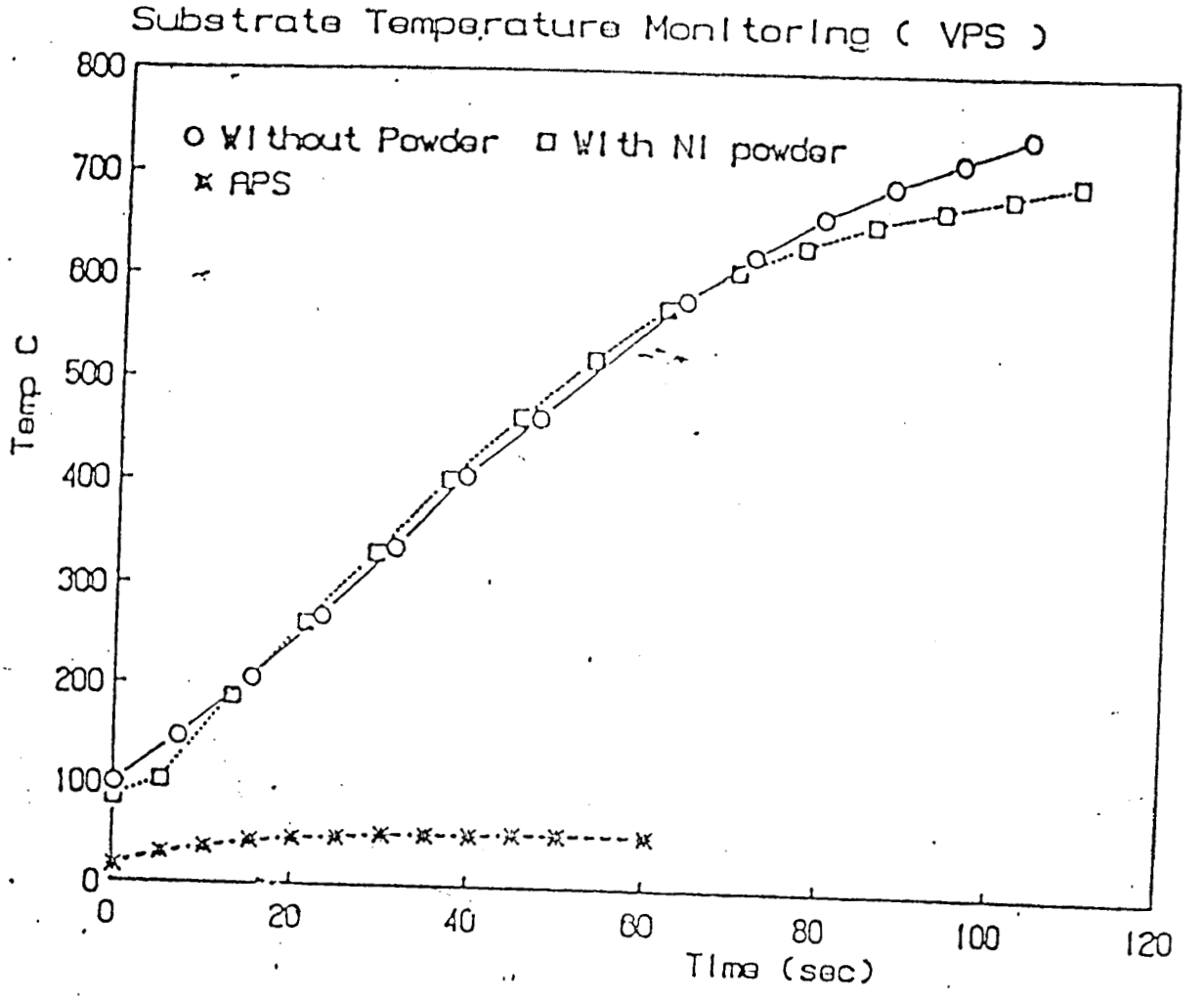

Fig. 4.1 Variation in substrate temperature with time during spraying

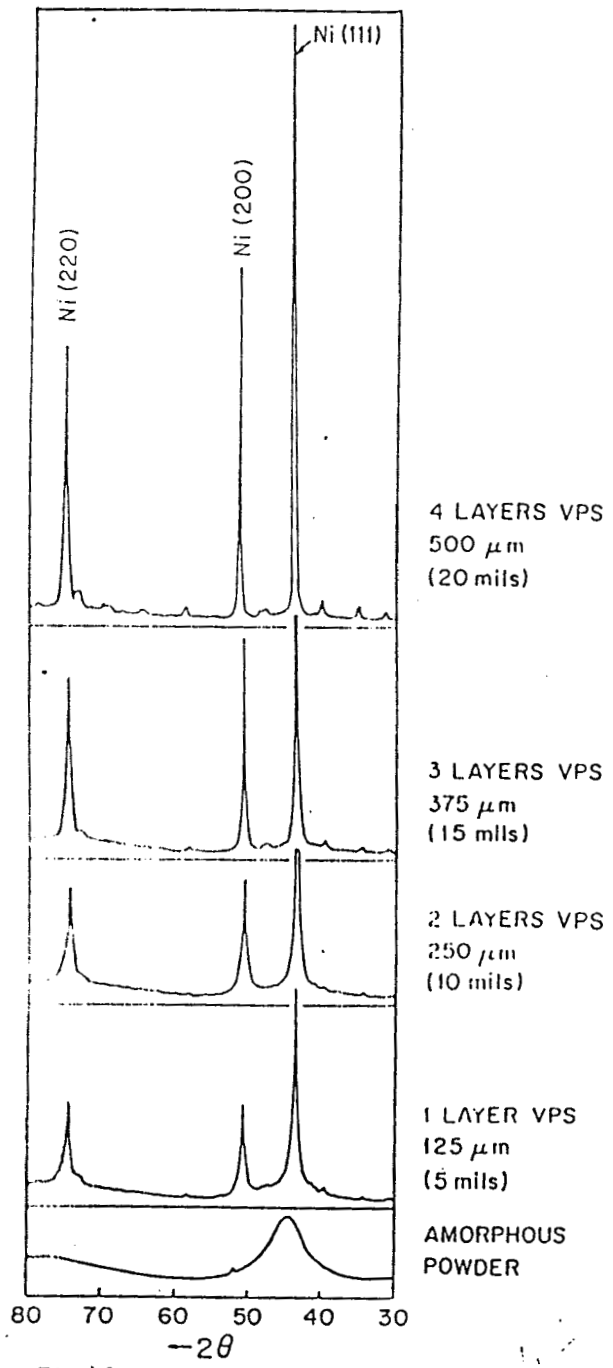

Fig.42: Sequentially arranged x-ray diffraction patterns from VPS coatings sprayed to different thickness. (Different Spray duration)

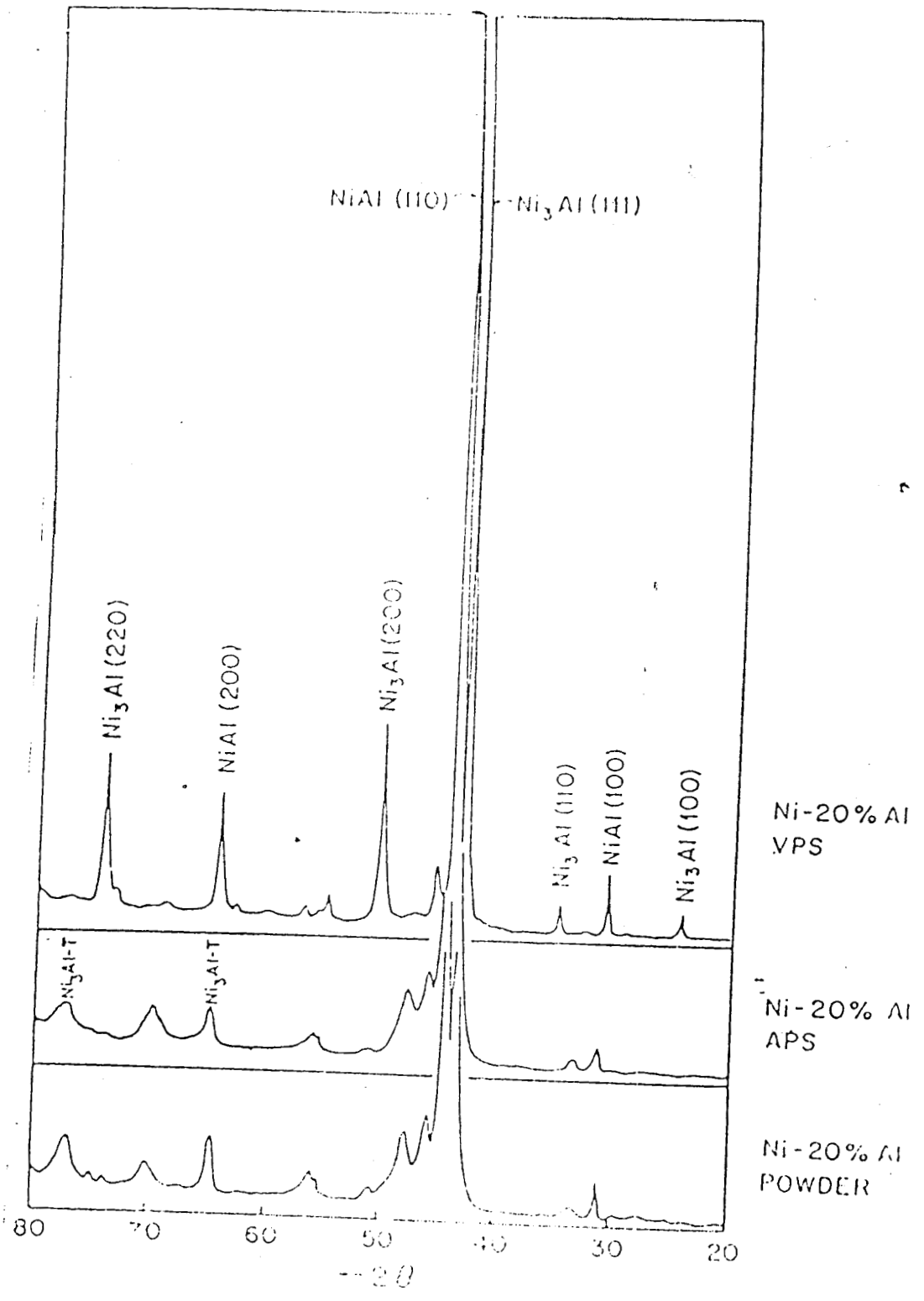

Fig. 4.2b - X-ray diffraction pattern from Ni - 20%Al alloy powder and its respective APS and VPS coatings (Ni_3Al - T = Martensitic Ni_3Al)

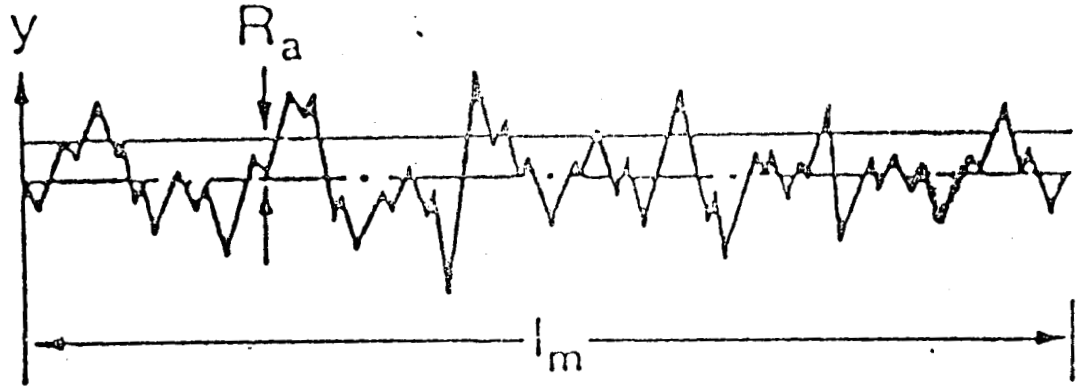

$$R_a = \frac{1}{l_m} \int_0^{l_m} |y| \, dx$$

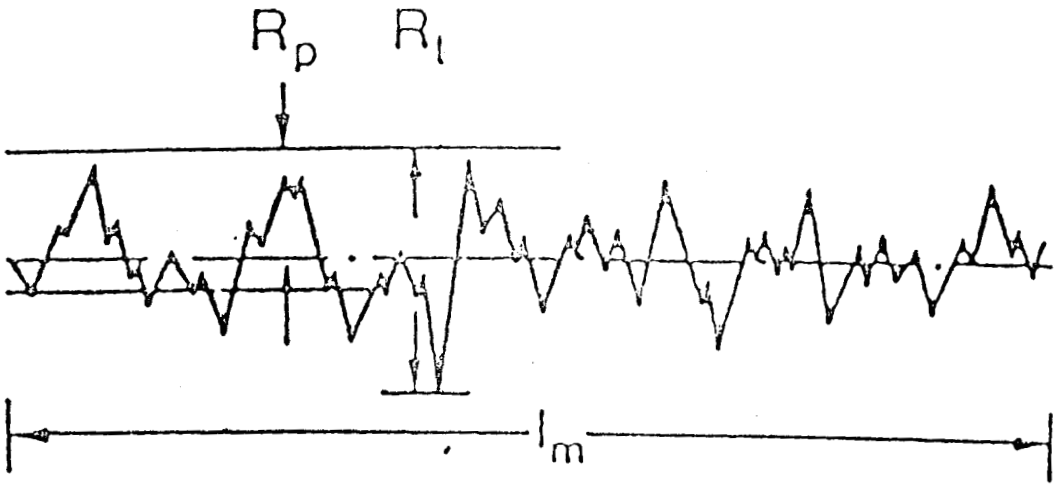

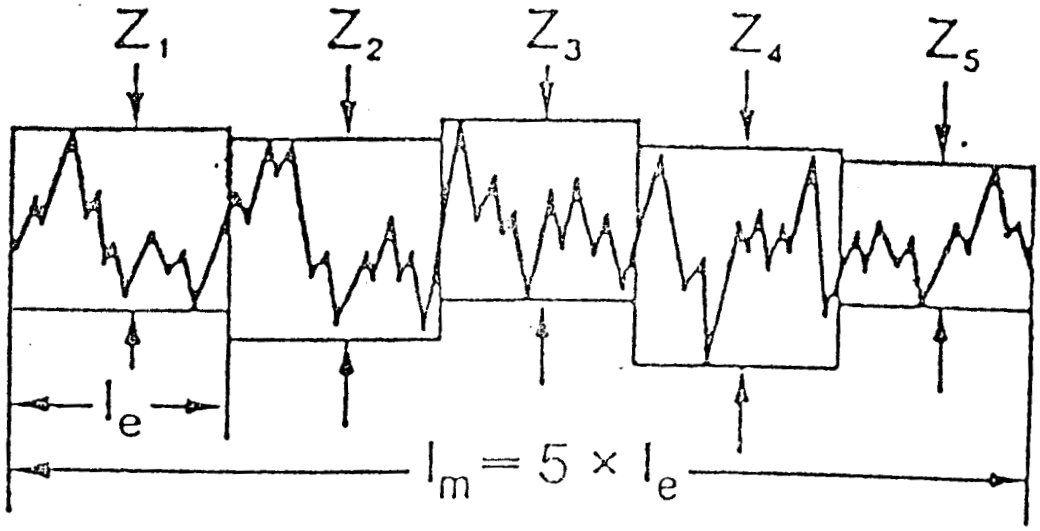

$$R_z = \frac{1}{5}(Z_1 + Z_2 + Z_3 + Z_4 + Z_5)$$

Fig. 4.3 Schematics illustrating the differences between R_a, R_p, R_t and R_z.

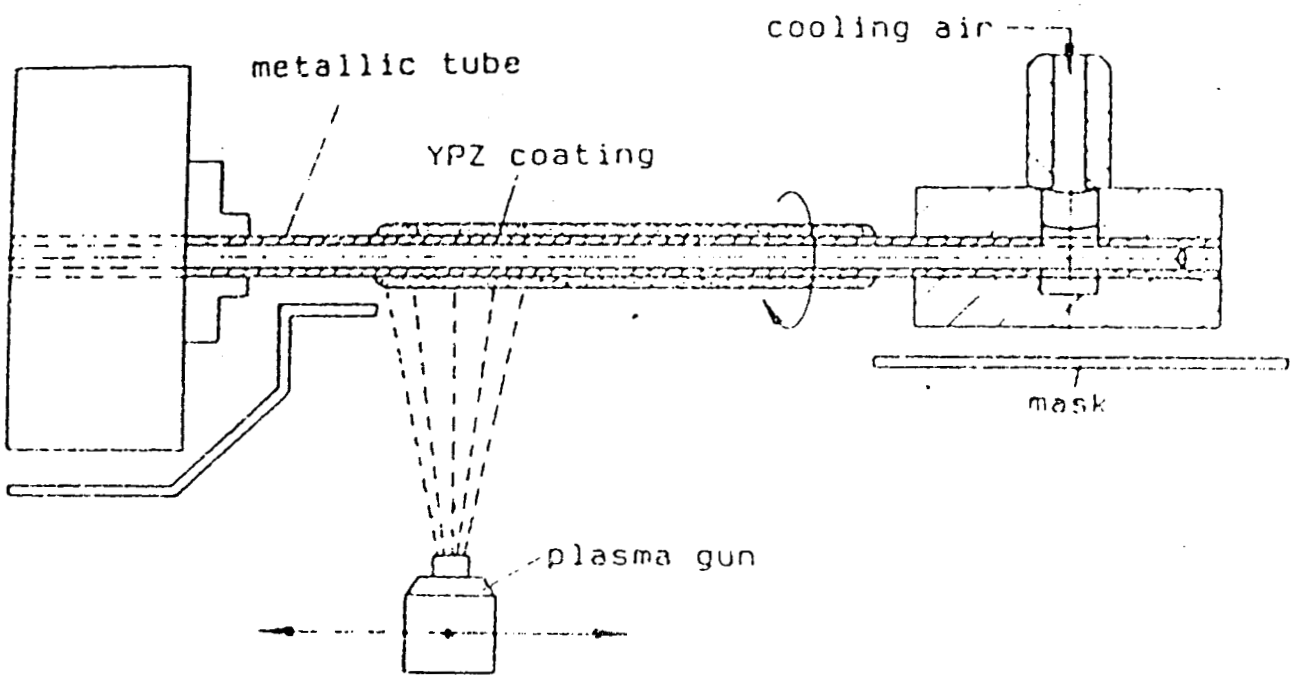

Fig. 4.4 - Production of specimens for mechanical tests of Plasma Sprayed Zirconia Coatings

The higher operating temperatures cause self annealing of the coating, leading to precipitation of equilibrium phases. The annealing leads to stress relief and recrystallisation of the grain, but no significant grain growth is observed. Thus VPS provides microcrystalline microstructures. The improved mechanical properties are attributed to the density and micro crustallinity of the coating.

Nicoll (1987) conducted studies specially relating to Textile industries, where the surface finish of the coating is more important than the process. The final surface roughness of the coating depends on

1. The surface roughness of the substrate after grit blasting.
2. The degree of fusion and flow of the selected powder : which in turn depends on the choice of plasma parameters, particle velocity and solidification characteristic of the materials.

The effect of powder injection and carrier gas was studied by Fanchais, Smith Nisc (1987). But NicoM has kept plasma parameter constant varying the size of plasma exit nozzle of the gun. this lowers the velocity, increases the dwell time of the powder and thus the melting characteristic constant plasma parameters. The powders of particle size 5.25 and 10-40 μm for Al_2O_3 and 5-25 and 10-50 μm for Cr_2O_3 was chosen. The chemical composition as well as the particle size distribution are given in table 4.2 The surface roughness was measured using Perth-O-Meter (Fig. 4.3)

Table – 4.2

Surface Roughness data various plasma gun nozzle diameter and ceramic powders

Material Reference	Surface Roughness (Micron)	Nozzles Size (mm) 6	7	8
Aluminum Oxide				
5 – 25 Micron	Ra	3.1	2.8	3.0
	Rp	6.8	6.2	6.8
	Rz	15.5	13.8	15.1
	Rt	18.6	18.4	18.9
10.40 Micron	Ra	3.7	3.6	3.9
	Rp	8.4	8.6	7.8
	Rz	18.8	19.2	20.1
	Rt	23.1	24.9	27.2
Chromium Oxide				
5-25 Micron	Ra	2.36	2.4	2.5
	Rp	5.16	5.1	5.1
	Rz	11.4	12.0	12.1
	Rt	13.9	16.2	15.1
10-50 Micron	Ra	2.8	2.9	3.2
	Rp	5.9	6.3	7.2
	Rz	14.0	14.6	15.7
	Rt	17.0	18.1	19.9

Table – 4.3

Bond strength and microhardness data for various plasma gun nozzle diameters and ceramic powders

			Nozzle Size (mm)		
			6	7	8
Aluminum-Oxide	Bond Strength	MPa	63.51 67.83	57.46 57.44	75.84 68.14
5 – 25 Micron	Micro Hardness	HV_{300}	751	809	622
Aluminum Oxide	Bond Strength	MPa	64.73 51.75	31.16 32.76	54.49 41.95
10-40 Micron	Micro Hardness	HV_{300}	896	945	845
Chromium Oxide	Bond Strength	MPa	75.44 78.45	46.46 49.39	51.95 65.74
5-25 Micron	Micro Hardness	HV_{300}	1142	1084	1018
Chromium Oxide	Bond Strength	MPa	38.88 49.69	52.44 51.35	55.06 42.59
10-50 Micron	Micro Hardness	HV_{300}	1117	1019	1038

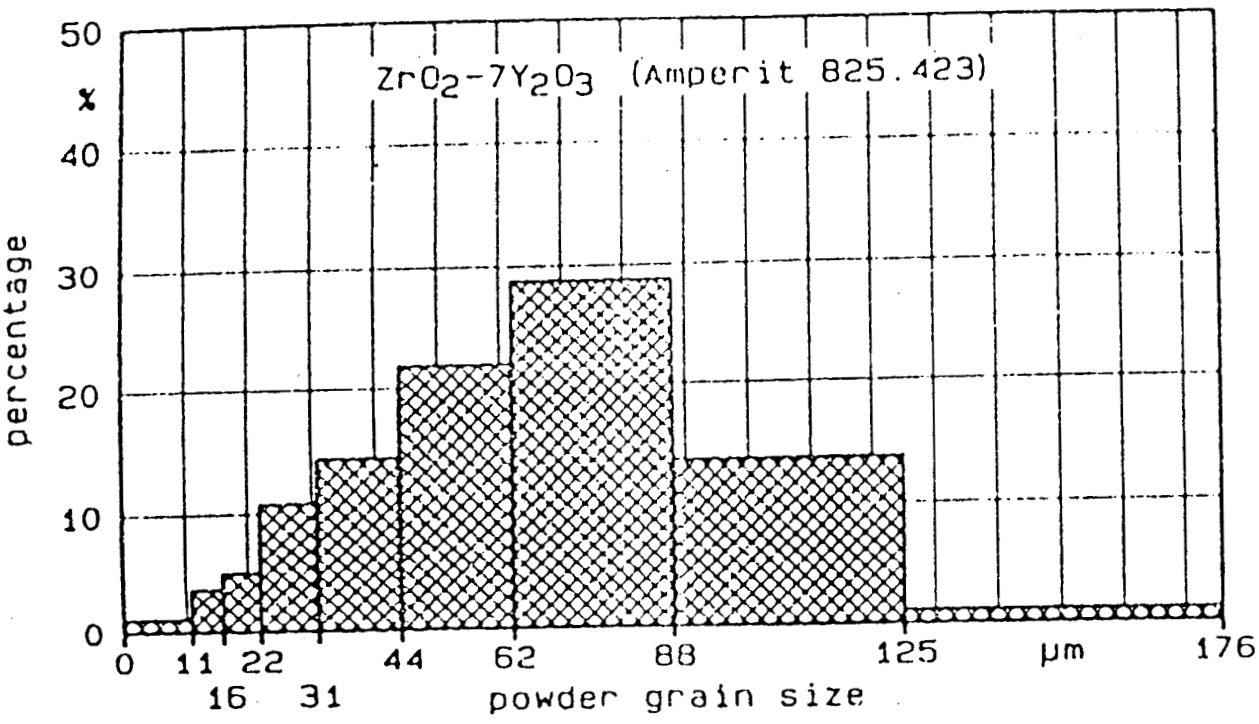

Fig. 4.5 - Grain size distribution of the powder

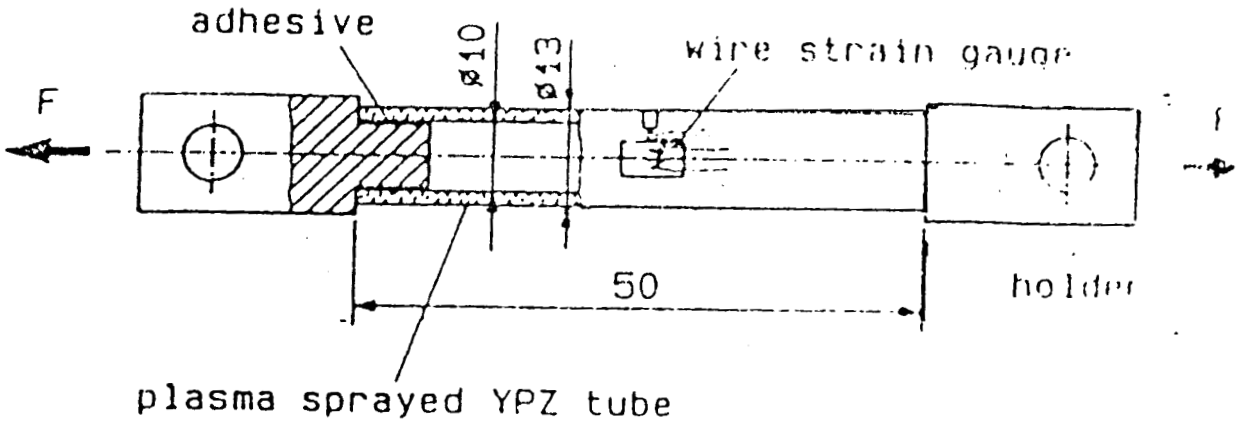

Fig. 4.6 - Specimen for measurements of Youngi Modulus of Plasma Sprayed Zirconia Coatings

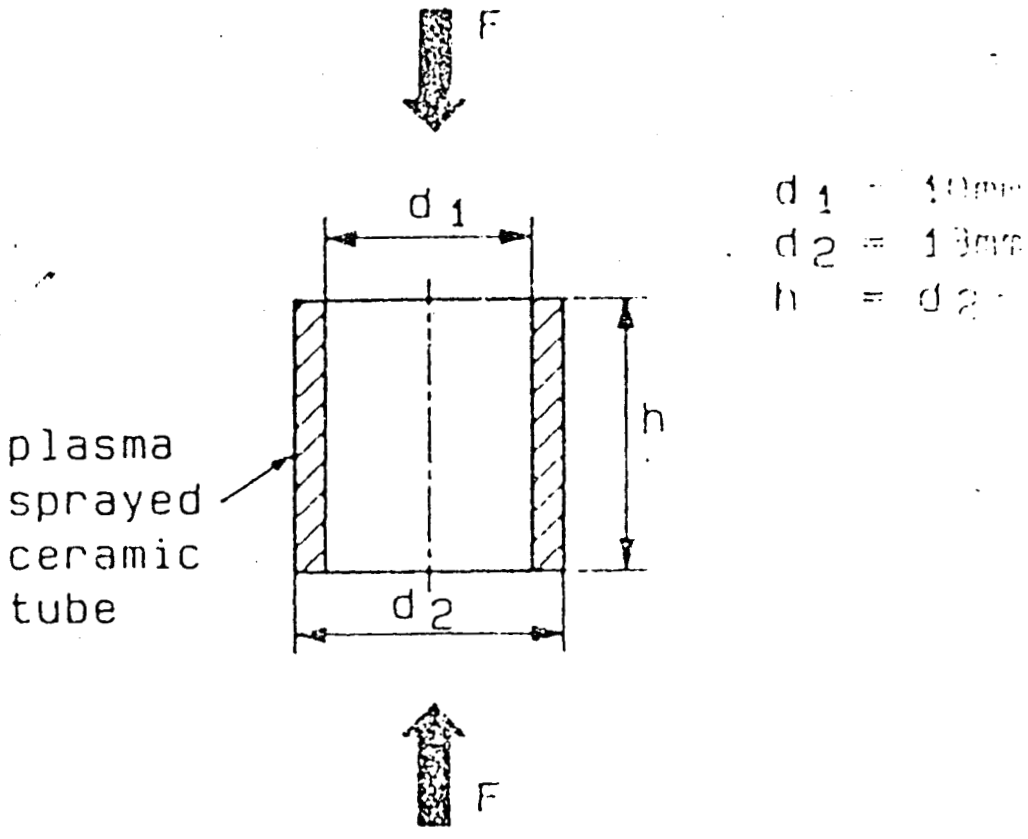

Fig. 4.7 - Specimen for measurements of compression strength for Plasma Sprayed Zirconia Coatings

The Al_2O_3 coatings show increasing surface roughness values increasing values with an increase in nozzle size. In both cases the values are lower than those of the Al_2O_3 coatings.

The Bond strength and micro hardness results are given in Table 4.3. The bond strength values using 5-25 micron powder are higher than those with 10-40 micron powder and the reverse is seen for the micro hardness values.

For the coatings provided using 10-50 micron powder, the bond strength values remain approximately at the 50 MPa level independent of nozzle size variation.

The results of mechanical testing and surface roughness indicate advantage in using 7 mm nozzle diameter for the Al2O3 powder. Changing the nozzle diameter for the Cr2O3 powder degrades both the mechanical properties and surface roughness.

4.1.1 Structure – Property Correlation of Plasma Sprayed Zirconia Coatings.

Hans – Dieter Steffens, (1994) conducted extensive research on the mechanical properties of Zirconia coatings. He prepared specimen (Fig. 4.4) using powders (Fig. 4.5) and concluded that Youngs Modulus for partially stabilized Zirconia coating is a function of porosity. Porosity increases as Young's Modulus

decreases. These data can be utilised as guide for calculation of thermally or mechanically induced strains and stresses on coatings.

4.2 STATIC INDENTATION STUDIES

Introduction

Ceramics are utilized in situations in which, they are often subjected to different forms of mechanical wear and / or erosion. During service, it is likely that the ceramic coatings may have to encounter two / three body abrasion. Usually fine ceramic particles from the sprayed coatings, fracture and get dislodged; these particles can further impinge on contacting surfaces or on being transferred, get entrapped in the counter surface, and tend to indent over / scratch the coated ceramics (Tong Zhaohe *et al,* 1992). Many such service applications involve elastic-plastic indentation, i.e., indenting particle radii are sufficiently small, that some irreversible deformation is associated with the indentation process (James Lankford et al, 1979b).

4.2.1 Nature of Indentation

The nature of indentation is largely dependent on the applied load and the material being indented; accordingly, the types of indentation can be as illustrated in Fig 4.8. Condition 'a' represents ideal indentation, while condition 'd' corresponds to indentation associated with radial cracking. Conditions 'b'

represents the pincushion indentation, as a result of sinking in of the material around the flat faces of the indenter. Condition 'c' represents the barrel shaped indentations as a result of ridging or piling up of material around the faces of the indenter. From this, it can be inferred that for realising an ideal indentation, one has to choose the correct geometry and apply the required load; though the diagonal across the corners of the indentation may be the same in all the four cases, the measurement will be erroneous in the cases of b – d.

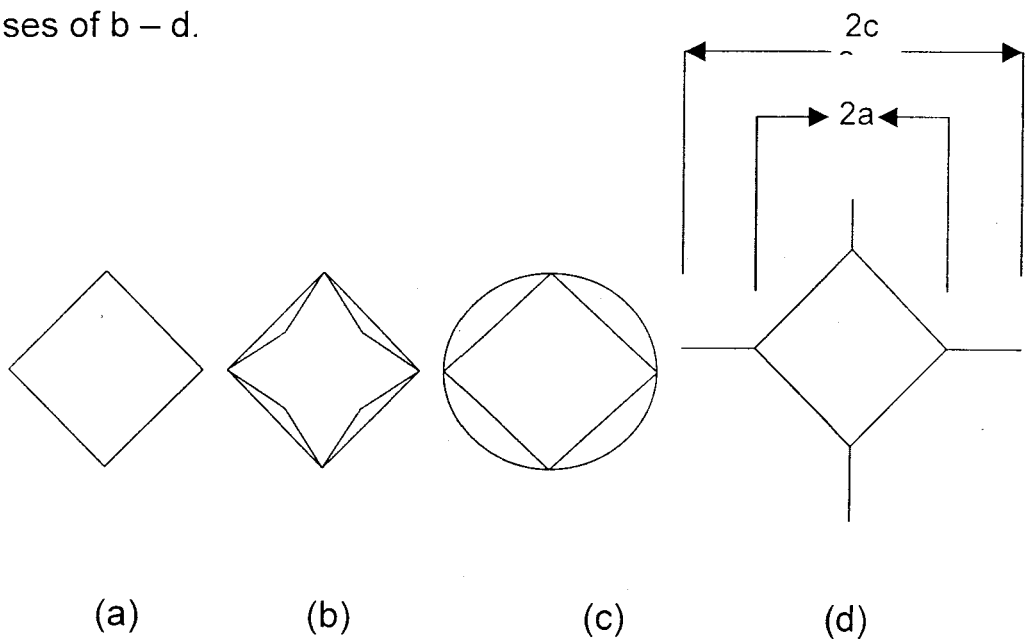

Fig. 4.8 Schematic representation of types of indentation

Indentation testing has been found useful for evaluating the response of the materials under such situations and also in the investigation of damage process in brittle materials. During indentation test, a suitably sharp indenter tip concentrates very high levels of stress and induces irreversible deformation in localised regions of the test specimen. During indentation, the material can

experience cracking / decohesion depending on the force of indentation. The status of the material during indentation can be monitored by suitable sensing techniques. Since, indentation testing is a noise free process; acoustic emission monitoring will be highly effective in studying the response of the material to indentation process and also to identify the threshold for possible crack initiation.

The main aim of the present investigation is to study the response of the plasma sprayed Alumina – Titania composites to static indentation, identifying the threshold load for crack initiation for different compositions and also to evaluate some of the mechanical properties of the Alumina-Titamia composite coating, from the data produced during static indentation tests. The response of the ceramic coating was evaluated in terms of depth of penetration, crack propagation and also the characteristics of the AE signal emanated by the ceramic coating being indented. Indentation experiments have been carried out as explained previously. Date acquired are presented in the following sections.

	COATING POWDER	PARTICLE SIZE (um)
BOND COAT	Nickel – Aluminium 95/ 5	45 – 105
TOP COAT	AT 40 Alumina - 60% Titania - 40%	10 – 45
	AT 13 Alumina - 87% Titania - 13%	10 – 45
	AT3 Alumina - 97% Titania - 03%	10 - 53

Table 4.4 Material Details

4.2.2 Load-Penetration observations

Indentation tests are normally used for hardness measurements. This test measures the average contact pressure when the indenter is pressed into a flat surface of a specimen. In recent times, depth-sensing indentation techniques have been widely used, which provide indentation load – depth curve in addition to the plastic residual impression. Such an indentation load-depth curve contains much information on the material properties.

The static indentation test was carried out using INSTRON universal testing machine with hydraulic loading facility. During indentation, the depth of penetration was plotted with respect to the indentation load.

Typical load-penetration characteristics of the three types of Alumina-Titania ceramic composites are illustrated in Fig. 4.9. The observed parametric influence of indentation load (P) and material hardness (H_v) on depth of penetration (h) for the ceramic composites exhibits a non-linear trend. Multiple regression analysis of the data on indentation depth has yielded the following relationship, with an error of about 5%.

$$h = 9.0 \frac{P^{0.6}}{H_v^{0.7}} \qquad 4.2.1$$

Zeng K, *et al*, (1996) have discussed on a general approach to determine mechanical properties of brittle materials, by controlled indentation. In any loading curve of the Vickers indentation process, the indentation load (P) and the corresponding displacement (h) will have a relation of the form $P = Ch^2$; where, C is a constant related to various mechanical properties and C can be obtained by curve fitting the loading date from an indentation P-h curve. Calculated values of C (N/mm2) are shown in Fig. 4.9.

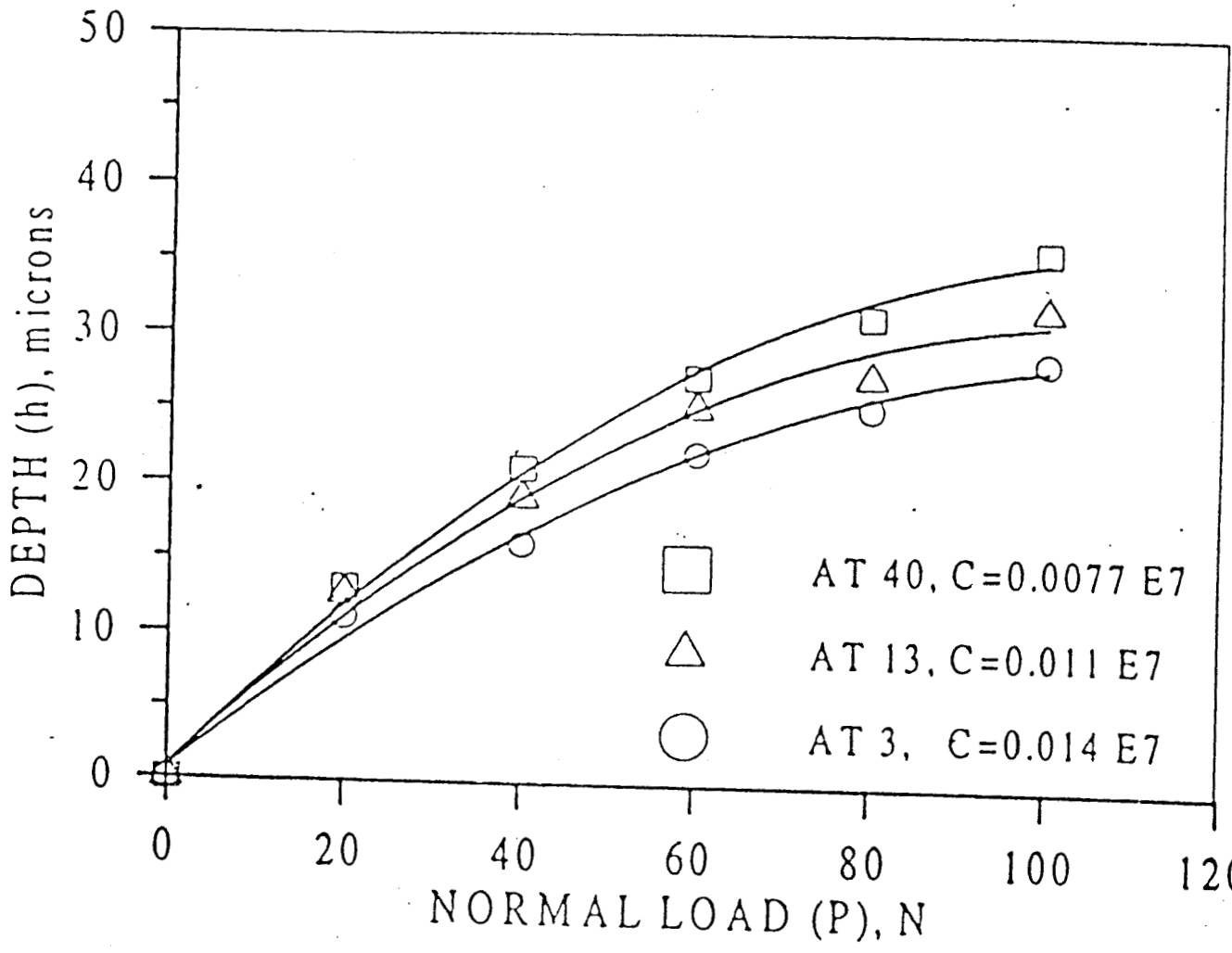

Fig. 4.9 - Typical variation of indentation depth with normal load

According to Zeng, et al, (1996) Compressive yield stress (oy) can be calculated (within 5% accuracy) using

$$\sigma_Y = (0.12) \tan^2 (22) \frac{P}{h^2} \qquad 4.2.2$$

Where, (P / h^2) is the constant, obtained from load – penetration curve for each composition.

Young's modulus (E) was then calculated, using,

$$H = \frac{2}{3} \left(1 + \ln \frac{E \cos 0}{3\sigma_y} \right) \sigma_y \qquad (4.2.3)$$

Where O is the half angle of indenter. (McColm, 1990)

Where H is the average pressure during loading.

$$H = \frac{P}{26.4h^2} \qquad \left(\text{Based on } H = \frac{0.464P}{a^2} \right) \qquad (4.2.4)$$

4.2.3 Observations on crack-indent size ratio(c/a)

During the indentation trial, normal load was applied on the test specimen, through diamond indenter and the indentation obtained was observed under optical microscope, to measure the size of the impression and any possible crack formation. Indentation trials (for

observation of indentation impression), were carried out using Zwick hardness tester at lower loads, and Instron Universal Testing machine at higher loads.

Microscopic observation of the indentations revealed that the Alumina - Titania ceramic composites experienced different magnitudes of indentation load for crack free indentation. This load, termed as critical load for crack initiation was around 50N for AT40, while it was 30N for AT13 and 20N for AT3. This is illustrated as extrapolated points in Fig. 4.10. Owing to the limitation of the testing machine, it was not possible to realise these low load observations using Instron testing machine.

It is seen from Fig. 4.10, that for all cases, the c/a increases up to certain load, above which, a reduction in c/a can be observed. Further referring to the figure, it can be seen that in the case of relatively harder AT3 and AT13 compositions, the c/a increases progressively, while for relatively tougher AT40 composition, a steady value of c/a can be observed up to about 200N. Beyond which, there is an increase in c/a value. the relatively higher toughness of AT40 compared to AT13 and AT3, causes the observed difference in the variation of c/a with applied load. Typical scanning electron micrographs of the indentations of different ceramic composites are illustrated in Fig. 4.11, 4.12, 4.13..

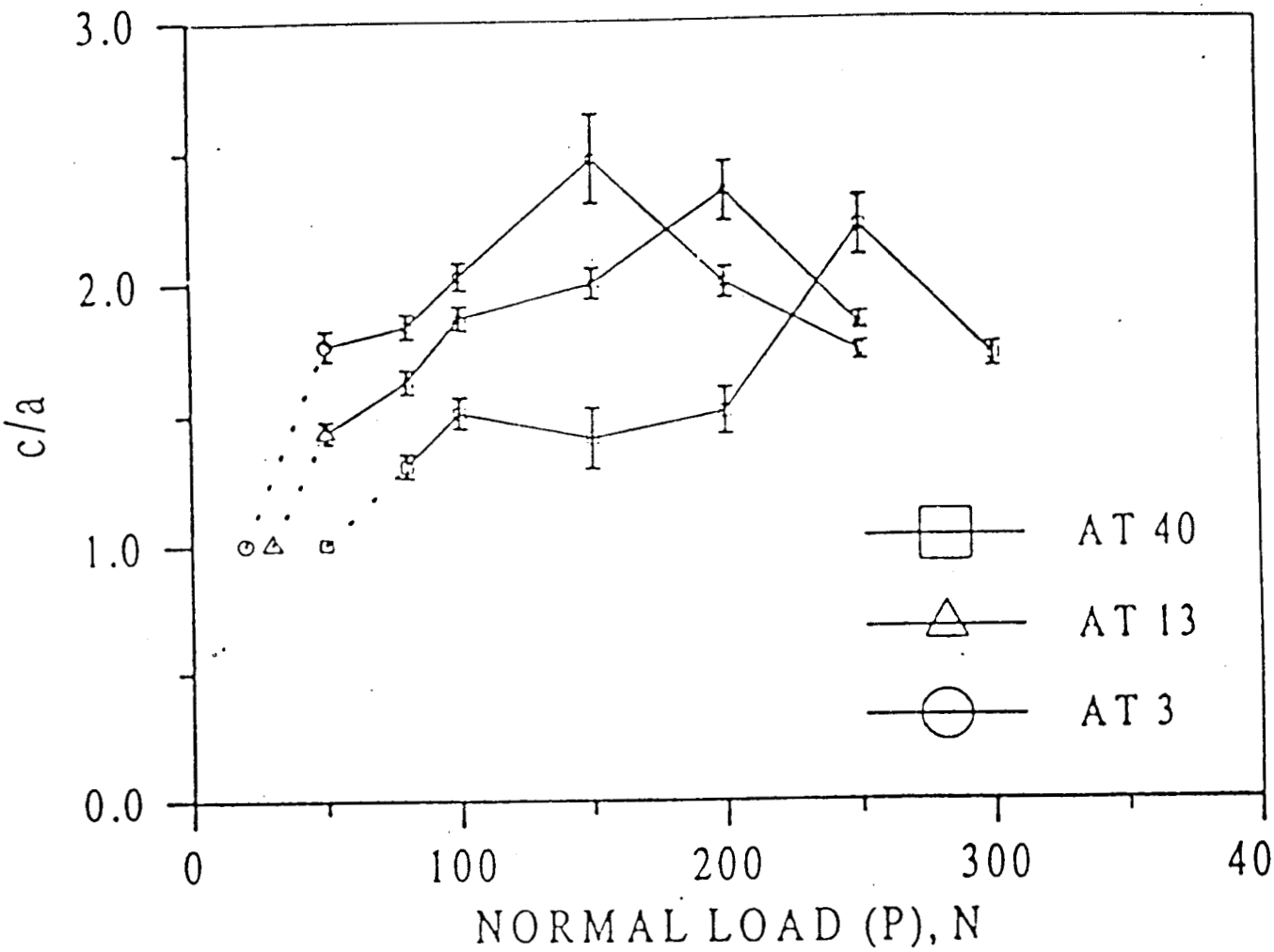

Fig. 4.10 - Typical variation of crack - indent size ratio with normal load

4.2.4 Fracture Toughness Measurement

Ceramics are hard, wear resistant materials, possessing low fracture toughness characteristics. Fracture toughness of ceramics can be evaluated through c/a measurement. Fracture values of different AT composites were determined from the crack – indent size ratios obtained during the initial stages of cracking, using (Cook *et al*, 1995).

$$K_c = 0.0141 \left(\frac{P}{A^{3/2}}\right)\left(\frac{E}{Hv}\right)^{2/5} \log_{10} 8.4 \left(\frac{a}{c}\right) \quad (4.2.5)$$

The properties evaluated, for the different coating system, by conducting static indentation tests are listed in table 4.5. Referring to the data presented in table 4.5, it can be seen that barring those for fracture toughness, all other data concerning mechanical properties are relatively lower compared to those of sintered ceramics. This difference can be attributed to the following.

PROPERTY	UNIT	AT40	AT13	AT3
AVERAGE PRESSURE (H)	GPa	2.9	4.2	5.2
YIELD STRENGTH (o_y))	MPa	1508	2155	2742
YOUNGS MODULUS (E)	GPa	83	116	139
FRACTURE TOUGHNESS (Kc)	MPa.m$^{1/2}$	4.8	4.0	3.6

Table 4.5. Evaluated properties of the coating materials

Indentation tests have been carried out on sprayed ceramic composites, containing certain amount of porosity and possible unmelt particles. Usually indentation of ceramics, especially the sprayed ceramics is a complicated material dependant process, involving elastic, plastic deformation and elastic recovery i.e. during indentation there will be an outward material flow around the indenter and during unloading, the material may coil back around the indenter, upsetting the formation of indentation. This calls for controlled indentation process, so that no undue material duress is introduced. In the present study, evaluation of mechanical properties through load penetration characteristics is in the higher range of loading, wherein all the ceramics have experienced certain amount of radial cracking. This could have resulted in the observed smaller values for physical properties. however, the test has facilitated fairly reasonable estimate of fracture toughness values.

4.2.5 AE response to indentation

Acoustic emission signals are the elastic waves released by a material under stress and as such they can be good indicators of the material response to a working environment. James Lankford, *et al*, (1979b) have studied the AE signal characteristics of different sintered ceramic materials along with scanning electron microscopy to establish the threshold load for crack initiation under indentation. The authors have found detectable AE activity only at the initiation of radial cracks on the indented surface. At loads, higher than

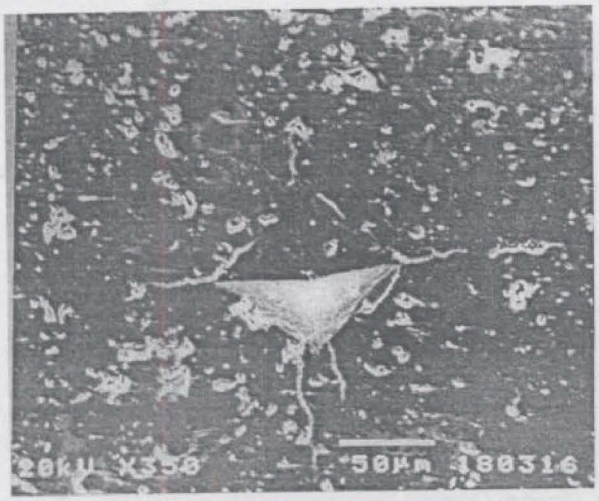

50 N

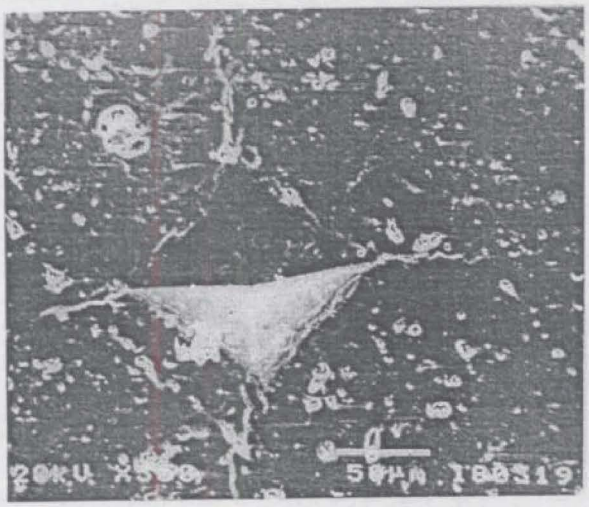

100 N

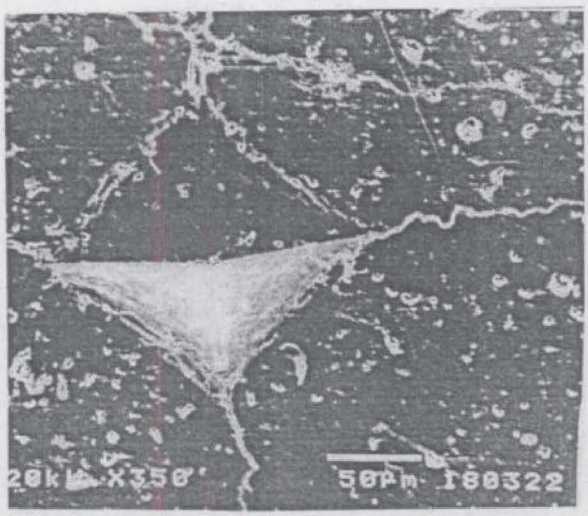

150 N

Fig. 4.11 Typical SEM of indentationm (AT3)

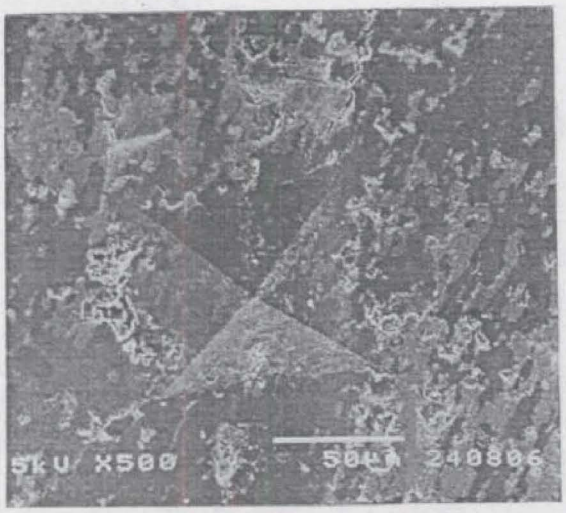

50 N

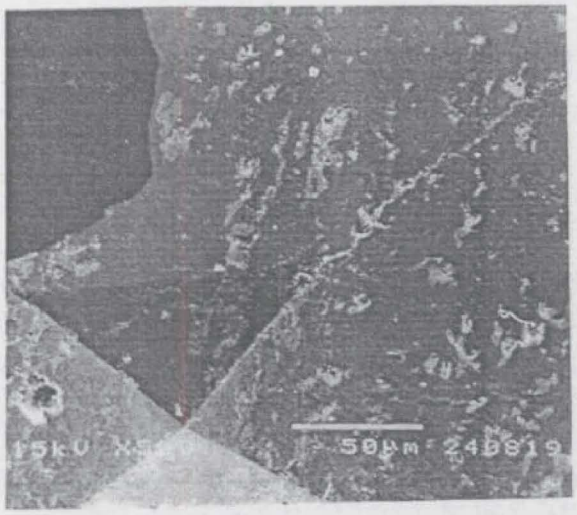

150 N

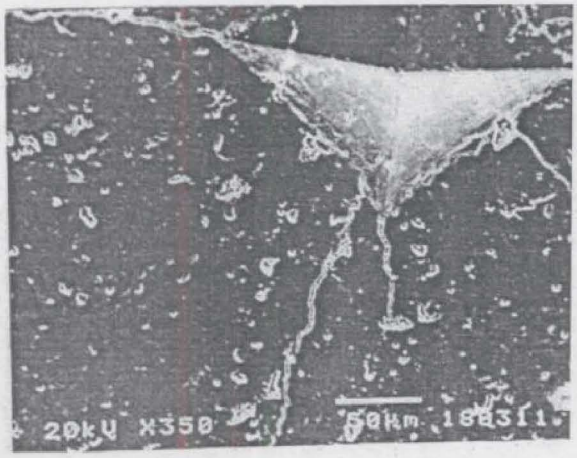

200 N

Fig. 4.12 Typical SEM of indentaion (AT13)

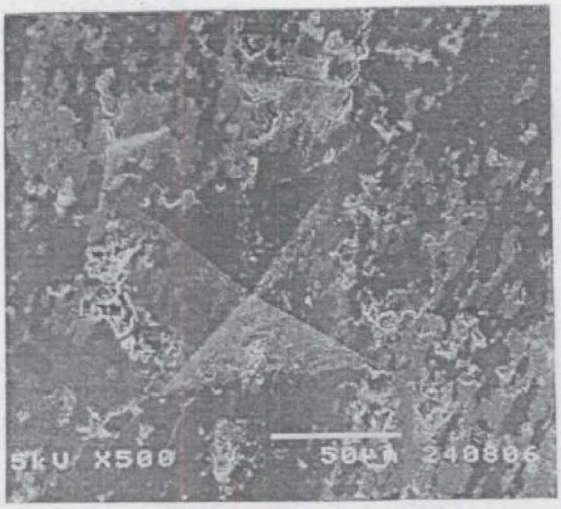

50 N

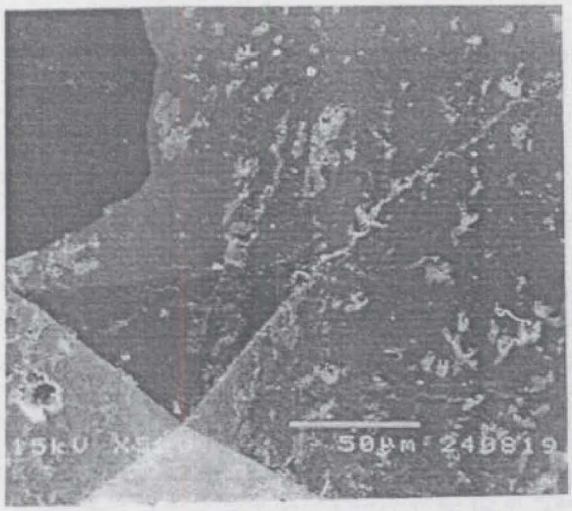

150 N

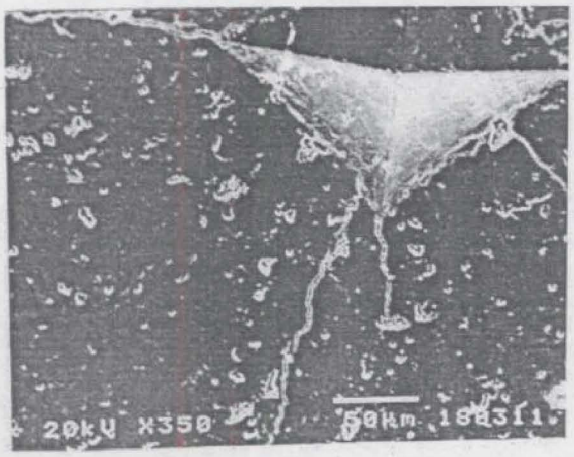

200 N

Fig. 4.12 Typical SEM of indentaion (AT13)

threshold, the AE activity has been found to increase with load. However AE activity was bit identified during crack free indentation. Unlike Lankford, Javad Akbari et al, (1994) have identified AE activity even during crack free indentations and the AE activity has been found to increase with load.

4.2.6 Observations on AE wave forms.

Typical AE signal waveforms and the corresponding power spectrum of the acoustic emission recorded at different stages of indentation are shown in Fig. 4.14 – 4.19. It can be clearly observed from the raw signals that lower order AE signals are emitted at low loads, even during crack free indentation. AE activity has been observed to increase with load for all the materials upto a certain extent. After reaching the stage of maximum AE activity, any further increase in load has only resulted in emissions of lower order. The load at which maximum AE activity is observed has been found to be different for different Alumina-Titania compositions. for AT3 composition, higher order AE activity has been observed around a load of 150N. Similarly, higher order emissions for AT13 and AT40 have been observed at normal loads of 200N and 250N respectively.

Referring to the illustration on power spectrum (Fig. 4.15), it is seen that AE signal acquired for AT40 ceramic is a composite signal, containing dominant peaks in the range of 1 – 300 kHz. With low loads, predominant peaks can be seen in the low

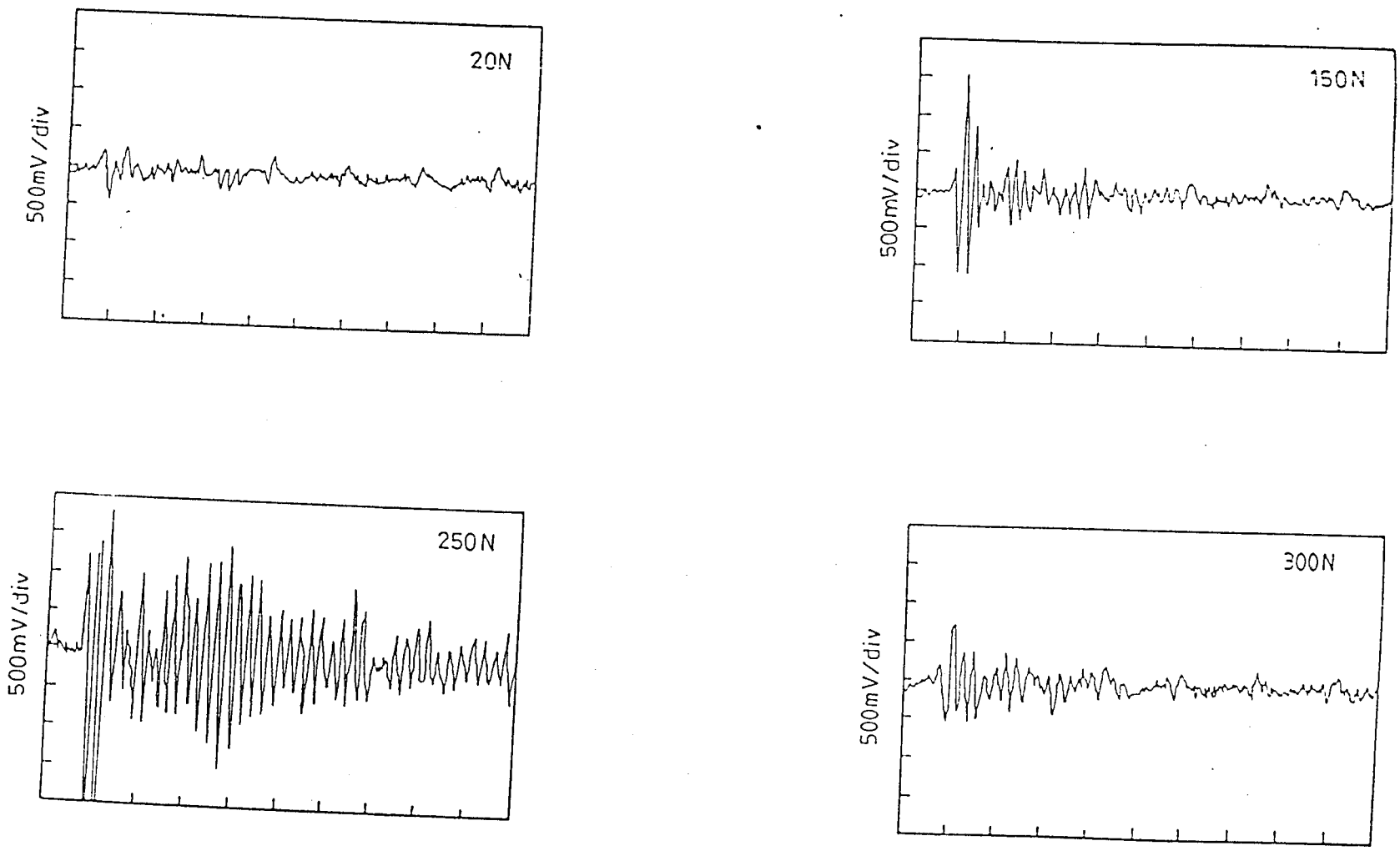

Fig. 4.14 Typical raw AE signals at different loads (AT40)

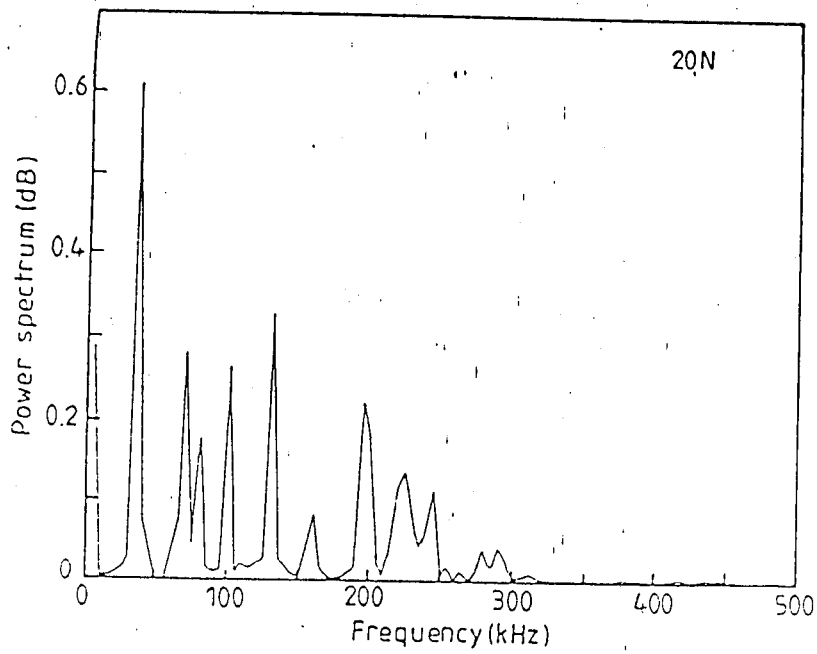

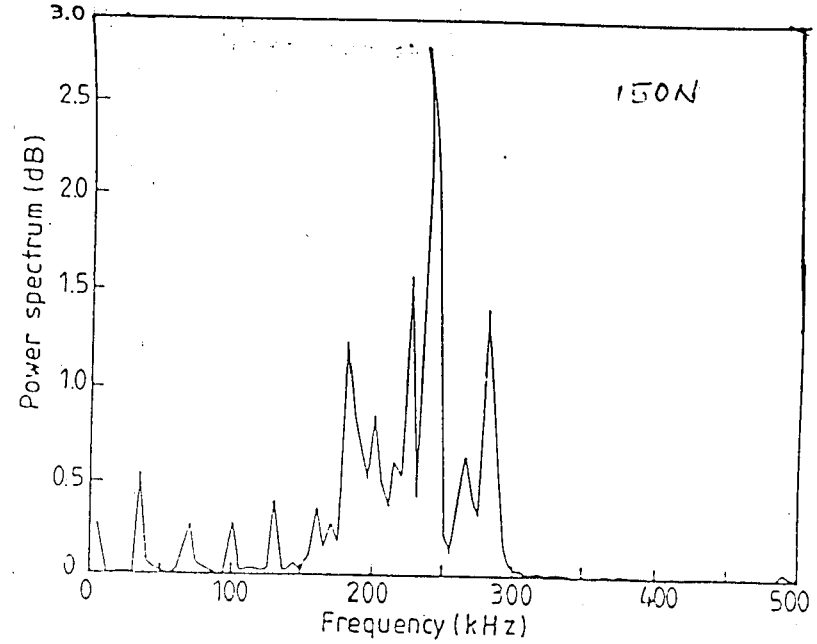

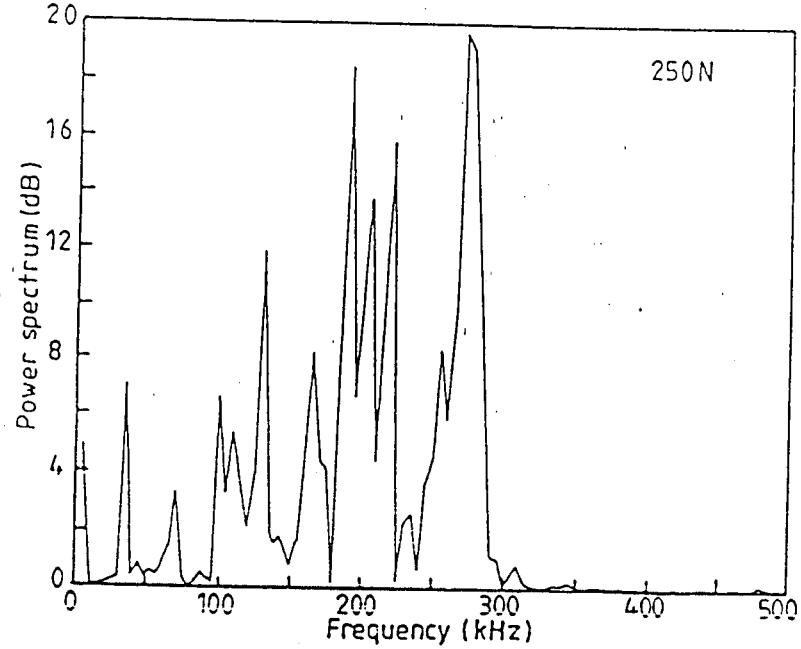

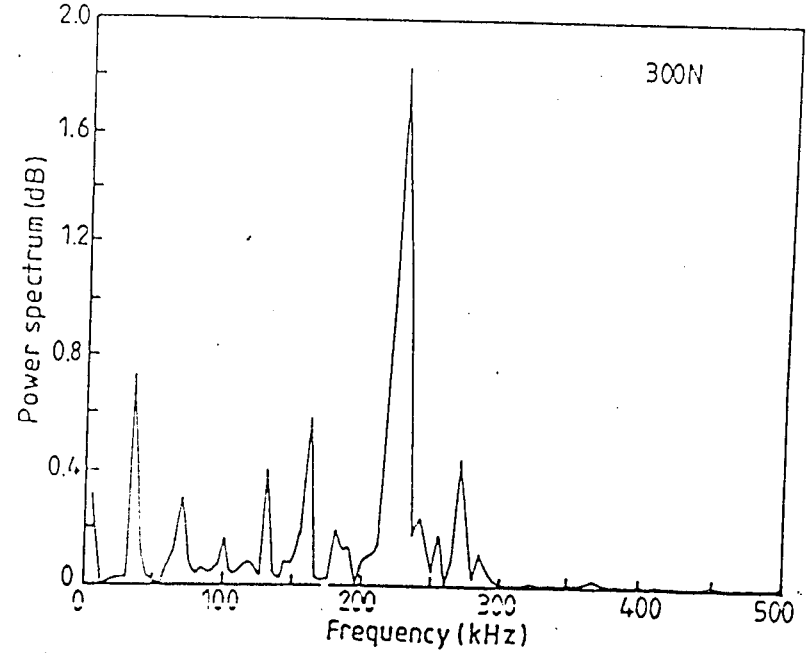

Fig. 4.15 - Typical power spectrum of AE signals at different loads (AT40)

Fig. 4.16 Typical raw AE signals at different loads (AT3)

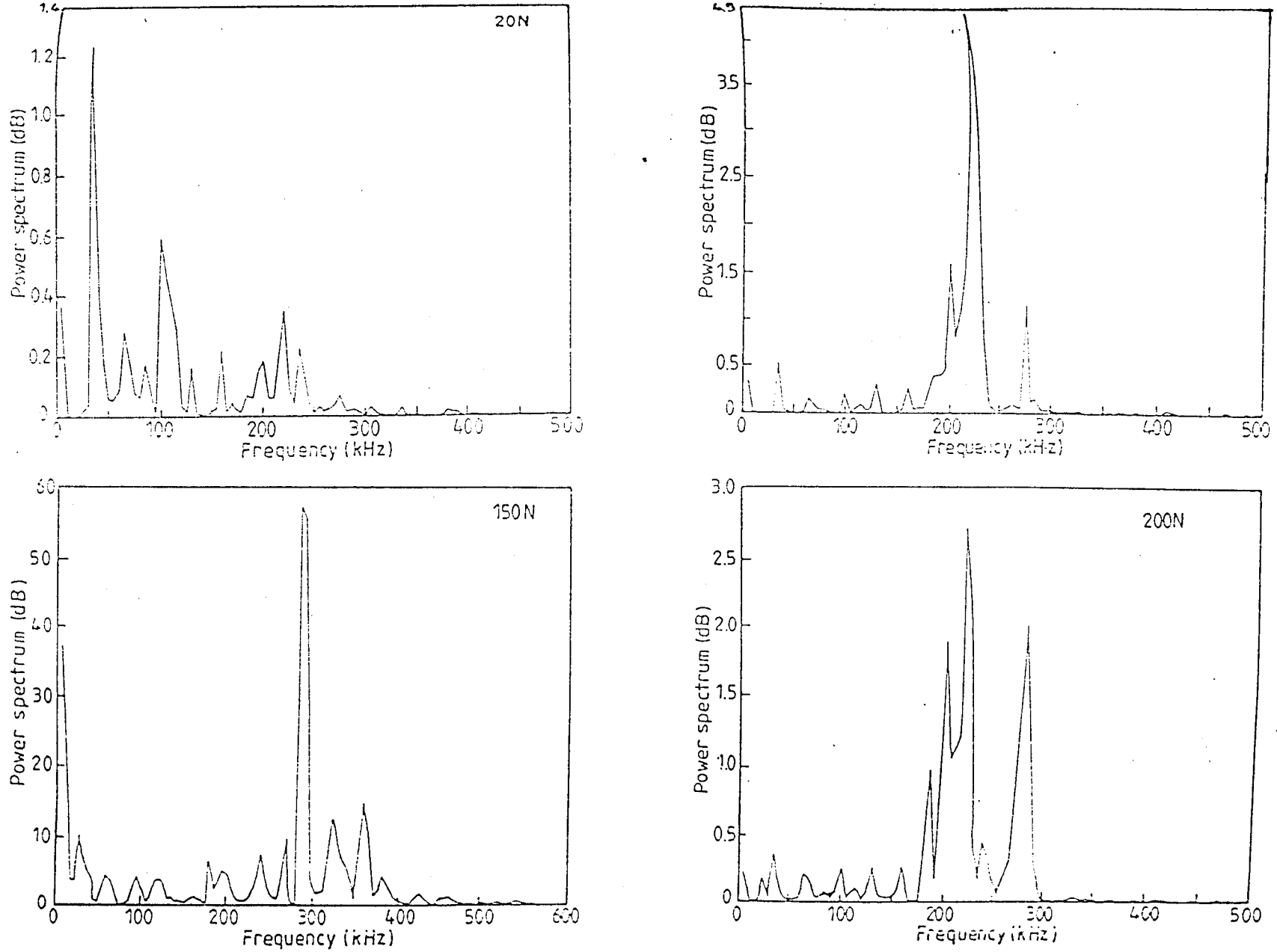

Fig. 4.17 Typical power spectrum of AE signals at different loads (AT 3)

Fig. 4.18 Typical raw AE signals at different loads (AT 13)

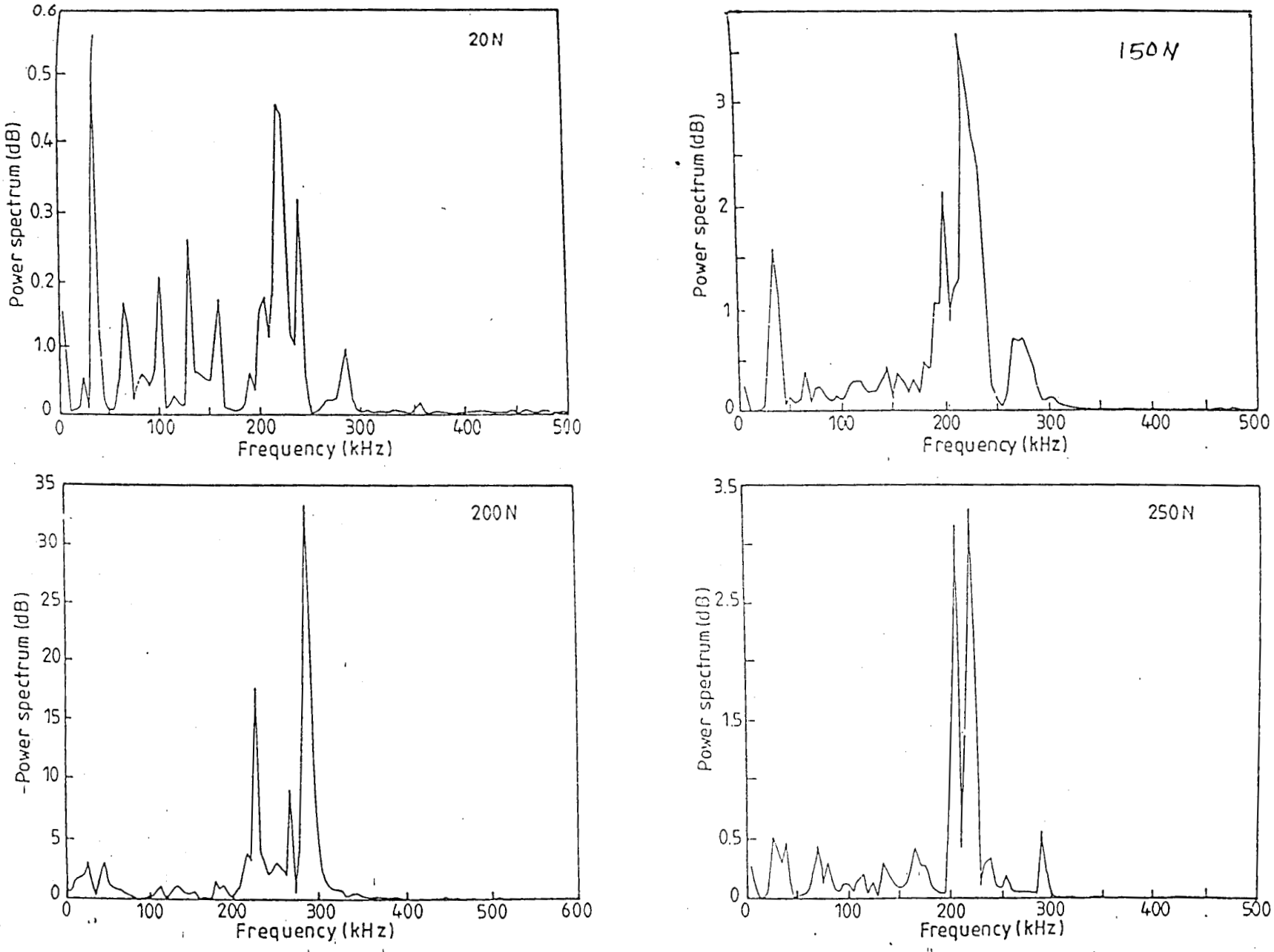

Fig. 4.19 - Typical power spectrum of AE signals at different load (AT12)

frequency range of 30 – 50 kHz. this indicates the deformation mode of the ceramic composite subjected to low indentation loads. With increasing load, there is a rise in the emission level with the individual peal amplitude increasing, upto 250N, above which, there is a reduction in the magnitude of signal emission. Also, with increase in load, there is a rapid increase in amplitude of peaks over the range of 150-300 kHz. The occurrence of higher amplitude peaks in the relatively higher frequency range indicates the on-set of cracking and associated burst mode acoustic emission.

In the case of AT3 ceramic also, the acquired AE signal (Fig. 4.17) is a composite one containing different peaks in the frequency range of 1 – 300 kHz. With low load (230N), relatively lower magnitude of emission is seen (dominating frequency in the range of 30-50 kHz), indicating that the ceramic composite undergoes only plastic deformation. As the load increases, there is an overall rise in peak amplitude, especially that of the peaks in the range of 200-300 kHz. A critical load of 150N is seen beyond which there is a reduction in the power of the AE sugnal acquired. The occurrence of predominant peaks with 200-300kHz indicates the on-set of cracking/distress in the material. Further loading has only resulted in reduced magnitude of emitted AE signal.

AE signal acquired for AT13 ceramic is also a composite signal (Fig. 4.19). Typically dominant peaks in the low frequency range of 30-50kHz for low loads and high amplitude dominating peaks in

the range of 200-300kHz with high indentation loads can be seen in the illustration. This ceramic composite also emitted AE signal of similar nature. A critical load of 200 N, at which maximum rise in peak amplitude occurs, can be seen.

AE signal acquired for AT13 ceramic is also a composite signal (Fig. 4.19). Typically dominant peaks in the low frequency range of 30-50kHz for low loads and high amplitude dominating peaks in the range of 200-300kHz with high indentation loads can be seen in the illustration. This ceramic composite also emitted AE signal of similar nature. a critical load of 200N, at which maximum rise in peak amplitude occur, can be seen.

Typical observed variation of the RMS values of the monitored AE signal, with the indentation load is plotted in Fig. 4.20. It is interesting to note that the nature of variation of the RMS value is similar to that of c/a value. The observed smaller magnitude of RMS value for AT40 can be attributed to the material being relatively softer compared to the other two and thus, deforms steadily, giving out low amplitude, continuous mode AE signals.
Typical influence of the indentation load on dominating frequency is illustrated in Fig. 4.21 It is interesting to note that upto around 20-30N for AT & AT13,a and 50N for AT40, relatively smaller order dominating frequency has occurred, indicating the continuous mode of acoustic emission (flow less indentation); while with increased loads, there is a rapid increase in the magnitude of dominating frequency. This is attributed to the occurrence of burst emission

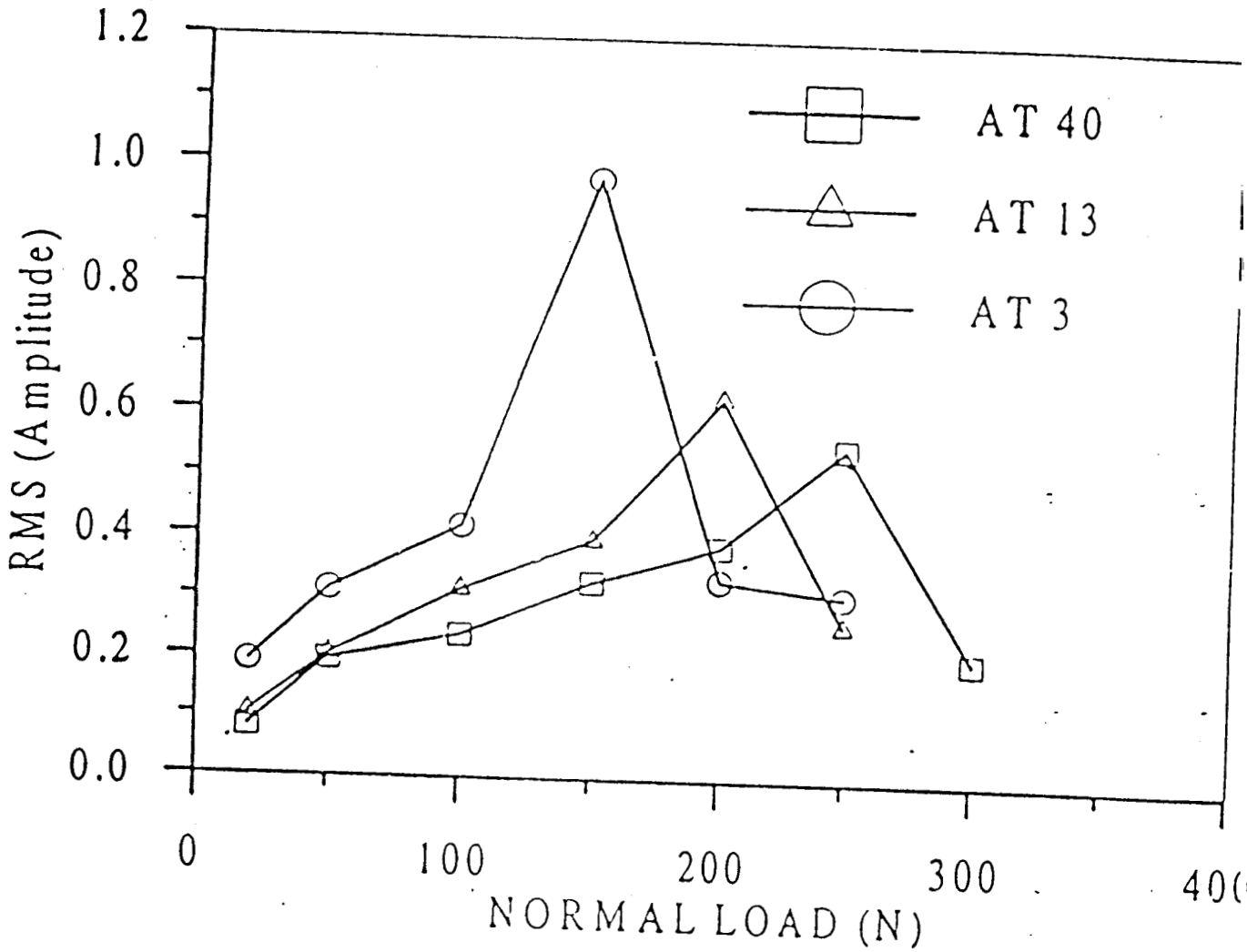

Fig. 4.20 - Typical variation of rms (AE) with normal load

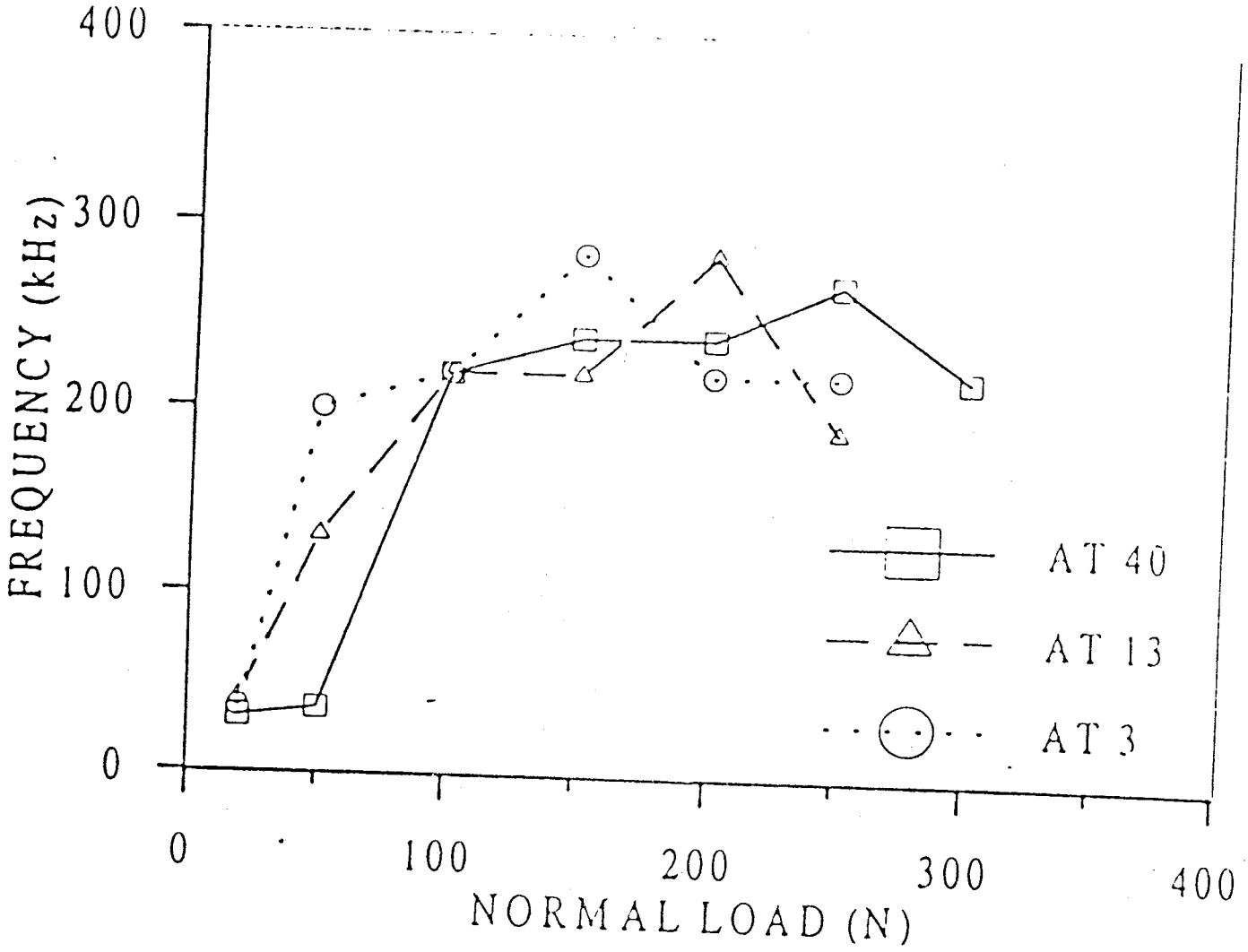

Fig. 4.21 - Typical variation of AE frequency with normal load

associated with cohesion cracking of the ceramic composites. The illustration of dominating frequency also resembles that of c/a values. Thus the observed characteristics of the AE signal clearly indicates the response of ceramic composites during indentation.

4.2.7 Discussions

Detection of AE signals at very low loads indicate, that elastic strain energy is also released at stress levels, which are far below the fracture stress. The results of signal analysis indicate that the AE characteristics of the signal generated by plastic deformation and cracking are significantly different. With increasing cracking rate, the high energy, high oscillation signals are observed.

In ceramics, because of their brittle nature, there will be very little plastic deformation before cracking. Thus, the strain energy release rate by plastic deformation is less than the energy released by cracking. This is the reason for the observed higher order AE signal during cracking mode compared to that during plastic deformation mode.

4.2.8 Summary of static indentations studies

Plasma-sprayed Alumina-Titania systems of three different grades were subjected to indentation loads, to study the material response to point loading. Summing up, it is observed that

1. Mechanical properties like elastic modulus and fracture toughness of the coating materials can be characterised by conducting displacement sensing indentation tests.
2. Initiation of radial crack was found to occur at 20N for AT3, 30N for AT13 and at 50N for AT40; further, the load for rupture was 150N for AT3, 200N for AT13, and 250N for AT 40 respectively.
3. It has been observed during low load indentation, deformation mode of the material response was associated with a dominating frequency of the AE signal in the range of 3-50kHz and, for cracking at higher loads, the dominating frequency was in the range of 200-300 kHz.

4.3 Controlling Glaze Surface Effects

Introduction

Demand is increasing for products with glazes that have unique aesthetic effects. These effects include variations in gloss, texture in the glaze and presence of specks or crystals. When present in or on the surface of a glaze, these effects can improve the appearance of the glaze for many consumers.

Studio potters have developed unique glaze surface effects for many years. Many attractive glazes have been produced. The problem with much of this work is that it is the result or random, uncontrolled variations. In many cases, the potter does not know what caused the beautiful result obtained and has no idea how to duplicate it. This is similar to the problem of duplicating ancient

Chinese porcelain, where an occasional outstanding result was sent to the Emperor, while the millions or ordinary pieces were marketed elsewhere.

For commercial operations, a glaze must be reproducible over time and over repeated glaze batches and production runs. Hence, the problem to be solved is to produce aesthetically pleasing variations to the appearance of a glaze in a controlled, reproducible way. This is not easily done, because materials that induce variations are by their nature reactive, often leading to random, uncontrolled variations.

4.3.1 Alumina as a Glaze Component

What then can be done in a controlled, reproducible way to produce aesthetically pleasing variations in glazes? Let us begin with a consideration of one material – alumina. That material is available in a wide variety of particle sizes (20 to – 400 mesh) and purities (90 to 99.999% $A1_2O_3$) as a result of refractory and abrasives industries markets.

As a glaze constituent, alumina is reported to have a nonlinear behaviouron the gloss. At low levels ($\leq$5 wt%), alumina increases gloss by suppressing phase separation between silica and boron oxide and / or alkaline-earth oxides. At high levels (>10wt%), alumina lowers gloss because of crystallization of alumina-contained phases, primarily anorthite ($CaO.A1_2.2SiO_2$).

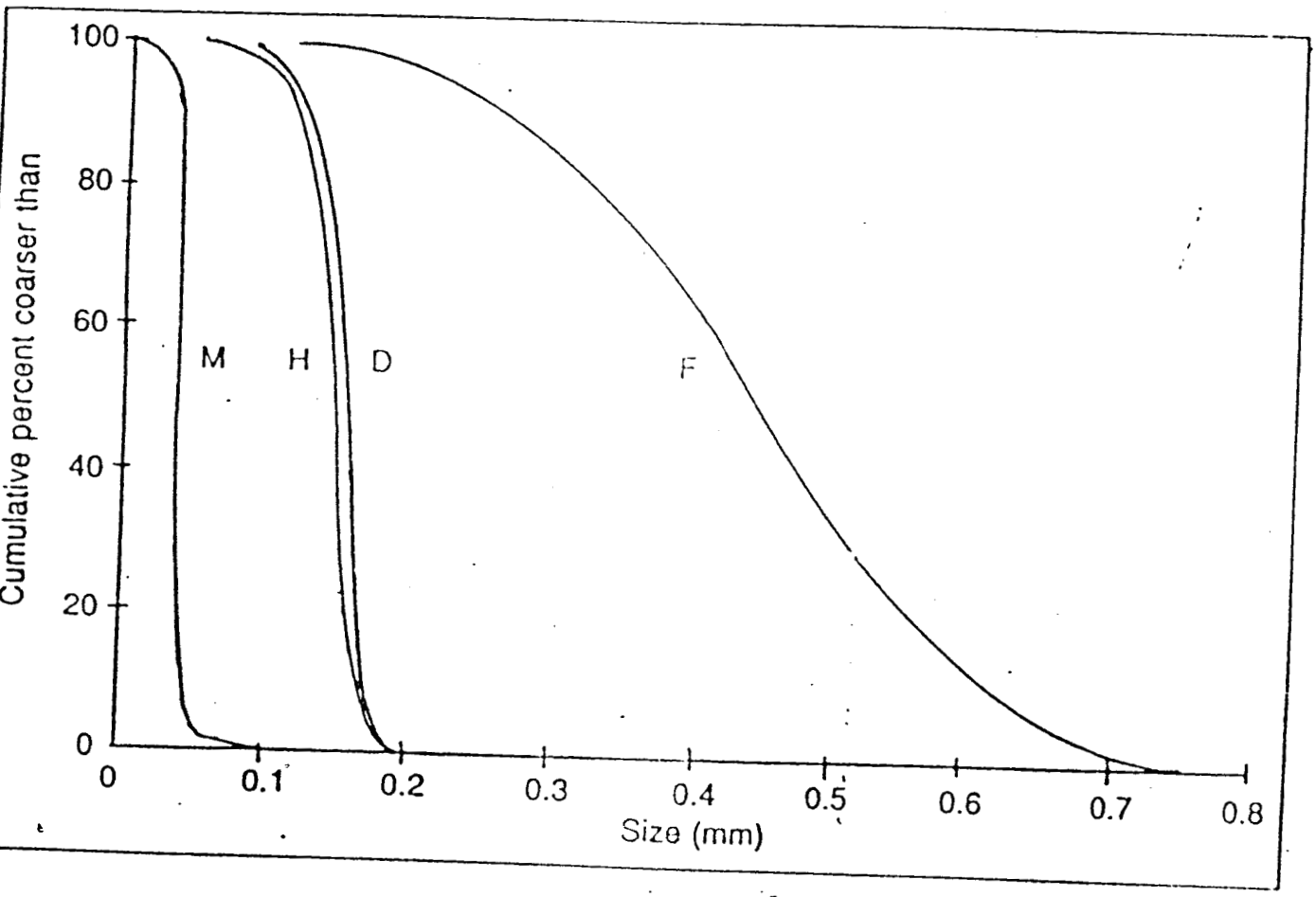

Fig. 4.22 - Particle sizes of four aluminas used for investigation

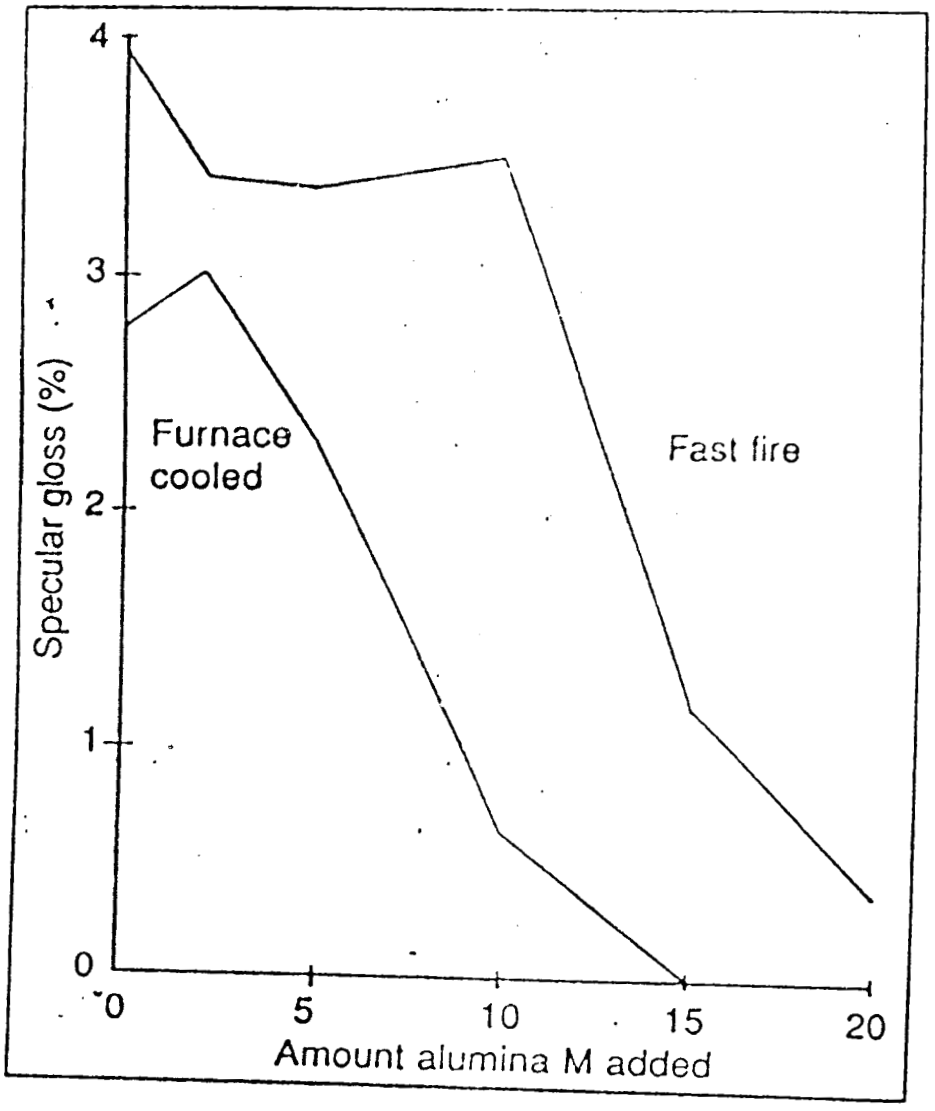

Fig. 4.23 - Specular gloss of tile was plotted vs. alumina M addition

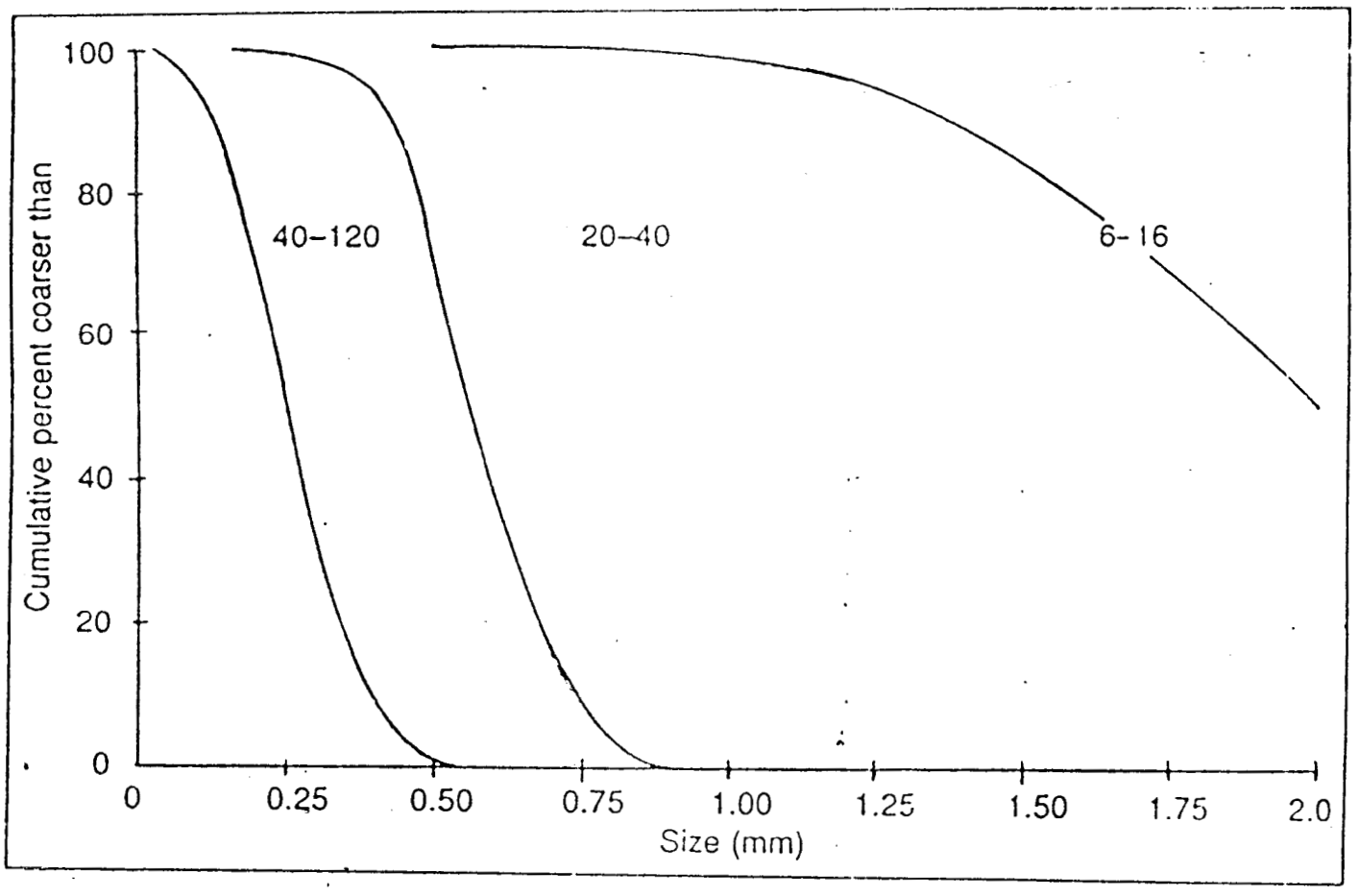

Fig. 4.24 - Particle sizes of synthetic specks

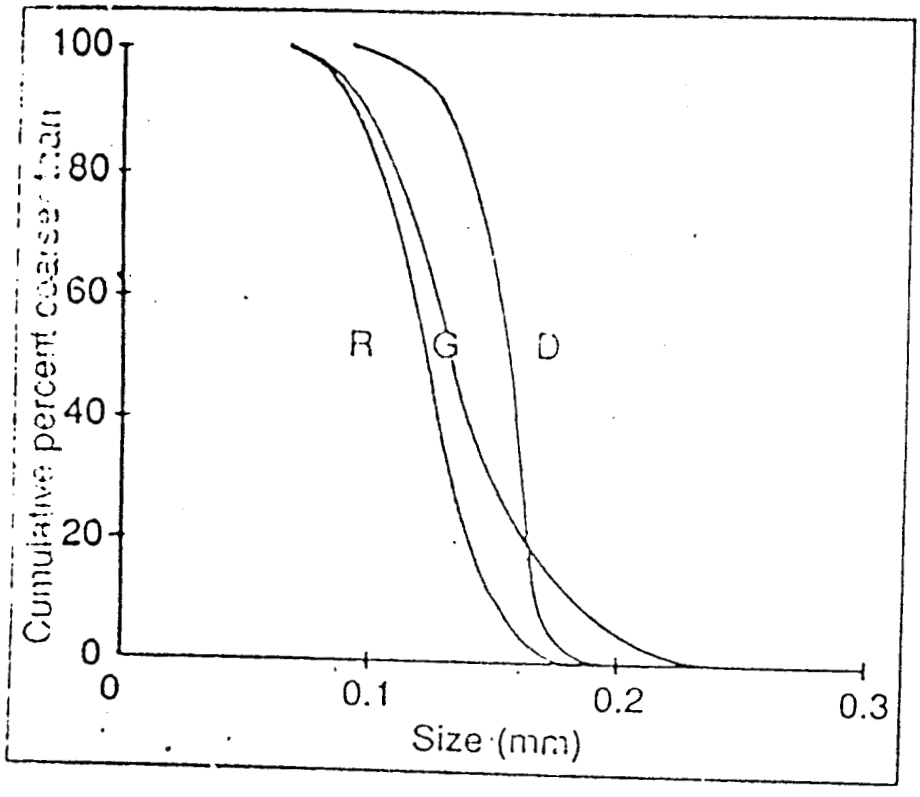

Fig. 4.25 - Particle sizes of (M) alumina M, (R) natural rutile and (C) black iron oxide

Let us first examine the effect of particle size. For that purpose, we add 2 wt% of several A1 aluminas of various particle sizes to a goiven base glaze. That base glaze contains 8.3 mol% alumina, added as frit, fledspar or clay. These raw materials react readily during the firing process to become part of the vitreous glaze structure. By contrast, pure alumina as a glaze raw material, even at –325 mesh particle size, is much less reactive. Various particle-size distributions (PSDs) of several aluminas are added to the base glaze. Alumina F has a d_{50} of 0.44 mm and range from 0.7 to 0.2 mm. Alumina Da has a $d_{50\ of}$ 0.158 mm and range from 0.18 to 1.10 mm. Alumina H has a d_{50} of 0.149 mm and a range from 0.18 to 0.10 mm. Alumina H is a pure, white alumina, and alumina D is a less-pure, dark alumina. Alumina M has a d_{50} of 0.04 mm and a range from 0.06 to 0.02 mm; it is a –325 mesh product usually used in glazes.

Tiles were coated with glazes containing 2 wt% of each of the four aluminas in the base glaze. The glaze containing 2 wt% of alumina F with d_{50} of 0.44 mm exhibited significant texture. Around individual alumina particles, the glaze was raised above the surface. The alumina particles were randomly dispersed over the surface, yielding a more-or-less uniform texture. It was a texture that could have application where slip resistance is desired.

The glaze with 2 wt% alumina F addition was coated on the same tile and on a tile with a glaze that had an added 5 wt% of a vanadium zircon blue pigment. In the latter glaze, the white

alumina particles yielded texture and gave a random pattern of white specks dispersed over the glaze surface. The glaze containing 2 wt% alumina D with d_{50} of 0.158 mm had a fairly smooth surface. The glaze exhibited a mottle of dark alumina particles in the clear base glaze. The mottle was fairly uniform, because it was produced using an alumina of narrow PSD. By contrast, the glaze containing 2 wt% alumina H, which is similar to alumina D in particle size, did not show visible differences over the surface. The colour of the glaze was whiter than the glaze with 2 wt% alumina M, the –325 mesh alumina, which indicated that particles of alumina H ; although not individually visible, were acting as an opacifier.

Thus, selection of an alumina crystal of appropriate particle size could be used to produce an aesthetic effect. The coarsest particles, where d_{50} is ~0.4 mm, yielded a texture to the glaze surface. where d_{50} was ~0.15 mm, particles of contrasting colour produced a mottled glaze. These same materials at d_{50} of ~0.4 mm blended completely into the glaze.

Another way that alumina can yield an aesthetic effect is by affecting the gloss. The base glaze contains 8.3 wt% alumina. Therefore, we expect additions of alumina to decrease the gloss. A series of tile with glaze having progressive additions of –325 mesh alumina (Alumina M) has been prepared. Photographs have been taken at a low angle to reveal the specular gloss, which differentiates a glossy glaze from a satin and a matte. The base

glaze and the glaze with 2 wt% alumina M are glossy. The glaze with 5 wt% alumina M is satin. The glaze with 10 wt% alumina M is low satin, almost matte. The glaze with 15 wt% alumina M is a dead matte.

These glazes were fired in an electric kiln equipped with a kiln sitter. The kiln ran at full power until the cone-one control cone deformed, which shut off the kiln. The ware cooled 2-3 h in the furnace until the ware was below 400°C, where no further crystallization was possible.

Similar glazes were fired in a pusher kiln that simulated fast firing. Again, the simulated fast firing. Again, the photographs were taken at low angle to reveal the specular gloss. The set point of the hot zone of the kiln when these glazes were fired was 1130 °C. The tile were pushed 2 in every 4 min, for a 44-min. cycle, cold to cold. a different result was obtained when this more rapid cooling cycle was used. The base glaze, the glaze with 2 wt% alumina M, the glaze with 5 wt% alumina M, the glaze with 10 wt% alumina M wre glossy. The glaze with 15 wt% alumina M was a low satin, and it incompletely smoothed out in the rapid fire. A glaze with 20 wt% alumina M was matte, and it was not fired out and porous.

The results of two firing methods were compared. The large difference in the gloss when 10 wt% alumina was added was

particularly noticeable. This illustrated the importance pf cooling rate in growing the crystals responsible for the matte effect.

The specular gloss of the tile was measured and plotted versus alumina M addition. To obtain the specular gloss the reflectance of the tile ws meased at 16 points across the visible spectrum, with and without the specular component included. The two sets of data were substrated to obtain the specular component of the gloss, and the 16 values were arranged. There was a large difference in these two curves, depending on the cooling rate of the glazes. Those cooled in ~15 min remained glossy until >10 wt% alumina M was added, whereas the tile cooled for 2-3 h were satin at 5 wt% alumina M and matte at slightly more than 10% alumina M.

Dark alumina D. with d_{50} of 0.158 mm and a range from 0.18 to 0.12 mm, was a suitable material to produce a mottled glaze, i.e., one with a variable color. We also observed the glazes produced by additions of 2 wt% alumina D and 5 wt% alumina D to the same base glaze. at 2 wt%, we had a mottle of gray and white, wheras, at 5 wt%, we had a mottle of black and gray. Two different – appearing glazes were formed by changing the concentration of the material used to produce the mottle.

A limitation on the usefulness of materials to produce a mottle is that most materials are available only commercially a fine powders or as coarse chunks. It is somewhat difficult to locate materials

available commercially with particle sizes in the vicinity of d_{50} of 0.15 mm. However, alumina is not the only material available in an appropriate particle size. There are other natural materials available in the appropriate particle size.

4.3.2 Natural Rutile as Glaze Component.

Natural rutile, beneficiated but not purified, is material that is available for purchase in an appropriate particle size. It has a d_{50} of 0.121 mm and range from 0.18 to 0.07 mm. Natural rutile has a composition of ~94 wt% TiO_2, 2 wt% SiO_2 and 1 wt% ZrO_2 and FeO_3.

Natural rutile was dispersed in the base glaze at 2 and 5 wt%. a dark colour resulted, primarily from the Fe_2O_3, and small (<1%) amounts of V_2O_5 and Cr_2O_3. There were substantial differences between the two concentration levels. At 2 wt% addition of natural rutile, we had a mottle of variable shades of gray. At 5 wt% addition of natural rutile, we had a mottle of black with dark-gray.

A coarse version of black iron oxide also is available. It has a d_{50} of 0.131 mm and range from 0.22 to 0.07 mm. This material was dispersed in the base glaze at 2 and 5 wt%. a 2 wt% addition of coarse black iron oxide produced a mottle of grays from black to light-gray. a 5 wt% addition of coarse black iron oxide produced a mottle of gray in black.

4.3.3 Synthetic Specks as a Glaze Component.

In addition to these natural materials, there are speciality firms that make synthetic specks. Specks are mixtures of pigments with frit fluxes and thermoplastic organic binders. The mixtures are heated to polymerise the thermoplastic medium and then brocken-up and screened into controlled particle-size fractions. Use of these synthetic materials provides some additional flexibility in the creation of unique aesthetic effects, beyond what is possible using natural materials. the use of synthetic specks greatly expands the number of materials that can be considered. In particular, it adds the variable of colour. Essentially, any colour that can be produced in a ceramic pigment can be prepared as a speck.

A second variable is particle size. a wide a\range of PSDs is commercially available. Particles range from chunks several millimetres in size down to mean sizes comparable to the natural materials described earlier. The coarsest speck (6-16 mesh) has a d_{50} of 2 mm and a range from 1 to 5 mm. The 20-40 mesh speck has a d_{50} of 0.56 mm and a range from 0.82 to 0.35 mm. The 40-120 mesh speck has a d_{50} of 0.26 mm and a range from 0.50 to 0.09 mm.

Three glazes were made by adding 2 wt% of one of these three specks to the base glaze. With the coarse (6-16 mesh) speck in the glaze, individual chunks of the speck extended above the glaze surface, producing texture in the glaze surface. With the 20-40

mesh speck in the glaze, the glaze surface was smooth, but individual specks were visible in the white matrix. With the 10-120 mesh specks in the glaze, there was a mottled surface similar to that obtained with natural materials of similar particle size.

Depending in the choice of frit flux, it also was possible to prepare a speck that, in the firing process, began to melt and spread out into adjacent areas of the glaze, but not dissolve completely. Various effects were achieved. The glaze with 2 wt% of the coarse (6-16 mesh) speck did not melt during firing. The glaze with 2 wt% of a speck with the same pigment, pigment concentration and PSD did begin to melt during firing. In this case, the pigment spread into adjacent areas of the glaze.

Glazes containing 2 wt% of a spreading speck in the base glaze were prepared. In the glazes with finer-particle-sized specks, the spreading effect manifested itself in a somewhat more diffuse mottle than was the case with the nonspreading specks. In the glaze with 2 wt% of the 20-40 mesh speck, individual particles were observed, but the interfaces were blurred instead of sharp. In the glaze with the 40-120 mesh speck, the mottle was more muted than with the non spreading speck, the mottle was more muted than with the non spreading speck, to the point that individual particles did not stand out.

In addition to the variations due to particle size and to spreading versus non spreading, there was a variation due to concentration of

the speck in the glaze. Three concentrations of the nonspreading 10-120 mesh speck in the base glaze were prepared. At a 1 wt% level, there was a light-purple mottle. At a 2 wt% level, the colour of the individual specks was clearer. At a 5 wt% level the mottle was between varying shades of the purple speck. The white of the base glaze was no longer apparent.

In summary, there are several ways to produce an aesthetically pleasing variation in the appearance of a glaze. Alumina can be used to adjust the gloss of the glaze. The specific levels of alumina needed depend on the cooling cylce used.

Most of the ways to produce these variations involve use of relatively coarse particles, with sizes ranging upward from a d_{50} of 1.1 mm. these include particles of alumina, rutile and iron oxide. Greater possibilities for variations come from the use of synthetic specks. Synthetic specks provide possibilities for variation in colour, particle size, spreading versus nonspreading and concentration of the speck in the glaze.

4.4 POLISHING PROCELAIN TILE

Introduction.

Polished porcelain tile's high gloss and hardness have ld to strong growth in the product's market share. Porcelain tile polishing is performed by grinding –tool friction on the tile surface,.

Long polishing trains are used in which tile thickness is decreased as much as 10% to produce smooth, high-gloss products. the polishing process actually consists of several operations.

In the process phase (levelling step), tools are used that contain coarse abrasive grains (diamond) to dress and level the tile surface to remove a great quantity of material. In the second process phase (actual polishing step); grinding tools are used that contain abrasives with progressively decreasing grain sizes to produce the desired end texture and gloss.

The main abrasive used in the grinding step is SiC embedded in an organic or inorganic matrix of variable composition, At present, the sequence of abrasives and time each abrasive works on the tile are based a\on experience, because there is insufficient knowledge of the effect of each abrasive on the tile surface.

This paper addresses the changes that result in the porcelain tile surface during the polishing operation. Exhaustive sampling has been accomplished along the length of an industrial porcelain-tile polishing line. the evolution of certain tile properties (mass. gloss and surface texture) has been observed using SEM.

Based on the evolution observed, an interpretation of the mechanisms that produce material removal during the polishing operation has been attempted. Finally, as suggested in the literature, scratch tests have been conducted using a single-point

Table – 4.6

Sample tile Positions in the Polishing Train, Grit and Abrasive Grain Size Distribution in the Last Tool to Work on the Sample			
Tile No	**Grit**	**Size range (um)**	**Diameter, d_{50} (um)**
2	36	600 – 425	
4	36	600 - 425	
6	36 – 46	600 – 425 / 425 – 300	
8	46	425 – 300	
10	46 – 60	425 – 300 / 300 – 212	
12	60 – 80	300 – 212 / 212 – 150	
16	80 – 100	212 – 150 / 150 – 106	
20	120	125 – 90	
24	120	125 – 90	
36	150 – 180	106 – 63 / 90 – 53	
44	240 - 280		44.5 – 36.5
52	400		17.3
54	600		9.3
56	600		9.3
58	800		6.5
60	800		6.5
68	1500		<6
72	LUX		

Table – 4.7

Estimated Number of Abrasive Grains per Unit Grinding Tool Volume (N) for Grits 36, 600 and 1500, as a Function of Grit Average Grain Size (d_{50}) and Grinding Tool Abrasive Mass Fraction (X_{SIC})			
Grit (um)	d_{50} (kg SIC / (kg tool)	X_{SIC} (number of SIC grains/(cm^3 tool)	**N**
36	525	0.12	1.0×10^9
600	32.8	0.6	2.0×10^{13}
1500	5.5	0.4	2.5×10^{15}

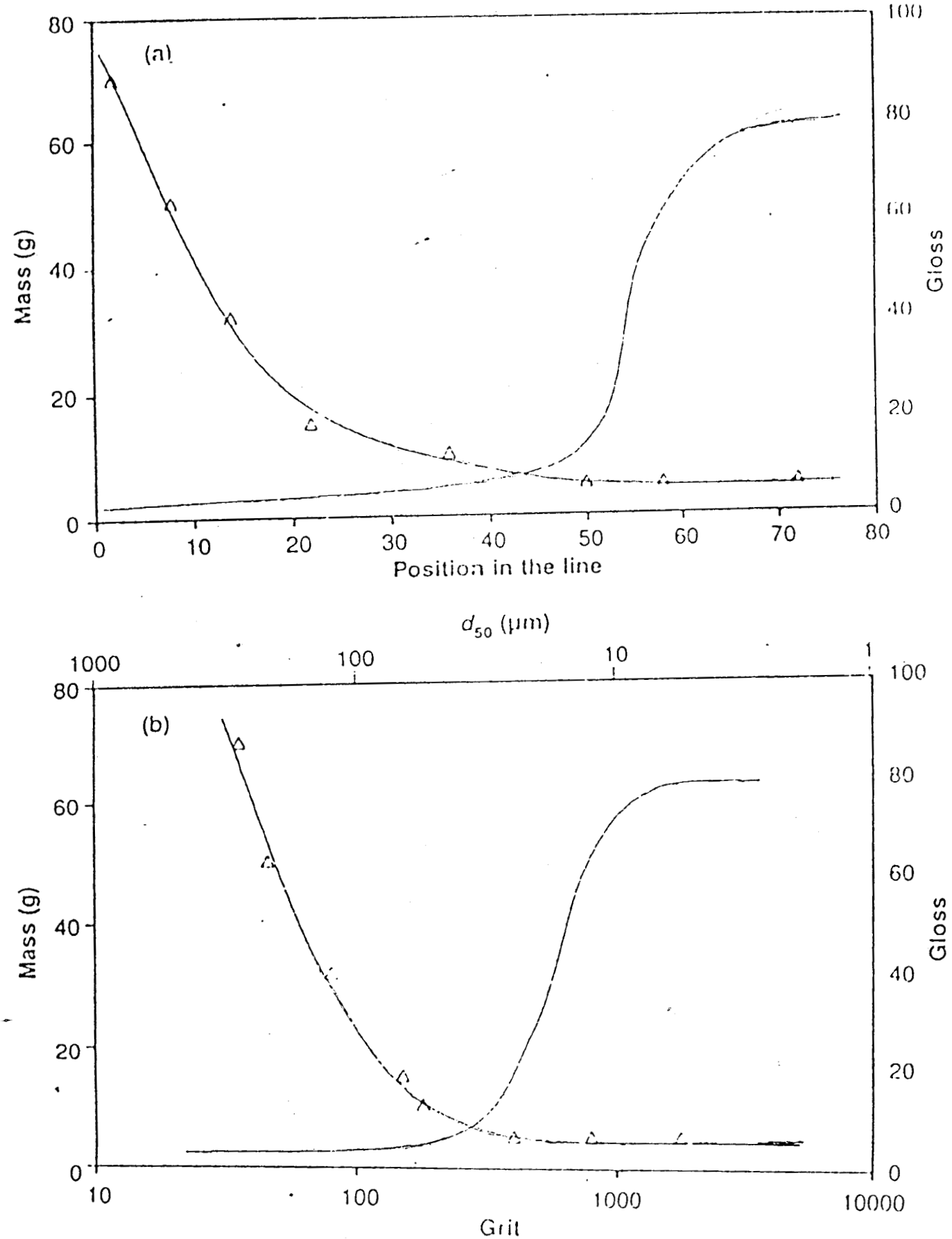

Fig. 4.26 - Variation of porcelain tile (△) mass and (□) gloss after the leveling step as a function of (a) relative position in the polishing grain and(b) grit or average abrasive grain diameter (d_{50})

176

diamond to elucidate the grinding mechanism. Another part of this study analyses the effect of porcelain tile micro-structure and mechanical properties on the wear mechanism.

4.4.1 Wear Mechanism

Samples were taken of the exiting the initial levelling step and at various positions in the polishing train corresponding to the actual polishing step, ranging from the first head to the last head. The grit used was as specified by the Federation of European Producers of Abrasives Products (FEPA). The average grain size (d_{50}) of each grit was determined. Waste samples were collected at various positions of the polishing train.

Surface gloss was measured using a reflectometer (Model Statistical Novo-Gloss, Rhopoint Instruments Ltd., Oxted, Surrey, U.K). Ten random gloss measurements were made of each sample tile surface using a 60° angle of incidence. The arithmetic mean and standard deviation were calculated for each sample.

Topographic maps were made using a roughness meter (Model R6000, Hommelwerke GmbH, Schwenningen, Germany) that had a pickup with diamond tip that had a pickup with a diamond tip that had a 90° angle and 5 mm radius. The surface topographies consisted of 101 profiles, 25 or 10 mm long, with respective spacings of 250 and 100mm, thus covering a surface of 25 x 25 mm or 10 x 10 mm^2.

The tile surfaces were observed using SEM, on some occasions with a backscattered electron signal (which highlighted compositional and topographical differences) and, on other occasions, with a secondary electron signal, which was more effective for studying the topography.

Scratch tests were conducted (Fraunhofer Institute, Freiburg, Germany) using controlled loading and sample advance speed during load application. a blunt conical diamond indenter of ~50 mm tip radius and 120° apex angle was used. Loading was increased by 1 N steps in the range 1-12 N.

4.4.2 Wear Mechanism : Leveling Step

In the leveling step, the grinding tool surface contains large diamond grain (250-300 mm) with sharp edges that come into contact with the tile under high pressure. These conditions produce severe wear in the tile because of brittle fracture mechanisms based on crack formation. Topographic maps of the tile have been prepared after the levelling step. Deep grooves are observed in the direction of sample advance. The grooves are produced by the set of fixed rollers that operate in the levelling step. The grooves indicate severe wear conditions with significant material detachment in the form of chips.

A topographic map has been made of the as-fired porcelain tile surface before polishing. The topographic map of the tile after

levelling reveals significant deterioration: surface topography height increases from 69 mm in the as-fired tile to 145 mm after levelling. Moreover, in the as-fired tile, part of the heights is due to tile curvature (visually perceivable), whereas after levelling, height is exclusively due to the depth of the grooves made in the surface, because initial curvature has been eliminated.

A cross section of a tile levelling shows the severity of material removal in the first grinding phase. The cross section shows deep subsurface cracks, with crack sizes up to 100 mm. The cracks confirm that material removal takes place by a brittle fracture mechanism in this step.

4.4.3 Wear Mechanism : Polishing Step.

Tile mass and surface gloss verses grit and relative position in the polishing train have been plotted. Mass loss is observed to vary greatly from grit 36 (600 mm) to approximately grit 280 (36.5 mm). This is the zone in which the deterioration produced by the foregoing levelling step is redressed, entailing significant material removal. At higher grits, sample mass undergoes little variation and is practically negligible after grit 400 (17.3 mm).

Gloss variation mirrors that found for material loss. Thus, the initially fast increase in gloss practically coincides with the end of the material removal period, indicating that the damage that results in the levelling step almost has been redressed and that the surface

is ready for the actual polishing step. Gloss finally tends toward a stable value from grit 1500 (d_{50} < 6,mm) and higher. This value depends on the porous texture of the tile. After the initial levelling step, the removal phase devoted to redressing surface deterioration accounts for up to 70% of the remaining industrial polishing train length. The other 30% accounts for actual surface polishing. This highlights the enormous deterioration produced in the tile and the need to optimise the levelling step to improve overall polishing process efficiency.

The great quantity if material removed during the first part of the polishing step and the mechanical characteristics of porcelain tile, suggest that wear is governed by a predominantly brittle mechanism, although without such an aggressive effect as in the levelling step. This type of wear is shown by the peaks and deep valleys in the fractured surface of tile 4 taken from the levelling zone (grit 36). The surface topography continues to exhibit peaks of considerable height (>100 mm) produced in the foregoing levelling step, pending their removal.

A micrograph of a porcelain-tile found in a sample of waste collected at this point in the polishing train (grit 36) shows spherical pores inside the chip) closed porosity) and sharp edges produced on detachment from the tile. The appearance of this chip also confirms that detachment occurs by a brittle fracture mechanism.

As the tile advances down the line, grit size decreases, decreasing grit ability to cut and remove material. After passing grit 60-80 (d_{50} ~ 250-180 mm), which has a lower material removal rate than grit 36, the surface of tile 12 continues to exhibit chipping, although most of it is covered with grooves. The grooves are not produced by a brittle mechanism but are characteristic of a gentler type of wear, i.e., plastic deformation. The surface topography of this tile continues to exhibit the deterioration of the levelling step, although peak height has decreased drastically.

Further progress in the transition from the brittle to ductile wear mechanism cab be observed in the pieces leaving grit 600 (d_{50} = 9.3 mm). In this polishing train zone, there is little material removal, while surface gloss increases rapidly. Although the tile surface continues to exhibit some chipping, most of the surface is formed by grooves characteristic of a blowing effect (plastic deformation). The waste coming from this last grinding tool basically consists of agglomerates of small porcelain-tile particles and binder particles.

Finally, tile 68, leaving grit 1500 (d_{50} < 6 mm), corresponding to the last stage of gloss stabilization without material removal, has a practically smooth appearance. The material removal symptoms observed in the previous zones (chipping and grooves) are no longer found here. Most of the discontinuities observed result from the surfacing of tile closed porosity with the removal of the top

layer. These observations indicate occurs practically entirely by plastic deformation, with no material removal.

The result confirm the wear modes of ceramics described in the literature, which indicate that, as the severity of contact increases (wear coefficient increases), the wear mode changes from blowing (pure plastic deformation) to powder formation and then to flake formation. This transition also occurs in the polishing train.

At large abrasive sizes (grit 36), flake formation predominates, which is confirmed by the porcelain-tile chips contained in the polishing waste, and it produces considerable material removal, These large flake like particles are formed by the propagation of large surface cracks, such as those observed a the end of the levelling step. Abrasive grain shape, which is angular, with sharp edges and conchoidal fracture, also facilitates this wear mode, because it enables reaching a profound depth of cut on maximizing contact pressure.

As abrasive grain size and , hence, contact severity decrease, small powder like particles, such as those observed in the debris from grinding tool 600, are formed by the propagation of surface micro cracks. This transition in the wear mode is accompanied by a drastic decrease in the material removal rate. Finally, for small abrasive grain sizes (grit 1500), the blowing effect is the dominant wear mode, which results in no typical wear particles.

The resulting mechanism changes are due to progressively decreasing grit contact pressure on the tile surface on decreasing grit size. Although the heads housing the various grinding tools apply a constant pressure across the polishing train, grit contact pressure is not constant. This occurs because, as grit size becomes smaller, the number of grains per unit area is significantly higher, despite the decreases in the abrasive mass fraction in progressing along the polishing train.

To illustrate this mechanism, the estimated number of abrasive grains per unit grinding tool volume for three grits (36,600 and 1500) shows an enormous increase in the number of abrasive grains per unit volume as grit size decreases. Therefore, the force applied to the tile is distributed over more contact points, so that the pressure each abrasive grain applies decreases significantly as the polishing train advances.

Obtaining ground surfaces, on a laboratory scale, simulating the conditions of an industrial grinding (polishing) operation is extremely complicated. Therefore, to evaluate the grinding mechanism, it has been suggested to conduct a scratching experiment on the tile rather than performing a grinding experiment.

A cone indenter with a spherical 50mm tip has been chosen to enable adequate observation of the formation of grooves and cracks responsible for material removal in the scratch tester loading

range. Because of the sharp edges of SiG grains, this indenter is representative of larger-sized grains.

SEM observation of the resulting groove cross section shows that multiple cracks form under the indenter track – mostly resulting from microflows already present in the material – because of its heterogeneous nature. However, close examination of the damaged area enables distinguishing certain types of cracks, characteristic of indentation in brittle materials.

At low loads, small cracks appear, similar to those typified as radial or lateral cracks, which propagate horizontally, causing chipping when they break through to the surface. On increasing the load, other cracks also appear, propagating vertically or obliquely inward into the piece. These cracks resemble those typified as cone cracks (characteristic of indentation using a spherical tip) or median cracks (characteristic of indentation using a sharp indenter). At higher loads, the foregoing types of cracks are found with chipping caused by lateral cracks that break through to the surface.

The scratch tests confirm the previous results. Wear by fracture occurs only on exceeding a critical load on each abrasive grain. This means that , if the abrasive particles are sufficiently small and numerous in the contact region, the load carried by each may be below the threshold needed to cause cracking. Then, at low loads or with small grains, fracture is suppressed and abrasive wear

occurs by plastic deformation. At higher loads, or with larger grains, brittle fracture takes place, leading to a sharply increased wear rate.

4.5 CHARACTERISATION OF RCP GLAZE SYSTEM

Introduction

Ceramic glaze properties are controlled mainly by microstructure, and the microstructure is controlled by processing technology. Besides processing, the microstructure or phase distribution of ceramic glazes is affected by other factors : raw materials, phase equilibrium relations, sintering, grain growth and phase change kinetics.

The microstructure of a glaze is mainly a product of heterogeneous nucleation. The glaze should not be considered as a single-phase at the grain boundaries and, frequently, extensive porosity. The characteristics of microstructure that can be determined are the number and identification of the phases present (including porosity), the relative amounts of each phase present and the characteristics of each phase present (such as size, shape and orientation).

The rutile-calcium phosphate glaze system is gradually attracting the attention of glaze technologies because of the promising opacity and brilliancy qualities it impacts on ceramic

bodies. Knowledge of the microstructure of this glaze system will aid in further development of methods of combating the rutile break-up effect and , hence , improve opacity. The purpose of this research is to identify the crystalline phases formed when a rutile-calcium phosphate glaze is sintered at 1100°C.

4.5.1 The Experiment

Two glazes slips designated R-C1 and R-C3 with variable amounts of commercial fritted rutile (10#frit) and 6% optimum calcium phosphate additions were prepared from the treated glazing materials. Various glaze slips were prepared for this study. Samples (100 g) of each of the batch glaze recipes were ball milled for 4 h in 60 Ml. of water, 1.5 g of sodium silicate and 180 g of milling stone.

The slurry was passed through a standard U.S. sieve No. 12 (<1.68 mm) and dried in an electric oven for 4 h. The dried powders were homogeneously mixed with 5% water and 0.5% starch (binder) and pressed into test bars (50 mm x 50 mm x 6mm) at 36 MPa. The test bars were fired at 1100°C with a glaze maturing time of 30 min and then free-cooled.

Phase constitution was examined using XRD (Model PW-1730, Philips, Eindhoven, Netherlands, and Model D-501, Siemens, Karlsruhe, Germany) with nickel-filtered CuK_a radiation, accelerator voltage of 30 kV, current of 10mA and 20 scan rte of

2 min^{-1} SEM was used to examine the microstructure, and EDX was used for elemental analysis of the glazes.

The whiteness of the glaze after it was fired at 1100°C was determined using a whiteness meter (Model JP 690-65) with an 86.5% white material as reference.

4.5.2 EDX Confirms Analysis

The XRD profiles of the two glaze samples sintered at 1100°C were plotted, and the peaks labelled according to the phase identified. The common phases in the two glazes were a-cristobalite, a-zinc titanium oxide and hydrocalumite. This was confirmed by the elemental analysis of the glazes using EDX.

Hydrocalumite is amorphous and has excellent fining properties in glass formation. Therefore, the predominance of hydrocalumite in the R-C1 glaze and the presence of reasonable concentrations of a-cristobalite, a-sodium calcium phosphate, and B-calcium hydrogen borate are major reasons for the glaze's amorphous, glassy microstructure, as evident from its waxy XRD peaks.

The parent materials of these phases act either as glass-network formers – in the case of silica for a-cristobalite, phosphorus pentoxide for a-sodium calcium phosphate or boron oxide for B-calcium hydrogen borate – or as fluxing agents – in the case of a=zinc titanium oxide. EDX examination shows low levels of

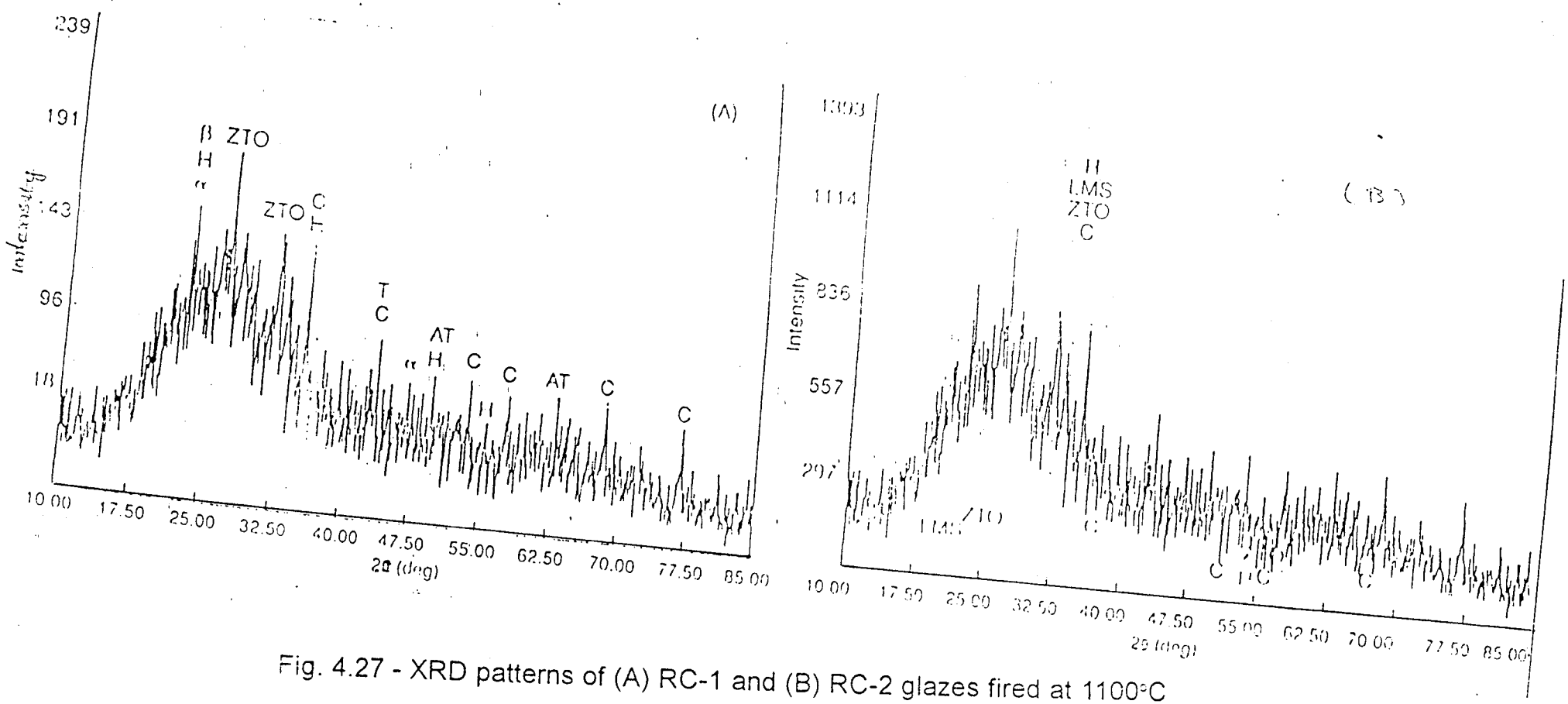

Fig. 4.27 - XRD patterns of (A) RC-1 and (B) RC-2 glazes fired at 1100°C

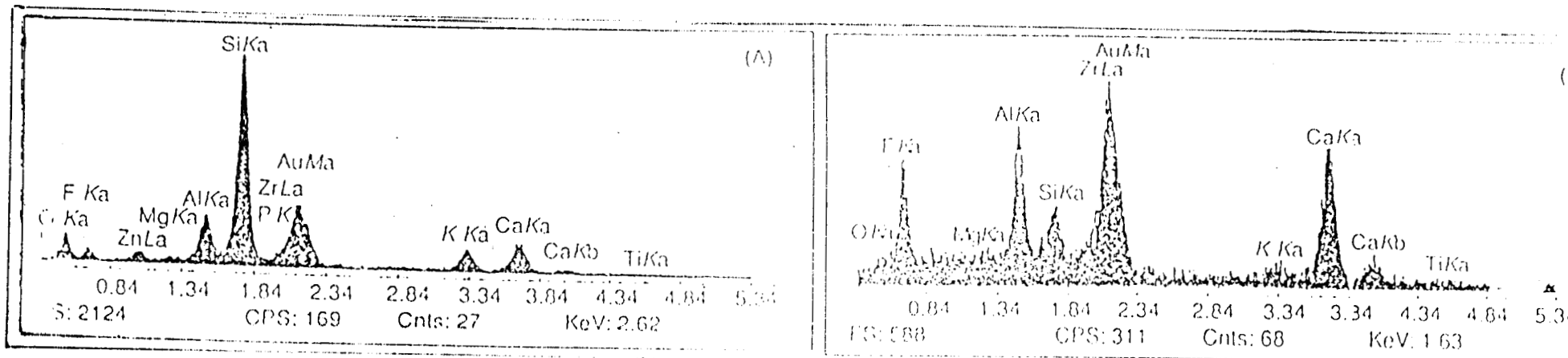

Fig. 4.28 - EDX patterns of (A) RC-1 and (B) RC-2 glazes fired at 1100°C

Table – 4.8

Abbreviations Used in XRD and EDX Patterns		
Abbreviation	Phrase description	***Formula***
LMS	lithium magnesium silicate	$Li_2Mg_{0.6}DiO_4$
ZTO	α – zinc titanium oxide	Zn_2TiO_2
C	α – *cristobalite*	SiO_2
H	hydrocalumite (synthesis)	$Ca_4Al_2O_6Cl_210H_2O$
α	α – sodium calcium phosphate	$NaCaPO_4$
B	B – clcium hydrogen borate	$Ca(H_2BO_3)_2\ 2H_2O$
T	tridymite	SiO_2
AT	α-aluminum titanium oside	Al_2TiO_2

Table – 4.9

Composition of the Glazes Studied						
Composition (mol%)						
Glaze	**Al_2O_3**	**SiO_2**	**Fe_2O_3**	**TiO_2**	**MgO**	**CaO**
R-C1	8.82	52.02	0.34	4.23	1.73	11.43
R-C2	8.69	50.44	0.22	5.74	7.79	10.80

Composition of the Glazes Studied						
Composition (mol%)						
Glaze	**K_2O**	**Na_2O**	**ZnO**	**P_2O_5**	**B_2O_3**	**LOI**
R-C1	3.07	0.80	7.64	2.25	0.98	6.43
R-C2	3.33	0.91	8.81	2.34	2.10	4.82

calcium and titanium in the R-C1 glaze, which supports the XRD results. The titanium-calcium system has an impact on glaze opacity; hence, it can promote crystal formation when present in appropriate amounts, as in the case of the R-C2 glaze.

The R-C2 glaze has a few distinct peaks because of the low concentration of hydrocalumite and other glassy phases and a comparatively higher concentration of the titanium – calcium system. these distinct peaks indicate the formation of crystalline phases, mainly contributed by lithium – and titanium – bearing phases, such as lithium magnesium sulphate and a-aluminium titanium oxide, respectively.

The higher concentration of the titanium and calcium is the probable reason for the higher opacity and whiteness, as evident from the whiteness results determined using the whiteness meter after firing at 1100oC, which indicates 71.6% and 79.4% whiteness for R-C1 and R-C2, respectively. The presence of fluorine peaks is due to the hydrofluoric acid used during the leaching process of the fired glaze samples prior to EDX examination. The detection of gold in the EDX results can be attributed to the gold used for coating the samples during the examination. The detection of gold in the EDX results can be attributed to the gold used for coating the samples during the examination. Detection of zircon is probably due to small amounts incorporated in the rutile frit under investigation.

SEM micrographs agree with the results of the ZRD examination. The SEM micrograph of R-C1 shows an almost amorphous phase with a concentration of extremely small crystalline phases. The micrograph of R-C2 shows distinct crystals.

4.5.3 Higher Whiteness and Opacity Found.

- a-cristobalite, a-zinc titanium oxide and hydrocalumite are common phases in the rutile-calcium phosphate glaze systems studied.
- More crystal formation is favoured in R-C2 than in R-C1; hence, R-C2 shows higher whiteness and opacity. This can be explained by the presence of higher concentration of amorphous, glassy phases, such as the borate phase of B-calcium hydrogen borate and to the hydrocalumite, which has fining properties in glass formation. This evident from the SEM images of the two glazes studied.
- R-C2 is recommended as the most efficient opaque glaze system of the two glaze systems studied because of its ability to form distinct crystals, which is a microstructural property promoting opacity of glazed tiles and associated ceramic building materials.

CHAPTER – 5

Conclusion and Discussion

5.1 Plasma sprayed coating materials are increasingly being used for surface modification to meet the desired tribological requirements. Even through Alumina Ceramics are commonly used, their applicability is restricted due to lower fracture toughness. Plasma Spray Technology facilitates deposition of high quality coatings for wear applications. Many of the properties of coatings depend upon their microstructure ; and microstructure is being depend on coating mechanism. coating properties may be modified by altering its microstructure. The stress-strain relation of the coating has been found to exhibit non0linear behaviour. The bending strength was found to decrease with increase in grain size. Thermal resistance of the coating can be enhanced by increasing the fracture strain of the coating.

5.2 Investigations on spray deposited ceramic composites indicated that there was a distinct phase change in the sprayed coatings compared to the spray powders used.

Physical property evaluation of Alumina-Titania Ceramic composite through load penetration relationship has yielded relatively smaller values barring fracture toughness. The AE tests conducted on coatings was found it useful for deciding

deformation response of Alumino-Titania ceramic composites to static indentation SEM studies on the abraded surfaces have illustrated that Alumina-Titania Ceramic Composites subjected to flexible abrasion is associated with material flow, glazing of the surface material, localised pull-out of glazed material due to attraction and formation of spalls.

In the present study, Alumina-Titania composites of varying proportion (AT3, AT13 and AT40) were tested to assess the response of the ceramic composites to typical abrasive environment through simulated tests.

Preliminary investigations on the spray deposited ceramic composites indicated that there was a distinct phase change in the sprayed coatings compared to the spray powders used; Al2O3 phase was observed to change over to predominantly y-Al2O3 phase after spraying and some of the rutile Titania was observed to have undergone reduction to Ti3O5. Hardness testing of the spray coated structures revealed in a reduction in hardness with increase in Titania content. Investigation by image processing of the sectioned surfaces of the coated composites indicated a porosity level of around 10+2%.

Physical property evaluation of Alumina-Titania ceramic composite through load penetration relationship has yielded relatively smaller values, barring fracture toughness. This calls for controlled, crack free indentation for especially for elastic

property evaluation through depth sensing technique. Critical loads for radial crack initiation have been identified for different compositions as, 20N for AT330N for AT13, and 50N for AT40. Also rupture loads of 150N, 200N and 250N we observed for AT3, AT13 and AT40 respectively. Acoustic emission response of the spray deposited materials to different indentation loads were observed and it was found that at low loads (around 20N), low frequency (30-50kHz) AE signals, associated with deformation modem, were emitted. It was also seen that the cracking of the sprayed ceramic composites at higher loads, as associated with burst mode of AE signal, with higher frequency (200-300lHz). Thus AE analysis was found to be useful for deciding the deformation response of Alumina Titania ceramic composites to static indentation.

However, lower critical loads were observed in the case of sliding indentation simulating rigid abrasion. Sliding indentation has resulted in relatively lower order acoustic emission in the case of AT13 composites, compared to AT3 and AT40, indicating reduced magnitude of distress experienced by AT13 composites. Plowing of ceramic composites has more dominant influence during sliding indentation, which has resulted in fairly more uniform response to scratching by 120^{o} point geometry compared to 140^{o} point geometry. SEM studies of the scratch / grooves have indicated formation of smooth grooves, grooves associated with formation of prows and

subsequent cracking over the groove walls, depending upon the normal load.

Among the ceramic composites tested AT13 composition exhibited higher wear resistance under flexible abrasion process compared to relatively harder AT3 or softer AT40 composition. The dominance of microplowing in case of softer AT40 and micro cutting and micro cracking in the case of AT3 resulted in the observed variation in wear resistance of different compositions. Regression model of the wear process indicates the level of influence of different material properties and also the test parameters on weight loss. The effect of abrasive particle size on weight loss due to abrasion was also clearly seen from the present investigation. While the weight loss due to abrasion increased with the abrasive particle size in case of AT3 and AT13, in case of AT40, higher order weight loss was observed with smaller size abrasive particles, especially at lower loads. Acoustic emission response of the sprayed composites to flexible abrasion process distinctly indicated different modes of material status at different stages of wear. SEM studies of the abraded surfaces have illustrated that Alumina-Titania ceramic composites subjected to flexible abrasion is associated with material flow, glazing of surface material. localised pull-out of glazed material die to attrition and formation of spalls.

5.3 Glazed surface effects can be produced using Alumino. The specific levels of alumina needed depend on the cooling cycle

used. Most of the ways to produce these variations involve use of relatively coarse particles. Synthetic specks provide possibilities for variation in colour, particle size, spreading vs. non-spreading and concentration of speck in the glaze.

REFERENCES

1. **Ahmed, M.M.I., R. A. Abdel-Karim, s.M./ El-Raghy. F. A. El-Rafie, and A.E. El-Mehairi (1991)**
Wear resistance of plasma coatings on mild steel.
Journal of Materials Science,**26**,517-522.

2. **Ajayi, O.O. and K.C. Kudema (1988)**
Surface damage of structural ceramics : Implications for wear modelling,
Wear, **124**, 237-257

3. **Alan P. Dimberg (1994)**
Coated abrasive superfinishing an alternative for roll refinishing.

4. **Alan V. Levy (1994)**
The performance of ceramic coatings on diesel engine combustion zone components.

5. **Albert Kay (1994)**
Successful Hypersonic spray applications in the steel industry.

6. **Anstis, G. R., P. Chantikyl, B. R. Lawn, and D. B.Marshall (1981)**
A critical evaluation of indentation techniques for measuring fracture toughness : I, Direct crack measurements.
Journal of American Ceramic Society, **64**, 533-538.

7. **Antonia Parares, Lanhua Wei, Brian R Lawn, Nitin P. Padture and Christoppher C. Berndt (1996)**
Mechanical characterization of plasma sparayed ceramic coatings in metal substrates by contact testing.
Material Science and Engineering, **A208**, 158-165.

8. **Aslund C. , L. Christensen (1994)**
A new production technique for spray powder.

9. **Arai, T., Jacobson, and S. Hogmark (1987)**
Evaluation of adhesion strengh of thin hard coatings.
Thin solid Films, **154,** 387-401.

10. **Axen, N. S. Jacobson, and S. Hogmark (1994)**
Influence of hardness of the counter body in three-body abrasive wear – an overlooked hardness effect.
Tribology International, **30,** 467-474.

11. **Axen, N., L. Kahlman, and I. M. Hutchings (1997)**
Correlations between tangential force and damage mechanisms in the scratch testing of ceramics.
Tribology International, **30,** 467-474.

12. **Beltzung, F., G. Zambelli, and E. Lopez (1989)**
Fracture toughness measurement of plasma sprayed ceramic coatings.
Thin solid films, **181**, 407 – 415.

13. **Bernard J. Hokey (1971)**
Plastic deformation of Aluminium Oxide by indentation and abrasion.
Journal of American Ceramic Society, **54**, 223-231.

14. **Berndt, C. C., and J.H. Yi (1987)**
Strength enhancement of plasma sprayed coatings. Proceedings of *National thermal spray conference*, Florida, September, 14-17

15. **Berndt C. C., J. H. Yi (1994)**
Strength Enhancement of plasma sprayed coatings.

16. **Boness, R. J. and S.L. McBride (1991)**
Adhesive and abrasive wear studies using acoustic emission techniques. *Wear*, **149**, 41-53

17. **Brian Lawn and Rodney Wilshaw (1975)**
Review Indentation fracture : principles and applications.
Journal of Materials Science, **10**, 1049 – 1081

18. **Bull, S.J. (1997)**
Failure mode maps in the thin film scratch adhesion test.
Tribology International, **30**, 491-498.

19. **Bull, S.J., D. S. Rickerby, A. Mathews, A. Leyland, A. R. Pace, and J. Valli (1988)**
The use of scratch adhesion testing for the determination of interfacial adhesion : The importance of fictional drag.
Materials Science and Engineering, **A140**, 583-592.

20. **Chalker, P.R., S. J. Bull, and D.S. Rickerby (1991)**
A review of the methods for the evaluation of coating-substrate adhesion.
Materials Science and Engineering, **A140**, 583-592.

21. **Champagne, B. S. Dallaire (1994)**
Particle injection in plasma spraying

22. **Chantikul, P., G. R. Ansits, B. R. Lawn, and D. b. Marshall (1981)**
A critical evaluation of indentation techniques for measuring fracture toughness : II, Strength method.
Journal of American Ceramic Society, **64**, 539 – 543.

23. **Chen, S.Y., T.N. Farris, S. Chandrasekhar (1991)**
Sliding microindentation fracture of brittle materials. *STLE.* **34**, 161-168

24. **Chicot, D., I. Hage. P. Demarecaux, and J. Lesage (1996)**
Elastic properties determination from indentation tests.
Surface and Coatings Technology, **81**, 269 – 274.

25. **Clive Nusum (1994)**
Applications in Thermal spraying

26. **Cook, S.G., J.E. King, and J.A. Little (1995)**
Surface and subsurface Vickers indentation cracks in SiC, Si_3N_4 and sialon ceramics.
Materials Science Technology, **11,** 1093 – 1098.

27. **David B.Marshall (1983)**
Controlled flows in ceramics ; A comparison of Knoop and Vickers indentation.
Journal of American Ceramic Society, **66**, 127-131.

28. **David L. Houck, William Whisenant (1994)**
Wear Resistance of Five Molybdenum-containing plasma sprayed coatings.

29. **Deckman, D.E., S. Jahanmir and S.M. Hsu (1991)**
Wear mechanisms of a-alumina lubricated with a paraffin oil.
Wear, **149,** 155-168.

30. **Diao, D. F., K. Kato, and K. Hayashi (1994a)**
The maximum tensile stress on a hard coating under sliding friction.
Tribology International, **27**, 267-272.

31. **Diao, D. F., K. Kato, and K. Hokkirigawa (1991b)**
Fracture mechanisms of ceramic coatings in indentation.
Journal of Tribology, ASME, **116,** 860-869.

32. **Donald H. Buckley, and Kazuhisa Miyoshi (1984)**
Friction and Wear of Ceramics. *Wear*, **100**, 333-353.

33. **Ekkehard, H. (1994)**
Microstructure and properties of plasma ceramics.
Journal of American Ceramic Society, **77**, 1274 – 1280.

34. **Erich Lugscheider (1987)**
Plasma sprayings for wear applications. Proceedings of *National thermal spray conference*, Florida, September, 105-122.

35. **Erich Lugscheilder (1994)**
Plasma spraying for wear applications.

36. **Evans, A. G. and E. A. Charels (1976)**
Fracture toughness determination by indentation.
Journal of American Ceramic Society, **59**, 371-372.

37. **Fauchais P., J. F. Coudert A., and M. Vardelle, A. Grimoud, P. Roumilhac (1994)**
State of the Art for the Understanding of the Physical Phenomena involved in plasma spraying at atmospheric pressure.

38. **Ferrari, m., j. H. Harding, and M. Marchese (1991)**
Computer simulation of plasma-sprayed coatings II. Effective bulk properties and thermal stress calculations.
Surface and Coatings Technology, **48**, 147-154.

39. **Filiaggi, m. J. and R. M. Pillar (1991)**
Mechanical testing of plasma-sprayed ceramic coatings on metal substrates : interfacial fracture toughness and tensile bond strength.
Journal of Materials Science, **26**, 5383-5395.

40. **Fouad Attar, and Thomas Johannesson (1996)**
Adhesion evaluation of thin ceramic coatings on tool steel using the scratch testing technique.
Surface and Coatings Technology, **78**, 87-102

41. **Gansert D. J., H. Herman (1994)**
Jet-Kote sprayed machine element coatings.

42. **Gowri,S.,G.Uma Shankar,K.Narayanasamy,R.Krishnamurthy**.
Expert system for process optimisation of atmospheric plasma spraying of high performance ceramics. *Journal of Processing Technology*,**63**,724-732.

43. **Griffiths, H. J., D. T. Gawne, and G. Dong (1997)**
The role of grit blasting in the production of high-adhesion plasma sprayed alumina coatings.
Journal of Engineering Manufacture, **211**, 1-9.

44. **Haiyan Liu, and Stephen M. Hsu (1996)**
Modeling of microfracture-induced wear transition in sliding of polycrystalline alumina ceramics. *Wear*, **195**, 169-177.

45. **Halling, J. and R.D. Arnell (1984)**
Ceramic coatings in the war on wear. *Wear*, **100**, 367 – 380.

46. **Hans-Dieter Steffens, Uwe Fisher (1994)**
Correlation between microstructure and physical properties of plasma sprayed zirconia coatings.

47. **Hans-Dieter Steffens, Mattias Wewel (1994)**
Recent developments in vacuum arc spraying.

48. **Heinrich Crutzner and Horst Weiss (1991)**
A novel shear test for plasma-sprayed coatings.
Surface and Coatings Technology, **45**, 317-323.

49. **Heinrich Kreye (1994)**
Optimization and Control of the spray conditions in the jet kote process.

50. **Heintze, G. N. and R. Mcpherson (1988)**
A further stidy of the fracture toughness of plasma-sprayed zirconia coatings.
Surface and Coatings Technology, **36**, 125-132.

51. **Hermanek F. J., Nicoil A. R., Robert H. Unger (1994)**
Manufacturing methods for plasma spray powders and the resulting coating quality.

52. **Hiratsuka, K., A. Enomoto, and T. Sasada (1992)**
Friction and wear of AL_2O_3,ZrO_2 and SuO_2 rubbed against pure metals
Wear, **151**, 361-373.

53. **Hobbis M.K., H. Reiter (1994)**
Residual Stresses in ZrO2-8% Y2O3 plasma sprayed thermal barrier coatings.

54. **Hockey, B. J. and B. R. Lawn (1975)**
Electron microscopy of microcracking about indentations in aluminium oxide and silicon carbide.
Journal of Materials Science, **10**, 1275-1284.

55. **Hokkirigawa, K. (1991)**
Wear mode map of ceramics. *Wear*, **151**, 219-228.

56. **Hohle H. M., D. Dietsch. (1994)**
Design of a computer controlled vacuum-plasma spray system for production application.

57. **Hreintze. G., N., R. McPherson (1994)**
Fracture toughness of Plasma-sprayed Zirconia coatings

58. **Ingard Kvernes, and Erich Lugscheider (1992)**
Surface engineering of diesel engine parts – New technological achievements in powders and coating microstructures.
Powder Metallurgy International, **24**, 7-13.

59. **James Lankford, and David L. Davidson (1979a)**
Indentation plasticity and microfracture in silicon carbide.
Journal of Material Science,**14,** 1669 – 1675.

60. **James Lankford, and David L. Davidson (1979b)**
The crack-initiation threshold in ceramic materials subject to elastic/plastic indentation.
Journal of Materials Science, **14**, 1662-1668.

61. **Jan Wigren (1994)**
Grit-Blasting as Surface preparation before plasma spraying.

62. **Javad Akbari,Yoshio Saito, Tadaaki Hanaoka, and Shinzo Enomoto (1994)**
Acoustic emission and deformation mode in ceramics during indentation.
JSME International Journal, **37**, 488-494.

63. **Jiaa, C. L. and D. A. Dornfeld (1990)**
Experimental studies of sliding friction and wear via coustic emission signal analysis. *Wear*, **139**, 403-424.

64. **Jianren Zhou, and Shyam Bahadur (1991)**
The effect of material composition and operational variables on the erosion signal analysis. *Wear,* **139**, 403-424.

65. **Julia-Schmutz, C. and H. E. Hintermann (1991)**
Microscratch testing to charecterise the adhesion of thin layers.
Surface and Coatings Technology, **48**, 1-6.

66. **Kato, K. (1990)** Tribology of Ceramics. *Wear*, **136**, 117-133.

67. **Kazuhisa Miyoshi (1988)**
Adhesion, friction and micromechanical properties of ceramics.
Surface and Coatings Technology, **36**, 487-501.

68. **Ke-shun shi, Zeng-ying qian, and Ming-sie zhuang (1988)**
Microstructure and properties of sprayed ceramic coating.
Journal of American Ceramic Society, **71**, 924-929.

69. **Khuri-Yakub, B.T.,**
Acoustic Characterisation of Structural Ceramics, pp. 401-412, In **David R. Rossington, Robert A. Condrate** and **Robert L. Snyder** (eds.)
Advance in Materials Characterisation – v15, Plenu,Press, New York, 1982.

70. **Kingswell, R., D.S. Rickerby, S.J. Bull, and K. T. Scott (1991)**
Erosive wear of thermally sprayed Tungsten coatings. *Thin Solid Films*, **198**, 139-148.

71. **Knight, J. C., T.F. Page, and I.M. Hutchings (1989a)**
Surface deformation behaviour of TiC and TiN coated steels : 1 Indentation response.
Surface Engineering, **5**, 213-225.

72. **Knight, J.C., T. F. Page and I.M. Hutchings (1989ab)**
The influence of substrate hardness on the response of TiN – coated steels to surface deformation. *Thin Solid Films*, **177**, 117-132.

73. **Knotek, O., R. Elsing and U. Balting (1988)**
On the influence of thermophysical data and spraying parameters on the temperature curve in thermally sprayed coatings during production.
Surface and Coatings Technology, **36**, 99-110.

74. **Lawn, B. R. and A. G. Evans (1977)**
A model for crack initiation oxide ceramics.
Powder Metallurgy International, **23**, 357-362.

75. **Lech Pawlowski (1991)**
The Science and Engineering of Thermal Spraying. John Wiley, England 1995.

76. **Lescribaa, D. and A. Vincent (1996)**
Iltrasonic charectarisation of plasma-sprayed coatings.
Surface and Coatings Technology, 36, 807-815.

77. **Lopez, E., F. Beltzung, and G. Zambelli (1989)**
Measurement of cohesion and adhesion strengths in alumina coatings produced by plasma spraying.
Journal of Materials Science Letters, **8,** 346-348.

78. **Ma, K. J. and A. Bloyce (1995)**
Observations of deformation and failure mechanism in TiN coatings after hardness indentation and scratch testing.
Surface Engineering, **10**, 46-51.

79. **Matejka, D. and B. Benko**
Plasma spraying of metallic and ceramic materials, John Wiley, UK, 1989.

80. **McColm, I. J.**
Ceramic hardness, Plenum Press, New York, 1990.

81. **Mcpherson, R. (1981)**
The relationship between the mechanism of formation, microstructure and properties of plasma sprayed coatings.
Thin Solid Films, **83**, 297-310.

82. **Mellali, M., P. Fauchais, and A. Grimaud (1996)**
Influence of substrate roughness and temperature on the adhesion / cohesion of alumina coatings.
Surface and Coatings Technology, **81**, 275-286.

83. **Merle L. Thorpe (1994)**
A Bond coat for metals on plastic.

84. **Nicoll. A. R. (1994)**
The effect of varying plasma gun nozzle diameter on the surface roughness; hardness and bond strength of Al_2O_3 and Cr_2O_3 coatings

85. **Novak, R., F. Cermak, and L. Kalivoda (1991)**
Study of AL_2O_3 and AiAL-AL_2O_3 coatings with acoustic emission analysis. *Materials Science and Engineering*, **A139**, 264-267.

86. **Noval R. C., A. P. Matarese, R. P. Huston (1994)**
Development of Thermal barriers coatings for diesel applications.

87. **Per Hedenqvist, and Strue Hogmark (1997)**
Experiences from scratch testing of tribological PVD coatings.
Tribology International, **30**, 507-516.

88. **Perrot, C. M. (1977)**
Elastic-Plastic indentation : Hardness and fracture. *Wear*, **45**, 293-309.

89. **Perry, A.J. (1983)**
Scratch adhesion testing of hard coatings.
Thin Solid films, **107**, 167-180.

90. **Perry, A.J., J. Valli, and P. A. Steinmann (1988)**
Adhesion scratch testing : A round-robin experiment.
Surface and Coatings Technology, **36**, 559-575.

91. **Pfender E., (1994)**
Fundamental Studies Associated with the Plasma Spray Process.

92. **Poech, M.H., S. Isfahani, and H. Opielka (1993)**
Size distribution analysis of powders used for thermal spraying.
Powder Metallurgy International, **25**, 233-237.

93. **Rhys-Jones, T.N. (1990)**
The use of thermally sprayed coatings for compressor and turbine applications in aero engines.
Surface and Coatings Technology, **42**, 1-11.

94. **Richard, C. S., G. Beranger, J. Lu, and j. F. Flavenot (1996)**
The influence of heat treatment and interdiffusion on the adhesion of plasma-sprayed NuCrALY coatings.
Surface and Coatings Technology, **82**, 99-109.

95. **Rickerby, D.S., G. Eckold, K. T. Scott, and I. M. Buckley-Golder (1987)** The inter-relationship between stress, processing parameters and microstructure of physically vapour deposited and thermally sprayed coatings. *Thin Solid Films*, **154**, 125-141.

96. **Robert A. Miller (1994)**
High resolution video monitoring of coating thickness during plasma spraying.

97. **Robert F. Cook, and George M. Pharr (1990)**
Direct observation and analysis of indentation cracking in glasses and ceramics.
Journal of American Ceramic Society, **73**, 787-817.

98. **Robert H. Unger (1994)**
Comparison of thermal spray bond coats.

99. **Ronald W. Smith (1994)**
Particle melting behaviour in a D.C. plasma jet; observations on several nickel base alloys.

100. **Sampath. S., H. Herman (1994)**
Micro Structure of Vacuum plasma sprayed coatings.

101. **Schweitzer, K. K., M.H. Ziehl, nd Ch. Schwaminger (1991)**
Improved methods for testing bond and intrinsic strength and fatigue of thermally sprayed metallic and ceramic coatings.
Surface and Coatings Technology, **48**, 103-111.

102. **Scott K. T., Restall J. E. (1994)**
Some aspects of the development and performance of ceramic thermal barrier coatings for gas turbines.

103. **Sekler, J., P. A. Steinmann, and H. E. Hintermann (1988)**
The scratch test : Different critical load determination techniques.
Surface and Coatings Technology, **36**, 519-529.

104. **Seong-Jai cho, Hahngue Moon, B. J. Hockey and S.M. Hsu (1992)**
The transition from mild to severe wear in alumina during sliding.
Acta metallurgica et materiala, **40**, 185- 192.

105. **Shigeyasu Amada, and Hiroshi Yamada (1996)**
Introdction of fractal dimensions to adhesive strength evaluation of plasma-sprayed coatings.
Surface and Coatings Technology, **78**, 50-55.

106. **Sobolev, V. V., J. M. Guilemany, J. Nuttings, and J. R. Miquel (1997)**
Development of substrate-coating adhesion in thermal spraying.
International Materials Reviews, **42**, 117 – 136.

107. **Sorokin, G. M., S.P. Grigoryev, and B. P. Saphonov (1991)**
Wear by abrasives : methodology and results of investigations.
Tribology International, **24**, 3-9.

108. **Steffens H. D., H, Kern, M. Fathi-Torbaghan (1994)**
An expert system for diagnosis of low pressure plasma spraying.

109. **Strafford, K. N. (1996)**
Tribological properties if coatings-expectations, performance and the design dilemma.
Surface and Coatings Technology, **81**, 106-117.

110. **Streb P., H. T. Steline, W. Simm, H. Oechsle, R. Dumole, P. A. Kammer (1994)**
New high energy combustion process for thermal spray coatings

111. **Suzanne H. Weissman, Mark F. Smith, William B. Chambers (1994)**
Diagnostics of a low-pressure plasma spray deposition system.

112. **Swain, M. V. (1975)**
Microscopic observations of abrasive wear of polycrystalline alumina.
Wear, **35**, 185-597.

113. **Swain, M. V. (1979)**
Microfracture about scratches in brittle solids.
Royal Society of London Proceedings A, **366,** 575-597.

114. **Swain, M. V. (1994)**
Indentation based mechanical characterisation of thin films on substrates. *Proceedings of Second Australian International Conference on Surface Engineering*, Adelaide, March, 79-94.

115. **Takashi Taniguchi, Minoru Akaishi, and Shinobu Yamaoka (1996)**
Mechanical properties of polycrystalline translucent cubic boron nitride as characterised by the Vickers indentation method.
Journal of American Ceramic Society, **79**, 547-549.

116. **Tanikella, B. V. and Ronald O. Scattergood (1995)**
Acoustic emission during indentation fracture.
Journal of American Ceramic Society, **78**, 1698-1702.

117. **Taylor M. L., J.G. Murphy, H.W. King. (1994)**
Brittle / Ductile Erosion of plasma sprayed ceramic and metallic coatings.

118. **Tong Zhaohe, Ding Chuanxian, and Yan Dongsheng (1992)**
A fracture model for wear mechanism in plasma sprayed ceramic materials. *Wear*, **155**, 309-316.

119. **Upadhyay, H. S. Spacil (1994)**
Intelligent processing for metal atomisation

120. Vijande-Diaz, R., J. Belzunce, and E. Fernandex (1991)
Wear and microstructure in fine ceramic coatings.
Wear, **148**, 221-233.

121. **Von Stebut, J., R. Rezakhanlou, K. Anoun, H. Michel, and M. Gantois.**
Major damage mechanisms during scratch and wear testing of hard coatings on hard substrates. *Thin Solid Films*, **181**, 555-564.

122. **Williams, A. (1996)**
Analytical models of scratch hardness.
Tribology international, **29**, 675-694.

123. **Yoshiaki ARTA (1994)**
New technology for processing and evaluating thermal sprayed coatings

124. **Yurkov, A. AL., E. Breval, and R. C. Bradt (1996)**
Cracking during indentation in Sialon-based ceramic: Kinetic microhardness and acoustic emission.
Journal of Materials Science Letters, 15, 987-990.

125. **Yushu Wang, and Stephen M. Hsu (1996b)**
The effects of operating parameters and environment of the wear and wear transition of alumina. *Wear*, **195**, 90-99.

126. **Yust, C. S., and H. J. Carignan (1985)**
Observations on the sliding wear of ceramics. *ASLE*, **28**, 245 – 252.

127. **Zeng, K., E. Soderlund, A. E. Giannakopoulos, and D. J. Rowcliffe (1996)**
Controlled Indentation : A general approach to determine mechanical properties of brittle materials.
Acta Metallurgica, **44**, 1127-1141.

128. **Zhou, L., L. Fang, N. X. Wang and J. E. Zhou (1994)**
Unlubricated sliding wear mechanism of fine ceramic Su3N4 against high-chromiun cast iron.
Tribology International, **27**, 349-357.